Nanoreinforced Shape Memory Polyurethane

by

Tara Beth Richardson

A dissertation submitted to the Graduate Faculty of
Auburn University
in partial fulfillment of the
requirements for the Degree of
Doctor of Philosophy

Auburn, Alabama
December 18, 2009

Keywords: shape memory polyurethanes, nanoreinforcement, nanocomposites, cellulose
nanofibers, conductive cellulose nanofibers, carbon nanotubes

Approved by

Maria L. Auad, Co-chair, Professor of Polymer and Fiber Engineering
Peter Schwartz, Co-chair, Department Head Polymer and Fiber Engineering
Gisela Buschle-Diller, Professor of Polymer and Fiber Engineering
Ann Beth Presley, Professor of Consumer Affairs

Abstract

Shape memory polymers (SMPs) are functional materials, which find applications in a broad range of temperature sensing elements and biological micro-electro-mechanical systems (MEMS). These polymers are capable of fixing a transient shape and recovering to their original shape after a series of thermo-mechanical treatments. Generally, these materials are thermoplastic segmented polyurethanes composed of soft segments, usually formed by a polyether macroglycol, and hard segments formed from the reaction of a diisocyanate with a low molecular mass diol. The hard segment content is a key parameter to control the final properties of the polymer, such as rubbery plateau modulus, melting point, hardness, and tensile strength. The long flexible soft segment largely controls the low temperature properties, solvent resistance, and weather resistance properties. The morphology and properties of polyurethanes (PU) are greatly influenced by the ratio of hard and soft block components and the average block lengths. However, in some applications, SMPs may not generate enough recovery force to be useful. The reinforcement of SMPs using nanofillers represents a novel approach of enhancing the performance of these materials. The incorporation of these fillers into SMPs can produce performance enhancements (particularly elastic modulus) at small nanoparticle loadings (~1-2 wt %). An optimal performance of nanofiller-polymer nanocomposites requires uniform dispersion of filler in polymers and good interfacial adhesion. The addition of nanofillers like cellulose nanofibers (CNF), conductive cellulose nanofibers (C-CNF), and carbon nanotubes (CNTs) allows for the production of stiffer materials with deformation capacity comparable to that of the

unfilled polymer. Additionally, the use of conductive nanoreinforcments such as C-CNF and CNTs leads to new pathways for actuation of the shape memory effect.

During this work, thermoplastic shape memory polyurethanes were synthesized with varying chemical composition and molecular weight. This was achieved by controlling the moles of reactants used, by using polyols with different molecular weights, and by using different diisocyanates. Using these controls, polymer matrices with different but controlled structures were synthesized and then reinforced with CNF, C-CNF, and CNTs in order to study the influence of chemical structure and polymer-nanoreinforcement interactions on polymer nanocomposite morphology, thermal and mechanical properties, and shape memory behavior.

Acknowledgments

First, I would like to thank my parents, Amy and David Richardson. My pursuit of graduate research would not have been possible without their love, support, and encouragement. I am very lucky to have been blessed with them and know that they are as proud of this accomplishment as I am. I owe a great deal of gratitude to William Jones, a wonderful companion and constant source of motivation. He provided a shoulder to lean on as well as many home cooked dinners and study breaks after long days spent in the laboratory and writing. I will be forever grateful for his encouragement and faith that I would, in fact, finally complete everything.

I would like to acknowledge and thank my graduate committee members, Prof. Maria L. Auad, Prof. Peter Schwartz, Prof. Gisela Buschle-Diller, and Prof. Ann Beth Presley, for their help and guidance during this project. In particular, Prof. Maria L. Auad was always there to listen and provide advice with any and all problems, be they research or life related. I cannot imagine what I would have done without her. Many thanks go to the Polymer and Fiber Engineering Department for use of their equipment and facilities. Additional thanks go to Prof. Auad's research group and undergraduate research fellows, Mirna Mosiewicki, Cihan Uzunpinar, Buket Demir, Samantha Bird, Angie Greer, and Marisa Hicks, for their support of the project. Norma Marcovich and Mirta I. Aranguren cannot be thanked enough for their guidance and instruction during collaborative research at the National University of Mar del Plata, in Mar

iv

Table of Contents

List of Tables

List of Figures

List of Abbreviations

SMP   Shape Memory Polymers

SME   Shape Memory Effect

SMB   Shape Memory Behavior

PU   Polyurethane

MDI   Methylenedi-p-phenyl Diisocyanate

TDI   Tolylene 2, 4 Diisocyanate

PTMG   polyether glycol

DMF   N, N'-dimethylformamide

CNF   Cellulose Nanofibers

C-CNF   Conductive Cellulose Nanofibers

CNT(s)   Carbon Nanotube(s)

SMB   Shape Memory Behavior

DSC   Differential Scanning Calorimetry

TGA   Thermal Gravimetric Analysis

FTIR   Fourier Transform Infrared

SEM   Scanning Electron Microscopy

AFM   Atomic Force Microscopy

DMA   Dynamic Mechanical Analysis

CHAPTER I.

INTRODUCTION

Shape Memory Materials/Polymers

Shape memory materials are stimuli-responsive materials that possess the ability to change their shape upon application of an external stimulus [Lendlein & Kelch, 2002; Chun et al., 2007]. They were first introduced in 1951 when Chang and Read discovered shape memory effect in an Au-47.5 at% Cd alloy [Chang & Read, 1951]. The designation of shape memory material covers a broad variety of materials (metal, ceramic, and polymer) [Chun et al., 2007]. Although a variety of materials have been found to exhibit shape memory effect, Ni-Ti alloy (Nitinol) is the most widely used shape memory material for commercial applications because of its shape memory performance, good processability, and excellent mechanical properties [Buhler et al., 1963; Wei & Sandstrom, 1998]. Additionally, Ni-Ti alloys have good biocompatibility and corrosion resistance which makes them desirable for biomedical applications. Shape memory materials are being pursued in research because of their unusual properties which are due to the phase transitions in the materials and include shape memory effect, pseudoelasticity or large recoverable strain, high damping capacity, and adaptive properties [Wei & Sandstrom, 1998]. A variety of external stimuli can be used to trigger the shape memory effect, making shape memory polymers useful for a range of applications. The external stimuli used to trigger a change in a shape may be heat [Auad et al., 2009; Kim et al., 1996; Kamieneski et al., 2007], magnetic field [Mohr et al., 1996], electric field [Jimenez et al., 2007], or light [Maitland et al., 2002; Lendlein

et al., 2005]. These polymers are capable of sensing the external stimuli and then exhibiting a predictable response such as a change in shape, position, strain, stiffness, natural frequency, damping, friction, and other static and dynamic characteristics to the environmental changes [Wei & Sandstrom, 1998].

Shape memory polymers have found applications in a wide range of fields. Several researchers have taken advantage of the large strain recovery behavior of shape memory polymers to create novel medical devices capable of performing in vivo functions such as gripping or releasing of therapeutic medical devices within blood vessels [Benett et al., 1997; Lee et al., 1997; Lee et al. 2000]. Shape memory polymers are also useful in industrial applications where manipulation of objects located in inaccessible locations is necessary [Lee & Fitch, 2000], aerospace applications [Gall et al., 2004], and smart textiles [Ding et al., 2004].

Shape Memory Alloys

Shape memory alloys (SMAs) derive their shape memory capabilities from their high temperature austenite and low temperature martensite phases. They are capable of recovering from up to 10% strains through temperature and stress-induced transformations between these phases [Smith, 2005]. The shape memory effect in SMAs works by plastic deformation applied at an ambient temperature that becomes elastic upon heating, allowing the material to return to its original shape. Despite the plastic to elastic transformation, the material experiences an increase in modulus with an increase in temperature [Monkman, 2000]. The thermodynamic stability of the austenite and martensite phases gives the material its ability to "remember" various shapes, which are constructed in the austenite phase. Despite their advantages, SMAs

have obvious drawbacks such as high manufacturing costs, limited recoverable deformation, appreciable toxicity, comparatively inflexible transition temperatures, and demanding processing and training conditions [Uo et al., 2001; Hornbogen, 2006; Liu et al., 2007].

Due to the disadvantages of shape memory alloys, increasing attention is being directed towards shape memory polymers [Rousseau, 2008]. Due to their light-weight, high shape recoverability, easy manipulation, economical value in comparison with shape memory alloys, and unusual properties, the development of shape memory polymers and composites is being actively pursued [Hayashi et al., 1991; Liang et al, 1991; Ahir & Terentjev, 2005]. For certain types of shape memory polymers, strains of up to 700% have been reported [Koerne et al., 2004] as opposed to shape memory alloys, shape memory ceramics, and glasses that normally have strains of less than 10, 1, and 0.1%, respectively [Wei et al., 1998; Winzek et al., 2004]. In contrast to their shape memory alloy counterparts, shape memory polymers rely on one or more glass transition temperatures to exhibit a change in shape and exhibit a decrease in elastic modulus with increasing temperature [Monkman, 2000]. Disadvantages of shape memory polymers include their relatively low modulus, usually 4-10 MPa against 200-400 MPa for SMAs [Wei et al., 1998; Cao & Jana, 2007], which results in small recovery forces [Cao & Jana, 2007; Koerne et al., 2004; Xu et al, 2006; Jeong et al, 2000], their response time is much longer than SMAs [Liu & Mather, 2005; Razzaq & Frormann, 2007], and the number of achievable cycles is lower than SMAs [Lin & Chen, 1998; Xu et al., 2006]. The molecular design of the polymer, however, can have a large impact on the achievable material properties and behavior [Rousseau, 2008]. The literature contains information on a broad variety of shape memory polymers based on common chemistries such as polyurethane (PU) [Chun et al., 2007], epoxy

[Gall et al., 2004; Liu et al., 2006], polyethylene [Ota, 1981; Machi, 1996], and polyolefin [Liu et al., 2002].

Categories of Shape Memory Polymers

It is accepted in academia and research that shape memory polymers can be divided into four categories which are distinguished by the differences in fixing mechanism and origin of "permanent" shape elasticity [Liu et al., 2002; Liu et al., 2007]. These categories split shape memory polymers into 1) covalently crosslinked glassy thermosets, 2) covalently crosslinked semicrystalline rubber, 3) physically crosslinked amorphous thermoplastics, and 4) physically crosslinked semi-crystalline block copolymers [Liu et al., 2007; Rousseau, 2008; Lendlein & Kelch, 2002]. Before these categories can be explored, it is important to discuss the molecular mechanism that makes shape memory a possibility in polymers. Shape memory polymers derive their ability to achieve temporary strain fixing and recovery from the intrinsic elasticity of the polymeric network [Liu et al., 2007]. However, it is important to note that shape memory behavior is not an intrinsic polymer property, so polymers do not exhibit this behavior by themselves but through a combination of polymer morphology, structure, and specific external processing conditions [Behl & Lendlein, 2007; Rousseau, 2008]. Shape memory behavior can be observed in elastomeric polymers that consist of two phases [Lendlein & Kelch, 2002; Rousseau, 2008; Ratna & Karger-Kocsis, 2008]. One of the phases allows for shape fixity through chemical or physical crosslinks while the other phase is responsible for reversibility or "remembering" the original/permanent shape through transitions such as a melting or glass transition temperature [Rousseau, 2008]. The two phases will exhibit separate and different phase transitions. The phase with the higher thermal transition, T_{perm}, is the phase which is

responsible for the permanent shape and acts as the physical crosslink, while the phase that allows for fixity exhibits a lower phase transition, T_{trans}, which can be either a melting or glass transition and allows for the fixation of the switching segments [Lendlein & Kelch, 2002]. Generally, the melting point is preferred since it is usually a much better defined and sharper transition [Ratna & Karger-Kocsis, 2008]. The material is processed to the desired shape above the switching temperature, T_{trans}, but below the T_{perm}. Upon deformation of the material in the rubbery state, the macromolecules rearrange along the deformation axis and reduce the entropy of the polymer network. It is possible to fix the temporary shape of the material by cooling it to a temperature that is below the switching temperature, T_{trans}. Cooling the material to a temperature below T_{trans} stores the energy so that the deformed network configuration is "frozen in". Generally, the polymer is capable of holding the deformed shape indefinitely. If the material is once again heated to a temperature above its reversible phase transition, the increase in molecular mobility from the entropy elasticity allows for the material to recover its permanent original shape [Rousseau, 2008, Lendlein & Kelch 2002].

The shape memory behavior of the first category of shape memory polymers, covalently crosslinked glassy thermoset networks, is based on the formation of a phase-segregated morphology. The shape memory effect of polymers with this morphology was discussed above. This is the simplest type of shape memory polymer [Liu et al., 2007]. The transition temperature, T_{trans}, is a melting temperature or a glass transition temperature. Shape memory polymers in this category generally show excellent shape fixity and recovery due to the high modulus, that can be adjusted through the extent of crosslinking and the absence of slippage

between chains, below the T_g and the excellent rubber elasticity, attributed to crosslinking, above the T_g [Rousseau, 2008; Liu et al., 2007].

Covalently crosslinked semicrystalline rubber comprises the second category of shape memory polymers. This category is similar to the first in that permanent shapes are established through crosslinking and cannot be reshaped after processing. However, the temporary shape is controlled through deformation above the T_m of the crystalline regions and subsequent cooling below their crystallization temperature [Rousseau et al., 2008]. The stiffness of these materials is sensitive to the degree of crystallinity and the degree of crosslinking, making it more compliant below the critical temperature. The temporary shapes of polymers in this class are fixed by crystallization as opposed to vitrification. Polymers in this class are expected to need lower temperatures relative to T_{trans} to experience a change in shape. The lower temperatures allow for full crystallization, which would create an expected increase in shape fixity [Rousseau, 2008]. In comparison to the first category, there is generally a wider range of attainable shape fixity and recovery. Included in this category are semi-crystalline rubbers, liquid crystalline elastomers (LECs), and hydrogels with phase separated microdomains [Liu et al., 2007].

The third category, physically crosslinked amorphous thermoplastics, consists of linear block copolymers and multiblock copolymers. The T_g of the soft segment regions are responsible for the shape memory behavior. After deformation at a temperature greater than the T_g of the polymer, the shape can be maintained by cooling the material below the glass transition temperature. Physical crosslinking of the hard segments through molecular interactions such as van der Waals, dipole-dipole interactions, or hydrogen bonding are responsible for the material's

permanent shape [Rousseau, 2008]. The majority of shape memory polymers in this category are amorphous segmented shape memory polyurethanes.

The final category of shape memory polymers, physically crosslinked semi-crystalline block copolymers, is similar to the third class. Some of the block copolymers in this category have soft segments that will crystallize and the melting temperature of the soft segments function as a shape memory transition as opposed to their T_g. The secondary shapes are therefore fixed by crystallization of the soft segments [Liu et al., 2007]. The most commonly reported shape memory polymers in this class are polyurethane based chemistries [Rousseau, 2008]. Segmented shape memory polyurethanes, which will be the focus of this research, fall into this category and represent the majority of this category of shape memory polymers.

Shape Memory Polyurethane

The biphasic morphology of polyurethane makes it an excellent candidate for a shape memory material [Lee et al., 2004; Chun et al., 2007]. Polyurethane is composed of soft and hard segments which phase separate due to the thermodynamic immiscibility that exists between the two [Chun et al., 2007; Lee et al., 2004; Takahashi et al., 1996]. It has been researched extensively since its discovery by Mitsubishi in 1988 [Liang et al., 1997; Richard & Gordon, 1993]. Much of this research has been devoted to the polyurethane morphology [Briber & Thomas, 1985; Christenson et al., 2003; Martin et al., 1996], crystal structure [Li et al., 2003], thermal behavior [Seymour & Cooper, 1973; Schneider et al., 1975], deformation behavior [Christenson et al., 2005; Desper et al., 1985], and rheological properties [Vlad & Oprea, 2001; de Vasconcelos et al., 2001; Yoon & Han, 2000].

7

Thermoplastic segmented polyurethane is synthesized through condensation polymerization of a diisocyanate and a long chain diol to form a prepolymer. The prepolymer is then further polymerized in the presence of a low molecular weight diol, the chain extender [Maiti et al., 2006; Mondal & Hu, 2007]. The soft segments, composed of long chain diols, are responsible for the reversible phase transformation that allows for the shape memory effect, whereas the hard segments, formed by the reaction of the diisocyanate and the chain extender, are responsible for memorizing the permanent shape [Auad et al., 2009; Hu et al., 2005]. Hard segments are capable of binding themselves via hydrogen bonding and crystallization, which makes the polymer solid below its melting transition temperature [Auad et al., 2009; Mondal & Hu, 2007]. Figure I-1 is a cartoon representation of the linear thermoplastic polyurethane soft and hard segment phase separated structure that is formed during the condensation reaction.
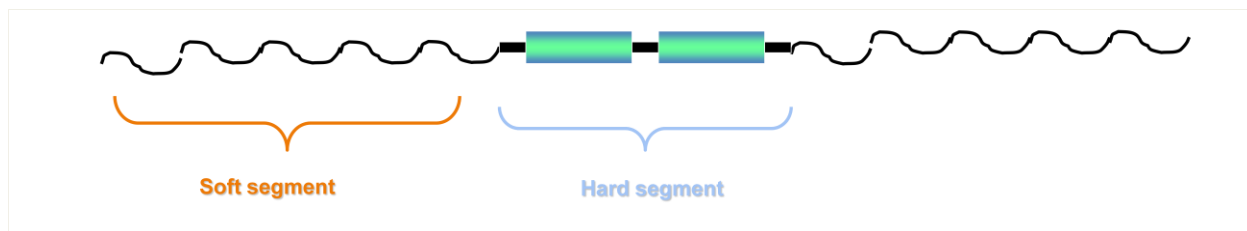
Figure I-1. Cartoon representing the soft and hard segment phase separated structure of a linear thermoplastic polyurethane.

The shape memory effect works by applying a specified initial deformation at an elevated temperature that is above the melting temperature of the soft segments of the polymer. These deformations can then be fixed by cooling the polymer to a temperature below the melting temperature of the soft segments of the polymer. The original shape can then be recovered by once again heating the polymer to a temperature above the melting temperature of the soft segments. The three cycles are known as deformation, fixing, and recovery [Hu et al., 2005;

Auad et al., 2009]. A graphical representation of the shape memory cycles is shown below in Figure I-2. Shape memory behavior can be evaluated in tension using a tensile tester equipped with a thermally controlled chamber or in compression using a dynamic mechanical analyzer (DMA). Depending on the instrument used, testing can be performed in strain or stress-controlled modes. Depending on the technique used to evaluate shape memory effect, slight variation may exist in the results. However, all testing is concerned with determining the shape fixity (R_f) and shape recovery (R_r). The shape fixity is defined as the ability of a shape memory polymer to fix the temporary shape upon completion of deformation after subsequent cooling and unloading [Chun et al., 2007; Tobushi et al., 2004; Li et al., 1997]. Shape recovery is the ability of the shape memory polymer to "remember" the original shape and recover it, after subsequent cooling and unloading, upon reheating to the rubbery state of the material [Rousseau, 2008]. The shape memory testing procedure and equations used in the calculation of shape memory behavior will be discussed in greater detail in Chapter II.
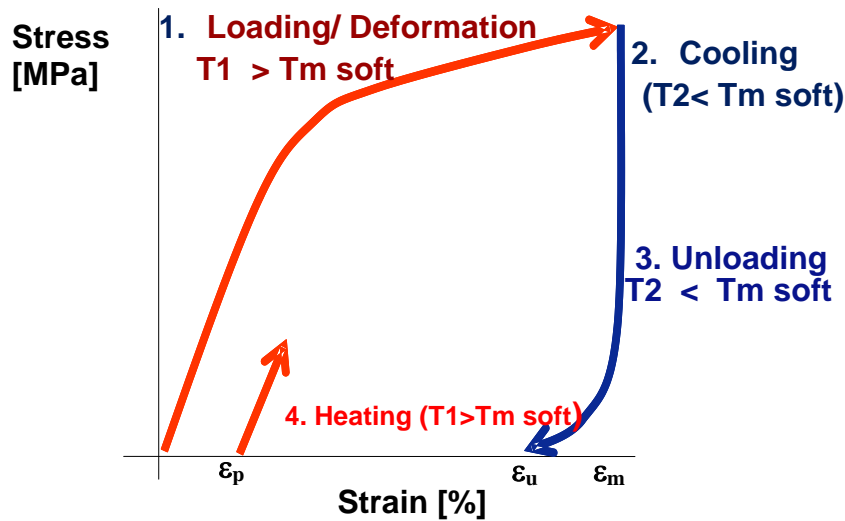
Figure I-2. Graphical representation of shape memory behavior testing cycles.

9

Polymers that exhibit a change in shape caused by a change in temperature posses what is referred to as thermally induced shape memory effect. The focus of this research will be on polymers exhibiting this type of shape memory effect. While some researchers have stated that shape memory effect is an intrinsic property of shape memory polyurethanes [Gall et al., 2004; Liu et al., 2007], this is not necessarily the case [Behl & Lendlein, 2007; Buckley et al., 2007; Li et al., 1998]. Rather, it results from a combination of the chemical structure and morphology together with the applied processing and programming technology [Lendlein & Kelch, 2002; Rousseau, 2008]. Therefore, shape memory effect can be engineered by controlling the molecular mass of the soft segment, the amount of hard segment content, the mole ratio of soft to hard segments, and the polymerization process.

Chemical Structure of Polyurethane

The use of shape memory polyurethanes presents several challenges. The first challenge of the research is control of the chemical structure of the polymer. A variety of different synthesis routes are available for the production of polyurethanes. A substantial change in polymer properties can be achieved by changing the segment lengths, the segment composition, or the percentage of hard/soft segments [Auad et al., 2009]. A great deal of research has been performed in this area. Lee et al. investigated the role of hard segment content on the structure and thermomechanical properties of the SMP [2004]. Others have investigated the effects of hard segment ordering, chain symmetry, block lengths, and segment shape on shape memory polyurethane properties [Kim et al., 1998; Mattoso et al., 2006; Prisacariu et al., 2003; Sheth et al., 2005; Yang et al., 2003; Lin et al., 1998]. However, little research has been performed on the impact that chemical structure has on shape memory behavior. This research will add to the

10

current body of knowledge on the direct effect of soft segment length and hard segment composition on shape memory behavior.

Shape Memory Polyurethane Nanocomposites

As previously discussed, shape memory polyurethanes present disadvantages such as weak recovery force and low stiffness in comparison to shape memory alloys. The second challenge of this research is overcoming these disadvantages. Current applications of SMPs are limited for this reason. An important goal of this research is to open the door to broader application areas by creating an increase in mechanical properties and recovery, while maintaining the shape memory behavior of the polymer material. It should be mentioned that the low recovery stress of shape memory polyurethane is mainly attributed to its low modulus. Other investigators have sought to overcome this challenge by increasing the stiffness or elastic modulus of the material [Rousseau, 2008]. Some studies have focused on creating improvements through the chemical structure of the material itself. For example, crosslink density has been increased and mesogenic units have been introduced to form liquid crystalline phases within the rubbery region of the polyurethane [Jeong et al., 2000, Rousseau, 2008]. Scientists have also investigated improving the recovery force and/or mechanical properties of shape memory polyurethanes by the addition microreinforcements to create composites. A composite is a material that is composed of two or more different materials in order to blend the best properties of each of the constituent materials. A wide variety of micro-reinforcements, such as silica, carbon or glass fibers, Kevlar®, cellulose whiskers or microfibrils, wood flour, clays, etc. have been utilized for composite construction [Gall et al., 2002; Gall et al., 2004; Seydibeyoglu & Oksman, 2008; Liang et al, 1997; Krishnamurthi et al., 2001]. Traditional composites utilizing microreinforcements require

11

addition of more than 40 wt% reinforcements to induce an increase in properties. Property enhancements include increases in thermal stability, stiffness, and strength of the employed polymer matrix. Additionally, in the case of shape memory polyurethanes, the use of microreinforcements has exhibited an increase in mechanical properties but at a detriment to the shape memory behavior [Liang et al., 1997; Ohki et al., 2004; Yang et al., 2005; Li et al., 2000]. However, utilization of reinforcements with such a large size does have its drawbacks. Reductions in strain to failure, impact strength, and fracture toughness are often observed [Friedrich et al., 2005]. The use of nanoreinforcements, a reinforcement in which one of the dimensions is in the nanometer range, is a new approach to enhance the properties of shape memory polymers. Nanocomposites differ from traditional composites, however, because they exhibit property enhancements with as little as 0.5 wt% reinforcement [Wouterson et al, 2007]. Due to their much higher surface area and the reduction in defects of the reinforcing phase at the nano level, nanoparticle incorporation offers a way to achieve the same property enhancements without many of the drawbacks witnessed from microreinforcements [Sternitzke et al., 1998]. Even nanocomposite materials with particle sizes exceeding 20 nanometers have exhibited the ability to increase properties over neat polymer matrices [Friedrich et al., 2005]. Additionally, previous studies have found that the higher surface area, or aspect ratio, of nanoreinforcements leads to a better polymer-nanoreinforcement interface than witnessed in microreinforcements. This improved interface is capable of producing polymer composites with increased properties, elastic modulus and strength in particular, at very small particle loadings (~1-2 wt%) [Bhattacharya & Tummala, 2002; Ash et al., 2001]. Previous studies performed by Gall et al. [2002] have shown that nanoreinforcements can increase stiffness and recoverable stresses of shape memory polyurethane materials. It is expected that shape memory polyurethanes with

12

enhanced recovery force, increased stiffness, and improved deformation capacity in comparison to the un-reinforced polymer matrix can be obtained through the addition of nanoreinforcements [Gall et al., 2002; Ryabov et al., 2001].

While use of nanoreinforcements has exhibited increased properties in polymer naocomposites, their use also presents a challenge. In order to obtain an increase in properties, it is imperative to achieve excellent dispersion and interfacial adhesion of the nanoreinforcements in the polymer matrix. This can be achieved through careful preparation of the nanoreinforcements. Two of the current methods to overcome problems in polymer nanocomposites include surface modification and chemical modification. Surface modification is often used with both natural and synthetic nanofillers. Physical methods of modification change the structural and surface properties of the fiber and therefore, create better interfacial adhesion with the polymer matrix. Physical treatments involve surface fibrillation and electric discharge. Additionally, chemical modifications are also used with nanofillers that are not inherently compatible with hydrophobic polymer matrices. In order to improve compatibility and dispersion, a hydrophobic coating needs to be developed on the fiber surface. When this type of chemical modification is performed on natural nanofillers, coupling agents such as silane, isocyanate, and titanate based compounds are often used [George et al., 2001]. In order to increase the interfacial adhesion of natural nanofibers into a polymer matrix many surface treatments such as bleaching, grafting of monomers, acetylation, acid hydrolysis, and delignification are utilized [Saheb et al., 1999]. Synthetic nanofillers employ the covalent attachment of functional groups to increase dispersion and adhesion [Chen et al., 2006, Auad et al., 2009; Hatchett & Josowicz, 2008]. This research

will employ modification of the selected nanoreinforcements to achieve optimal dispersion and adhesion within the shape memory polyurethane matrix.

Nanoreinforcements

The nanoreinforcements chosen for investigation during this research are cellulose nanofibers (CNF), conductive cellulose nanofibers (C-CNF), and carbon nanotubes (CNT). Cellulose, which constitutes the primary structural material in a wide variety of plant life, is one of nature's most abundant materials [Eichhorn & Young 2001]. It possesses attractive attributes of low cost, low density, high stiffness, and biodegradability [Zadorecki & Michell 1989; Boldizar et al., 1987]. Cellulose fibers are composed of assemblies of microfibrils, which form slender and nearly endless rods [Mark 1980; Marchessault & Sundarrjan 1983]. Upon exposure to strong acids, the microfibrils are degraded into microcrystals that are similar in structure to the parent microfibril but with shorter lengths ranging from a few hundred nanometers to a few microns. Additionally, cellulose possesses polar groups that can interact with segmented polyurethanes [Marcovich et al., 2006]. During polyurethane synthesis it is possible for the –OH group of cellulose to co-react with the polyurethane. This interaction leads to strong interfacial adhesion that is necessary for property enhancement in nanocomposites. Researchers have shown that use of cellulose microfibrils can induce property enhancements [Orts et al., 2005]

Cellulose nanofibers coated with polyaniline, in order to achieve conductive cellulose nanofibers (C-CNF), presents a new approach to creating conductive polymers through the use of nanoreinforcement. Polyaniline was chosen for this application due to its good environmental stability, low cost, and easy polymerization. Conducting polymers have gained attention due to

14

the possibility of commercial applications. However, conductive polymers present a challenge for applications due to their low mechanical properties [Malmonge et al., 2001]. In this research, a way to overcome this challenge will be investigated. By coating a nanoreinforcement, such as CNF, with polyaniline, and then creating a nanocomposite, it is expected that a non-conductive polymer will not only gain the conductive properties of the polyaniline but will also experience an increase in mechanical properties due to the nanoreinforcement material.

The use of synthetic carbon nanotubes as a nanoreinforcement presents another challenge. While carbon nanotubes possess a number of advantages, such as excellent mechanical properties, increased electrostatic discharge, chemical stability, low density, and conductivity, their poor surface reactivity and high aspect ratio create dispersion problems in nanocomposites [Chen et al., 2006; Auad et al., 2009]. Synthetic CNT are generally incompatible with organic molecules, including polymers. Entanglements are usually encountered due to the extremely high aspect ratio and can cause difficulty when preparing CNT nanocomposites [Ajayan et al., 2000; Zhou et al., 2003; Cadek et al., 2004; Andrews et al., 2002; Sun et al., 2002]. For this reason, several researchers have focused on surface functionalization of CNT to aid in nanofiller dispersion [Auad et al., 2009; Cui et al., 2003; Gong et al., 2000]. During these studies, various functionalization methods have been described including covalent bonding methods in which carboxyl groups on the CNT surface are converted to organic groups in order to improve the surface group reaction efficiency between the CNT and the SMPu [Auad et al., 2009]. This research will employ a surface functionalization method in order to overcome the challenges associated with dispersion and agglomeration.

Research Objectives

There are four main objectives associated with this research:

i)   The first objective is to obtain a basic understanding and comprehension of the morphology and thermal and mechanical properties of segmented shape memory polyurethanes with a variety of chemical structures, segment lengths, and hard/soft segments percentages.

ii) After gaining control of the structure of the segmented shape memory polyurethane, the second objective is to overcome dispersion problems associated with nanoreinforcement materials through modification of the reinforcement surface or structure.

iii) The third objective is to offer new information on the property effects of nanoreinforcement on segmented shape memory polyurethanes with different chemical compositions by reinforcement of the polyurethane matrix.

iv) Finally, the last objective is to increase the recovery force of the nanoreinforced segmented shape memory polyurethane while maintaining the shape memory effect. The tasks to fulfill these objectives are discussed in the following chapters of this text.

REFERENCES

1. Ahir, S. V.; Terentjev, E. M. Photomechanical Actuation in Polymer-nanotube Composites. *Nat. Mater.*, **2005**, *4*, pp 491-495.

2. Ajayan, P. M.; Schadler, L. S.; Giannaris, C.; Rubio, A. Single-walled carbon nanotube-polymer composites: strength and weakness. *Advanced Materials*, **2000**, *12*, pp 750-753.

3. Andrews, R.; Jacques, D.; Oian, D.; Rantell, T. Multiwall Carbon Nanotubes: Synthesis and Application. *Acc. Chem. Res.*, **2002**, *35* (12), pp 1008-1017.

4. Ash, B. J.; Stone, J.; Rogers, D. F.; Schadler, L. S.; Siegel, R. W.; Benicewicz, B. C.; Apple, T. Investigation into the Thermal and Mechanical Behavior of PMMA/Alumina Nanocomposites. *Mat. Res. Soc. Symp. Ser.*, **2001**, pp 661-666.

5. Auad, M. L.; Mosiewicki, M. A.; Richardson, T.; Aranguren, M. I.; Marcovich, N. E. Tailored Shape Memory Polyurethane Reinforced with Microcrystalline Cellulose Nanofibers. Accepted for publication in *Journal of Applied Polymer Science*, **2009**.

6. Auad, M. L.; Mosiewicki, M. A.; Uzunpinar, C.; Williams, R. J. J. Single-wall Carbon Nanotubes/Epoxy Elastomers Exhibiting High Damping Capacity in an Extended Temperature Range. *Composites in Science and Technology*, **2009**, *69* (7-8), pp 1088-1092.

7. Behl, M.; Lendlein, A. Shape Memory Polymers. *Materials Today*, **2007**, *10* (4), pp 20-28.

8. Benett, W. J.; Krulevitch, P. A.; Lee, A. P.; Northrup, M. A.; Folta, J. A. Miniature plastic gripper and fabrication method. United States Patent, 5, 609, 608 (1997).

9. Bhattacharya, S. K.; Tummala, R. R. Epoxy Nanocomposite Capacitors for Application as MCM-L Compatible Integral Passives. *Journal of Electronic Packaging*, **2002**, *124* (1), pp 1-6.

10. Boldizar, A.; Klason, C.; Kubat, J.; Naslund, P.; Saha, P. Prehydrolyzed Cellulose as Reinforcing Filler for Thermoplastics. *Intern. J. Polymeric Mater.*, **1987**, *11*, pp 229–262.

11. Briber, R. M.; Thomas, E. L. The Structure of MDI/BDO- Based Polyurethanes: Diffraction Studies on Model Compounds and Oriented Thin Films". *Journal of Polymer Science: Polymer Physics Ed.*, **1985**, *23*, pp 1915-1932.

12. Buckley, C. P.; Prisacariu, C.; Caraculacu, A. Novel Triol-crosslinked Polyurethanes and Their Thermorheological Characterization as Shape-Memory Materials. *Polymer*, **2007**, *48*, pp 1388-1396.

13. Cadek, M.; Coleman, J. N.; Ryan, K. P.; Nicolosi, V.; Bister, G.; Fonseca, A.; Nagy, J. B.; Szostak, K.; Beguin, F.; Blau, W. J. Reinforcement of Polymers with Carbon Nanotubes: the Role of Nanotube Surface Area. *Nano Letters,* **2004**, *4* (2), pp 353-356.

14. Cao, F.; Jana, S. C. Nanoclay-tethered Shape Memory Polyurethane Nancomposites. *Polymer*, **2007**, *48* (13), pp 3790-3800.

15. Chang, L. C.; Read, T. A. Tran AIME, **1951**, *189*, pp 47.

16. Chen, W.; Auad, M. L.; Williams, R. J. J.; Nutt, S. R. Improving the Dispersion and Flexural Strength of Multiwalled Carbon Nanotubes-stiff Epoxy Composites Through β-hydroxyester Surface Functionalization Coupled with the Anionic Homopolymerization of the Epoxy Matrix. *European Polymer Journal*, **2006**, *42*, pp 2765-2772.

17. Christenson, E. M.; Anderson, J. M.; Hiltner, A.; Baer, E. Relationship between Nanoscale Deformation Processes and Elastic Behavior of Polyurethane Elastomers. *Polymer*, **2005**, *46*, pp 11744-11754.

18. Christenson, C. P.; Harthcock, M. A.; Meadows, M. D.; Spell, H. L.; Howard, W. L.; Creswick, M. W.; Guerra, R. E.; Turner, R. B. Model MDI/Butanediol Polyurethanes: Molecular Structure, Morphology, Physical and Mechanical Properties. *Journal of Polymer Science Part B: Polymer Physics*, **2003**, *204*, pp 1401-1439.

19. Chun, B. C.; Cho, T. K.; Chung, Y-C. Blocking of Soft Segments with Different Chain Lengths and its Impact on the Shape Memory Property of Polyurethane Copolymer. *Journal of Applied Polymer Science,* **2007**, *130*, pp 1435-1441.

20. Cui, S.; Canet, R.; Derre, A.; Couzi, M.; Delhaes, P. Characterization of Multiwall Carbon Nanotubes and Influence of Surfactant in the Nanocomposite Processing. *Carbon*, **2003**, *41* (4), pp 797-809.

21. Desper, C. R.; Schneider, N. S.; Jasinski, J. P. Deformation of Microphase Structures in Segmented Polyurethanes. *Macromolecules*, **1985**, *18*, pp 2755-2761.

22. Ding, X. M.; Hu, J. L.; Tao, X. M. Effect of Crystal Melting on Water Vapor Permeability of Shape-Memory Polyurethane Film. *Text Res J*, **2004**, *74*, pp 39-43.

23. Eichhorn, S. J.; Young, R. J. The Young's Modulus of a Microcrystalline Cellulose. *Cellulose*, **2001**, *8*, pp 197-207.

24. Friedrich, K.; Fakirov, S.; Zhang, Z., Eds. *Polymer Composites: from nano-to macro-scale*. Springer: New York, 2005.

25. Gall, K.; Dunn, M. L.; Liu, Y.; Finch, D.; Lake, M.; Munshi, N. A. Shape Memory Polymer Nanocomposites. *Acta Materialia*, **2002**, *50*, pp 5115-5126.

26. Gall, K.; M. Dunn, M.; Liu, Y. Internal Stress Storage in Shape Memory Polymer Nanocomposites. *Appl. Phy. Lett*., **2004**, *85*, pp 290.

27. Gall, K.; Kreiner, P.; Turner, D.; Hulse, M. Shape-memory Polymers for Microelectromechanical Systems. *J. Microelectromech. Syst.*, **2004**, *13*, pp 472-483.

28. George, J.; Sreekala, M. S.; Thomas, S. A Review on Interface Modification and Characterization of Natural Fiber Reinforced Plastic Composites. *Polymer Engineering and Science*, **2001**, *41* (9), pp 1471-1485.

29. Gong, X.; Liu, J.; Baskaran, S.; Voise, R. D.; Young, J. S. Surfactant Assisted Processing of Carbon Nanotube/polymer Composites. *Chemistry of Materials*, **2000**, *12* (4), pp 1049-1052.

30. Hatchett, D. W.; Josowicz, M. Composites of Intrinsically Conducting Polymers as Sensing Materials. *Chem. Rev.,* **2008**, *108*, pp 746-769.

31. Hayashi, S.; Fujimura, H.; Tamura, Y. Development of Polymeric Shape Memory Material. *Proc. 2nd Jpn Int. SAMPE*, **1991**, pp 76.

32. Hornbogen, E. Comparison of Shape Memory Metals and Polymers. *Advance Engineering Materials*, **2006**, *8*, pp 101-106.

33. Hu, J. L.; Ji, F. L.; Wong, Y. W. Dependency of the Shape Memory Properties of a Polyurethane upon Thermomechanical Cyclic Conditions". *Polymer International*, **2005**, *54*, pp 600-605.

34. Jeong, H. M.; Kim, B. K.; Choi, Y. J. Synthesis and Properties of a Thermotropic Liquid Crystalline Polyurethane Elastomer. *Polymer*, **2000**, *41*, pp 1849-1855.

35. Jimenez, G. A.; Jana, S. C. Proc SPE ANTEC, **2007**, pp 18-22.

36. Ji, F. L.; Hu, J. L.; Li, T. C.; Wong, Y. W. Morphology and Shape Memory Effect of Segmented Polyurethanes. Part I. With Crystalline Reversible Phase. *Polymer*, **2007**, *48,* pp 5133-5145.

37. Kamieneski, E. L.; Mandelbaum, S.; Vemuri, P.; Weiss, R. A. Proc SPE ANTEC, **2007**, pp 2714-2717.

38. Kim, B. K.; Lee, S. Y.; Xu, M. Polyurethanes Having Shape Memory Effects. *Polymer*, **1996**, *37*, pp 5781-5793.

39. Kim, H. D.; Huh, J. H.; Kim, E. Y.; Park, C. C. Comparison of Properties of Thermoplastic Polyurethane Elastomers with Two Different Soft Segments. *Journal of Applied Polymer Science*, **1998**, *69* (7), pp 1349-1355.

40. Koerner, H.; Price, G.; Pearce, N. A.; Alexander, M.; Vaia, R. A. Remotely Actuated Polymer Nanocomposites – Stress-recovery of Carbon-Nanotube-Filled Thermoplastic Elastomers. *Nature Materials*, **2004**, *3*, pp 115-120.

41. Krishnamurthi, B.; Bharadwaj-Somaskandan, S.; Shutov, F. Nano- and Micro-fillers for Polyurethane Foams: Effect on Density and Mechanical Properties. API Polyurethanes Expo Conference Proceedings, Columbus, OH. September 30- October 3, 2001.

42. Lee, A. P.; Northrup, M. A.; Ahre, P. E.; Dupuy, P. C. Polymer Microfold and Fabrication Process". United States Patent, 5,658, 515 (1997).

43. Lee, A. P.; Fitch, J. P. Micro Devices Using Shape Memory Polymer Patches for Mated Connections". United States Patent 6,086,599 (2000).

44. Lee, S. H.; Kim, J. W.; Kim, B. K. Shape Memory Polyurethanes having Crosslinks in Soft and Hard Segments. *Smart Mater. Struct., ***2004, ***13*, pp 1345-1350.

45. Lendlein, A.; Kelch, S. Shape-memory Polymers. *Chem. Int. Ed*., **2002**, *41*, pp 2034-2057.

46. Lendlein, A.; Jiang, H.; Junger, O.; Langer, R. Light-induced Shape-memory Polymers. *Nature*, **2005**, *434*, pp 879-882.

47. Liang, C.; Rogers, C. A.; Malafeew, E. Investigation of Shape Memory Polymers and Their Hybrid Composites. *J. Intell. Mater. Syst. Struct*., **1997**, *8,* pp 380-386.

48. Liang, C.; Rogers, C. A.; Malafeew, E. Preliminary Investigation of Shape Memory Polymers and Their Hybrid Composites. *Smart Struct. Mater.*, **1991**, *AD-24/AMD-123*, pp 97-105.

49. Lin, J. R.; Chen, L. W. Study on Shape-memory Behavior of Polyether-based Polyurethanes. I. Influence of the Hard-segment Content. *Journal of Applied Polymer Science*, **1998**, *69*, pp 1563-1574.

50. Liu,C.; Chun, S. B.; Mather, P. T.; Zheng, L.; Haley, E. H.; Coughlin, E. B. Chemically Cross-linked Polycyclooctene: Synthesis, Characterization, and Shape Memory Behavior. *Macromolecules*, **2002**, *35* (27), pp 9868-9874.

51. Liu, C.; Rousseau, I. A.; Qin, H.; Mather, P. T. Tailored Shape Memory Polymers: Not all SMPs are Created Equal. *Proc. First World Cong. Biomim. Artificial Muscles*, **2003**.

52. Liu, C.; Mather, P. T. A Shape Memory Polymer with Improved Shape Recovery. *Mater. Res. Soc. Symp. Proc.*, *Symposium W: Mechanically Active Materials*, Boston, MA, **2004**, 855E, W4.7.1.

53. Liu, C.; Qin, H.; Mather, P. T. Review of Progress in Shape-memory Polymers. *J. Mater. Chem.*, **2007**, *17*, pp 1543-1558.

54. Liu, Y.; Gall, K.; Dunn, M. L.; Greenberg, A. R.; Diani, J. Thermomechanics of Shape Memory Polymers: Uniaxial Experiments and Constitutive Modeling. *Int. J. Plast.*, **2006**, *22*, pp 279-313.

55. Li, F.; Zhang, X.; Hou, J.; Xu, M.; Luo, X.; Ma, D.; Kim, B. K. Studies on Thermally Stimulated Shape Memory Effect of Segmented Polyurethanes. *Journal of Applied Polymer Science*, **1997**, *64*, pp 1511–1516.

56. Li, F.; Qi, L.; Yang, J.; Xu, M.; Luo, X.; Ma, D. Polyurethane/conducting Carbon Black Composites: Structure, Electric Conductivity, Strain Recovery Behavior, and Their Relationships. *Journal of Applied Polymer Science*, **2000**, *75*, pp 68-77.

57. Li, F.; Chen, Y.; Zhang, X.; Xu, M. Shape Memory Effect of Polyethylene/Nylon 6 Graft Copolymers. *Polymer*, **1998**, *39*, pp 6929-6934.

58. Li, Y.; Liu, J.; Yang, H.; Ma, D.; Chu, B. Multiphase Structure of Segmented Polyurethanes: Its Relation with Spherulite Structure. *Journal of Polymer Science Part B: Polymer Physics*, **2003**, *31*, pp 853-867.

59. Machi, S. New Trends of Radiation Processing Application. *Radiat. Phys. Chem.*, **1996**, *47*, pp 333-336.

60. Maiti, P.; Radhakrishnan, G.; Aruna, P.; Ghosh, G. Novel Polyurethane Gels: The Effect of Structure on Gelation. *Macromol. Symp.*, **2006**, *241*, pp 51-59.

61. Maitland, D. J.; Metzger, M. F.; Schumann, D.; Lee, A.; Wilson, T.S. Photothermal Properties of Shape Memory Polymer Micro-actuators for Treating Stroke. *Laser Surg. Med.*, **2002**, *30*, pp 1-11.

62. Malmonge, J. A.; Compoli, C. S.; Malmonge, L. F.; Kanda, D. H. F.; Mattoso, L. H. C.; Chierice, G. O. Effect of the Doping Medium on Blends of Polyurethane and Polyaniline. *Synthetic Metals*, **2001**, *119*, pp 87-88.

63. Marchessault, R. H.; Sundarrjan, P. R. In *Cellulose. The Polysaccharides*. Academic Press: New York, 1983; pp 11-95.

64. Marcovich, N. E.; Auad, M. L.; Bellesi, N. E.; Nutt, S. R.; Aranguren, M. I. Cellulose Micro/Nanocrystals Reinforced Polyurethane. *Journal of Materials Research,* **2006**, *21* (4), pp 870-881.

65. Mark, H. Fifty Years of Cellulose Research. *Cellulose Chem Technol*, **1980**, *14*, pp 569–81.

66. Martin, D. J.; Meijs, G. F.; Renwick, G. M.; Gunatillake, P. A.; McCarthy, S. J. Effect of Soft-segment CH$_2$/O Ratio on Morphology and Properties of a Series of Polyurethane Elastomers. *Journal of Applied Polymer Science*, **1996**, *60*, pp 557-571.

67. Mattoso, L. H. C.; Baker, D. A.; Avloni, J.; Wood, D. F.; Orts, W.J. 41st International Symposium on Macromolecules Proceedings (2006).

68. Merline, D.; Reghunadhan Nair, C. P.; Gouri, C.; Bandyopadhyay, G. G.; Ninan, K.N. Polyether Polyurethanes: Synthesis, Characterization, and Thermoresponsive Shape Memory Properties. *Journal of Applied Polymer Science*, **2007**, *107*, pp 4082-4092.

69. Mohr, R.; Kratz, K.; Weigel, T.; Lucka-Gabor, M.; Moneke, M.; Lendlein, A. Initiation of Shape-memory Effect by Inductive Heating of Magnetic Nanoparticles in Thermoplastic Polymers. *Proc. Natl Acad Sci USA*, **2006**, *103* (10), pp 3540-3545.

70. Mondal, S.; Hu, J.L. Shape Memory Study of Thermoplastic Segmented Polyurethane: Influence of Hard Segment. *Polymer-Plastics Technology and Engineering,* **2007**, *46*, pp 939-942.

71. Monkman, G. J. Advances in Shape Memory Polymer Actuation. *Mechatronics*, **2000**, *10*, pp 489-498.

72. Ohki, T.; Ni, Q-Q.; Ohsako, N.; Iwamoto, M. Mechanical and Shape Memory Behavior of Composites with Shape Memory Polymer. *Composites Part A: Applied Science and Manufacturing*, **2004**, *35(9)*, pp 1065-1073.

73. Ota, S. *Radiat. Phys. Chem.*, **1981**, *18(1-2)*, pp 81-87.

74. Orts, W.; Shey, J.; Imam, S. H.; Glenn, G. M.; Guttman, M.E.; Revol, J-F. Application of Cellulose Microfibrils in Polymer Nanocomposites. *Journal of Polymers and the Environment*, **2005**, *13*(4), pp 301-306.

75. Prisacariu, C.; Olley, R. H.; Caraculacu, A. A.; Basset, D.C.; Martin, C. The Effect of Hard Segment Ordering in Copolyurethane Elastomers Obtained by Using Simultaneously Two Types of Diisocyanates. *Polymer*, **2003**, *44*, pp 5407-5421.

76. Rabani, G.; Luftmann, H.; Kraft, A. Synthesis and Characterization of Two Shape-memory Polymers Containing Short Aramid Hard Segments and Poly (ε-caprolactone) Soft Segments. *Polymer*, **2006**, *47*, pp 4251-4260.

77. Ratna, D.; Karger-Kocsis, J. Recent Advances in Shape Memory Polymers and Composites: A Review. *J Mater Sci.,* **2008**, *43*, pp 254-269.

78. Razzaq, M. Y.; Frormann, L. Thermomechanical Studies of Aluminum Nitride Filled Shape Memory Polymer Composites. *Polym. Compos.*, **2007**, *28*, pp 287-293.

79. Richard, F.; Gordon, P. E. *Mater. Technol.*, **1993**, *8*, pp 254.

80. Rousseau, I. A. Challenges of Shape Memory Polymers: A Review of the Progress Toward Overcoming SMP's Limitations. *Polymer Engineering and Science*, **2008**, *48* (11), pp 2075-2089.

81. Ryabov, S. V.; Kercha, Y. Y.; Kitel'nikova, N. E.; Gaiduk, R. L.; Shtompel, V. I.; Kosenko, L. A.; Yakovenko, A. G.; Kobrina, L. V. *Polymer Science*, **2001**, *43*(12), pp 1256-1260.

82. Saheb, D. N.; Jog, J. P. Natural Fiber Polymer Composites: A Review. *Advances in Polymer Technology*, **1999**, *18*, pp 351-363.

83. Schneider, N. S.; Paik Sung, C. S.; Matton, R. W.; Illinger, J. L. Thermal Transition Behavior of Polyurethanes Based on Toluene Diisocyanate. *Macromolecules*, **1975**, *8*, pp 62-67.

84. Seydibeyoglu, M. O.; Oksman, K. Novel Nanocomposites Based on Polyurethane and Micro Fibrillated Cellulose. *Composites Science and Technology,* **2008**, *68*, pp 908-914.

85. Seymour, R. W.; Cooper, S. L. Thermal Analysis of Polyurethane Block Polymers. *Macromolecules*, **1973**, *6*, pp 48-53.

86. Sheth, J.P.; Klinedinst, D. B.; Wilkes, G. L.; Yilgor, I.; Yilgor, E. Role of Chain Symmetry and Hydrogen Bonding in Segmented Copolymers with Monodisperse Hard Segments. *Polymer*, **2005**, *46 (18)*, pp 7317-7322.

87. Smith, R. C. *Smart material systems. Model development*. Society for Industrial and Applied Mathematics: Philadelphia, 2005.

88. Sternitzke, M.; Derby, B.; Brook, R. J. Alumina/silicon Carbide Nano-composites by Hybrid Polymer/powder Processing: Microstructures and Mechanical Properties". *J Am Ceram Soc*, **1998**, *81* (1), pp 41-48.

89. Sun, Y.; Fu, K.; Lin, Y.; Huang, W. Functionalized Nanotubes: Properties and Applications. *Accounts of Chemical Research*, **2002**, *35* (12), pp 1096-1104.

90. Takahashi, T.; Hayashi, N.; Hayashi, S. Structure and Properties of Shape-memory Polyurethane Block Copolymers". *Journal of Applied Polymer Science*, **1996**, *60*, pp 1061-1069.

91. Tobushi, H.; Matsui, R.; Hayashi, S.; Shimada, D. The Influence of Shape-holding Conditions on Shape Recovery of Polyurethane-Shape Memory Polymer Foams. *Smart Mater. Struct.*, **2004**, *13*, pp 881-887.

92. Uo, M.; Watari, F.; Yokoyama, A.; Matsumoto, H. *Biomaterials,* **2001**, *22*, pp 677.

93. de Vasconcelos, C. L.; R. R. Martins, R. R.; Ferreira, M. O.; Pereira, M. R.; Fonseca, J. L. C. Rheology of Polyurethane Solutions with Different Solvents. *Polymer International*, **2001**, *51*, pp 69-74.

94. Vlad, S.; Oprea, S. Evaluation of Rheological Behavior of Some Thermoplastic Polyurethane Solutions. *European Polymer Journal*, **2001**, 37, pp 2461-2464.

95. Wei, Z. G.; Sandstrom, R. Shape Memory Materials and Hybrid Composites for Smart Systems. Part I Shape-memory Materials. *Journal of Materials Science*, **1998**, *33*, pp 3743-3762.

96. Wei, Z. G.; Sandstrom, R.; Miyazaki, S. Shape Memory Materials and Hybrid Composites for Smart Systems: Part II Shape –memory Hybrid Composites. *J. Mater. Sci.*, **1998**, *33*, pp 3763-3783.

97. Winzek, B.; Schmitz, S.; Rumpf, H.; Sterzl, T.; Hassdorf, R.; Thienbaus, S.; Feydt, J.; Moske, M.; Quandt, E. Recent Developments in Shape Memory Thin Film Technology. *Materials Science and Engineering A*, **2004**, *378*, pp 40-46.

98. Wouterson, E. M.; Boey, F. Y. C.; Wong, S. –C.; Chen, L.; Hu, X. Nano-toughening Versus Micro-toughening of Polymer Syntactic Foams. *Composites Science and Technology,* **2007***, 67*, pp 2924–2933.

99. Xu, J.; Shi, W.; Pang, W. Synthesis and Shape Memory Effects of Si-O-Si Cross-linked Hybrid Polyurethanes. *Polymer*, **2006**, *47*, pp 457-465.

100. Yang, B.; Huang, W. M.; Li, C.; Chor, J. H. Effects of Moisture on the Glass Transition Temperature of Polyurethane Shape Memory Polymer Filled with Nano-carbon Powder. *European Polymer Journal*, **2005**, *41*, pp 1123-1128.

101. Yang, J. H.; Chun, B. C.; Chung, Y-C.; Cho, J. H. Comparison of Thermal/Mechanical Properties and Shape Memory Effect of Polyurethane Block-Copolymers with Planar or Bent Shape of Hard Segment. *Polymer*, **2003**, *44(11),* pp 3251-3258.

102. Yoon, P. J.; Han, C. D. Effect of Thermal History on the Rheological Behavior of Thermoplastic Polyurethane. *Macromolecules*, **2000**, *33*, pp 2171-2183.

103. Zadorecki, P.; Michell, A. J. Future Prospects for Wood Cellulose as Reinforcement in Organic Polymer Composites. *Polymer Composites*, **1989**, *10*, pp 69–77.

104. Zhou, J.; Kim, J. D.; Peng, H. Q.; Margrave, J. L.; Khabashesku, V. N.; Barrera, E. V. *Nano Letters*, **2003**, *3* (8), pp 1107-1113.

CHAPTER II.

SEGMENTED SHAPE MEMORY POLYURETHANES

INTRODUCTION

Shape memory polymers (SMPs) belong to a class of "smart" polymers that possess the ability to "memorize" a permanent shape, be deformed and fixed to a temporary shape under specific conditions, and then later recover to the original, stress-free condition by influence of an external stimulus [Liu et al., 2007]. Shape memory materials have drawn considerable interest in recent years because of their capacity to remember their initial shape at different conditions, their superior properties, and potential applications in a wide variety of fields such as medical, industrial, electronic, and textiles [Ratna & Karger-Kocsis, 2008; Liu et al., 2007; Chen et al., 2007; Cho et al., 2004].

Segmented shape memory polyurethane is a material that exhibits shape memory behavior through the interactions of its chemical structure, which is made up of hard and soft segments [Lee et al., 2004; Auad et al., 2009]. It differs from conventional polyurethane through its segmented structure and wide range of glass transition temperature or soft segment crystal melting temperature [Mondal & Hu, 2007]. Segmented shape memory polyurethanes possess structure-property relationships which are easily controlled and very diverse. Due to this control, it is possible to set the shape recovery in a wide range of temperatures (i.e., between -30 to 70°C) by changing the chemical structure of the network [Lee et al., 2004; Auad et al., 2009].

Properties can vary from rubbery to glassy and from a linear thermoplastic polymer to an elastomeric thermosetting plastic [Chen et al., 2007]. These unique properties are predominantly influenced by the phase separation process that occurs due to the thermodynamic immiscibility of the soft and hard segments [Li et al., 1996; Chen et al., 2007, Auad et al., 2009]. It is possible, however, to control the degree of phase separation through control of block length, copolymer composition, crystallization of hard and soft segments, synthesis conditions, and thermal history [Chen et al., 2007]. The ability to control these aspects of the polymer structure and synthesis is responsible for the wide variety of properties and applications that are achievable for these materials [Lee et al., 2004].

In this chapter, two series of thermoplastic shape memory polyurethanes were synthesized and characterized. One system utilized tolylene 2, 4 diisocyanate (TDI) for the hard segments and polyether glycol (PTMG) (TERATHANE®) with molecular weights of 2000 and 2900 g/mol (PTMG 2000 and PTMG 2900) as the soft segments while other system was composed of methylenedi-p-phenyl diisocyanate (MDI) and the soft segments were PTMG 2000 or PTMG 2900. This portion of the research focuses on the effect of hard segment content, composition of the network, and chemical structure of the reactants on the thermal, mechanical, and shape memory properties of the tailored shape memory polyurethanes. Molecular weight, morphology, thermal and mechanical properties, shape memory behavior, and rheological behavior of the samples were evaluated. The main goal of this chapter is to evaluate the effect of the molecular structure, phase separation process, and processing time on the final properties of shape memory polyurethanes.

Many studies have been performed on shape memory polyurethanes composed of MDI hard segments and polycaprolactone (PCL) soft segments [Chen et al., 2007; Jeong et al., 2000; Ji et al., 2007; Kim et al., 1996; Kim et al., 1998; Li et al., 1996; Mondal & Hu, 2007]. Additionally, many reports in literature have also focused on shape memory polyurethanes with hard segments composed of MDI and soft segments composed of poly(tetramethylene oxide) (PTMO) [Lin & Chen, 1998; Aneja & Wilkes, 2003; Auad et al., 2009]. However, very few reports in literature have evaluated the use of TDI for the hard segment composition of shape memory polyurethanes. This portion of the research is important due to the selection of raw materials for the hard and soft segments. Since there has been little research performed on shape memory polyurethanes with the chosen compositions, it is expected that this research will add to the body of knowledge on the effect of the shape memory polyurethane structure on the overall performance of the polymer itself. Additionally, this research will be a systematic study of the chemical and physical properties of shape memory polyurethanes in relation to their shape memory behavior, which is an area that has not been widely explored.

MATERIALS

Thermoplastic shape memory polyurethanes were prepared from polyether glycol (PTMG) (TERATHANE®) with molecular weights of 2000 and 2900 g/mol PTMG 2000 and PTMG 2900), and two diisocyanates with different structures, tolylene 2, 4 diisocyanate (TDI), and methylenedi-p-phenyl diisocyanate (MDI). 1-4 butanediol (BD) was used as a chain extender. The solvent utilized was N,N-dimethylformamide (DMF). The BD and DMF were stored under 4 Å molecular sieves for a period of at least 4 days prior to use. All utilized reactives were purchased from Sigma-Aldrich.

A high-performance polyester thermoplastic polyurethane was kindly donated by Huntsman (Irogran PS455-203, Huntsman, USA) for comparison purposes. The chemical structure of this polyurethane is substantially different than synthesized polyurethanes, however, the mechanical and thermal properties and the shape memory behavior are comparable.

METHODS

Two series of thermoplastic shape memory polyurethane copolymers were synthesized by a two step solution polymerization. Pre-polymerization method or two-step process was selected for the shape memory polyurethane preparation because a more uniform and controlled distribution of domain sizes and properties can be obtained than with the one-step method [Ahn et al., 2007; Cho et al., 2004]. Figure II-1 shows a graphical representation of the soft and hard segments that are formed during the two steps of the reaction. First, PTMG (PTMG 2000 or PTMG 2900) was dissolved in DMF. This solution was added drop-wise to a 500mL round bottom flask containing a magnetic stir bar and a solution containing diisocyanate (MDI or TDI) and DMF. The mixture was allowed to react for 45 minutes at 80°C under strong stirring and nitrogen. During this step of the reaction, the soft segments of the polyurethane were formed. Fourier transform infrared (FTIR) spectroscopy was utilized to insure the reaction between the diisocyante (TDI or MDI) and the PTMG (PTMG 2000 or 2900) was complete.
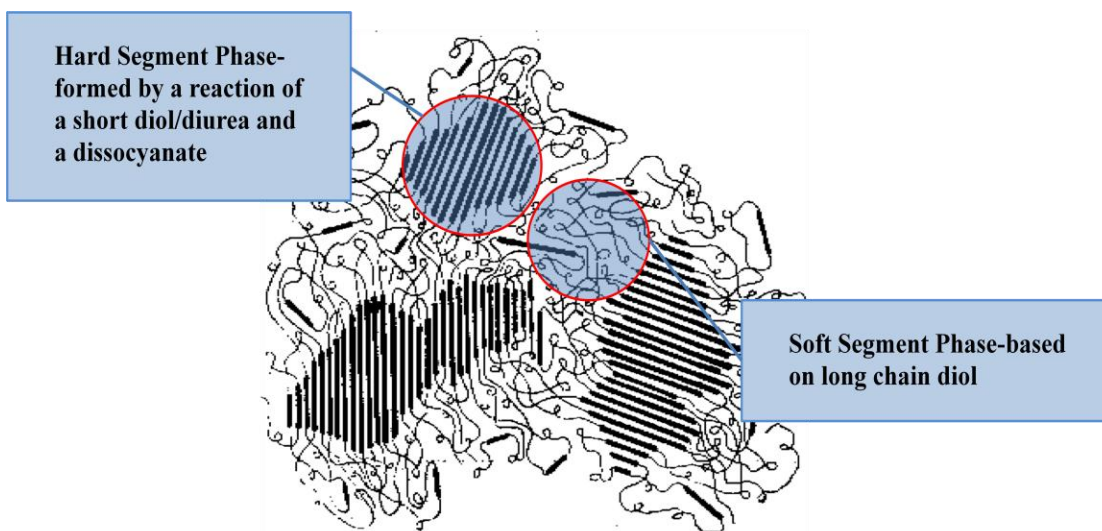
Figure II-1. Representation of polyurethane hard and soft segments.

In the second step, the soft segments were chain extended by addition of BD in order to form the phase segregated hard segment domains. BD is added to the reaction mixture according to the desired diisocyanate to BD ratio (see Table II-1). This step of the reaction was allowed to take place for 5 minutes until a considerable increase in the solution viscosity occurred. The solution was cast into open Teflon® molds and placed in an oven at 80°C for 24 hours to allow for solvent evaporation. In order to obtain linear polyurethanes, the isocyanate (NCO) to hydroxyl (OH) ratio was 1.0 for all synthesized samples. The formula used to calculate the molar ratio of the reactants was:

$$M_{isocyanate}*X + M_{BD}*(X-1) = \%HS*(M_{isocyanate}*X + M_{BD}*X - M_{BD} + M_{PTMG}) \qquad (1)$$

where $M_{isocyanate}$ is the molecular mass of the isocyanate, X is the molar amount of isocayante to be used, M_{BD} is the molecular mass of 1-4 butanediol, and M_{PTMG} is the molecular mass of the PTMG. Information regarding the molar fractions, the sample name designations, and the hard

segment weight percentages are shown in Table II-1. By controlling the molar ratio of the

reactants, it is possible to control the weight percentages of hard and soft segments. The reaction

scheme is shown in Figure II-2.

Sample designation	TDI moles	MDI moles	BD moles	PTMG (2000) moles	PTMG (2900) moles	wt% of hard segments
MDI 2000/45		5	4	1		45
MDI 2000/39		4	3	1		39
MDI 2000/32		3	2	1		32
MDI 2000/23		2	1	1	1	32
MDI 2900/32		4.3	3.3		1	23
TDI 2000/32	3.9		2.9	1		32
TDI 2900/32	5.5		4.5		1	32

Table II-1. Formulations of prepared shape memory polyurethanes.
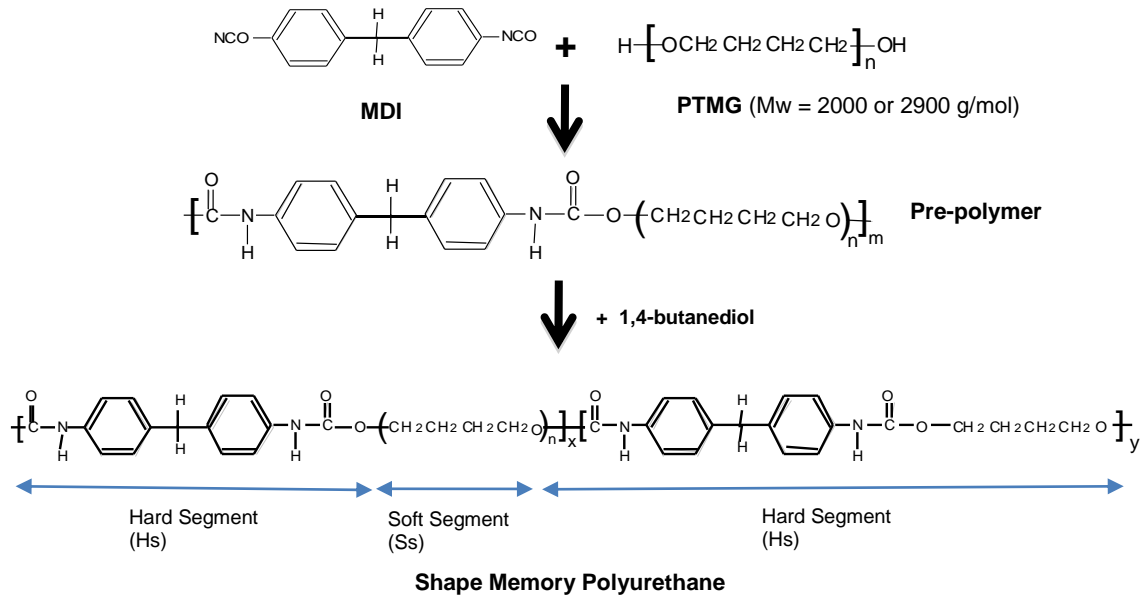
Figure II-2. Reaction scheme for the preparation procedure of linear thermoplastic polyurethanes.

The chemical structure of the diisocyanates chosen for the polyurethane systems can be seen in Figure II-3. Due to the substitution of the isocyanate groups, the crystallization of MDI is more regular. This contributes to an increase in the degree of crystallinity of the polyurethane itself which directly affects its morphology and properties.
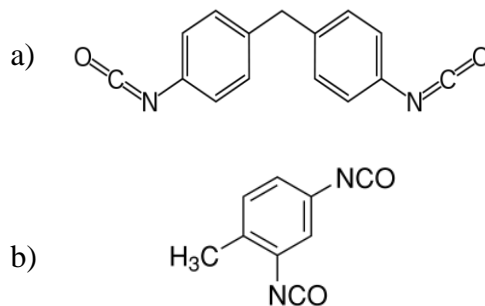
Figure II-3. Chemical structure of a) methylenedi-p-phenyl diisocyanate (MDI) and b) tolylene 2, 4 diisocyanate (TDI).

The commercial polyurethane was received from Huntsman in pellet form. In order to construct polyurethane films, 30.0 wt% of polyurethane pellets was dissolved in DMF. This solution was then cast in open Teflon$^®$ molds and placed in an oven at 80°C for 24 hours to allow for solvent evaporation.

TECHNIQUES

Fourier Transform Infrared (FTIR)

The completion of the reaction between the diisocyanate and long chain diol was observed using Fourier Transform Infrared (FTIR; Nicolet 6700) equipped with an attenuated total reflectance (ATR) stage. A small amount of the reactive solution was taken from the reaction flask periodically and evaluated.

Gel Permeation/Size Exclusion Chromatography (GPC)

Gel permeation/size exclusion chromatography (Viscotek270 Dual Detector with Viscotek 3580 Refractive Index Detector) was utilized to evaluate the molecular weight of the polyurethane samples. DMF was the eluting solvent.

Differential Scanning Calorimetry (DSC)

Thermal analysis was performed using temperature-modulated differential scanning calorimetry (TA Instruments DSC Q2000). Modulated DSC is generally used to characterize melting and recrystallization in polymers that exhibit multiple melting endotherms. Samples were equilibrated -80°C. Heating and cooling rates of 10°C/min and modulation rate of ± 1.0°C every 60 seconds were used. Samples were heated from -80°C to 280°C. Subsequently, they were

cooled to -80°C at a cooling rate of 10°C/min. Samples were then reheated to 280°C and cooled once again to -80°C. The enclosure was purged with dry nitrogen. Thermal transitions were evaluated.

Rheological Analysis

Rheological measurements were performed using a TA Instruments AR-G2 rheometer equipped with disposable parallel plates (diameter = 25mm). In order to determine the temperature at which the samples were in the molten state, temperature ramp sweeps were performed over a range of temperature (80 - 270°C). The remaining rheological experiments were strain sweeps which were performed on samples in the molten state in order to determine the linear viscoelastic range for frequency sweep experiments.

Thermal Gravimetric Analysis (TGA)

Thermal gravimetric analysis (TGA; TA Instruments Q500) was employed to determine the decomposition temperature of the polyurethane films. Samples were evaluated from room temperature to 400°C at a heating rate of 10°C/min. The enclosure was purged with dry nitrogen.

Scanning Electron Microscopy (SEM)

A scanning electron microscope (SEM; Philips Model SEM 505) was used to observe the fragile fractured surfaces of the shape memory polyurethane films. Liquid nitrogen was used during the fracture of the samples to insure that temperatures were below the glass transition of the soft segments. Samples were coated with gold to aid in conductivity for viewing.

Atomic Force Microscopy (AFM)

Atomic force microscopy (AFM; Veeco Instruments Inc., Dimension 3100) in tapping mode was used to evaluate sample morphology. Samples were cast as usual and allowed to dry at 80°C for solvent evaporation. The samples were then melted, a temperature of 220°C for the MDI system and 170°C for the TDI system was used, and allowed to condition at the specified temperature for 5 minutes in order to erase any thermal history. Images were taken at room temperature immediately following.

Tensile Analysis

Stress/strain measurements were obtained by testing 5mm x 25mm specimens at room temperature using a Universal Testing Machine (INSTRON 4400R Model 1122) in accordance with ASTM D 1708. The gauge length was 15mm. For evaluation of Young's modulus (E) and yield stress (σ_y) an extension speed of 10 mm/min was used. An extension speed of 100 mm/min was used for determination of elongation at break (ε_b). At least five replicates of each sample were tested and the average values were reported.

Shape Memory Behavior (SMB)

Thermal cyclic tests were performed on microtensile specimens of 5 mm x 25 mm using a universal testing machine equipped with a heating chamber (INSTRON 8501). Samples were first conditioned to a specified temperature, T_1, which was above the melting transition temperature of the soft segments, T_m soft, for ten minutes and then subsequently elongated to a maximum deformation of 100 or 200% of the original length at a speed of 10, 20, or 30 mm/min. The samples were then cooled below the glass transition temperature of the soft segments

(~ -20°C) and unloaded. Finally, the samples underwent the recovery process by heating once again for 10 minutes at the initially specified temperature. Figure II-4 is representative of the procedure followed to evaluate shape memory behavior, which was previously discussed in Chapter I.
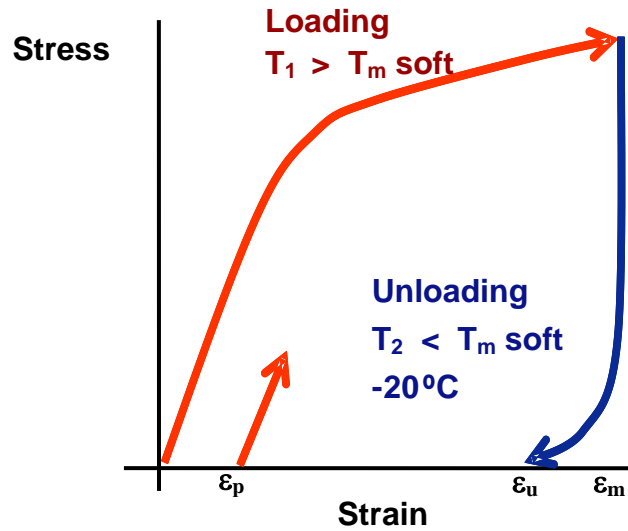
Figure II-4. Representative stress versus strain graph for the testing of shape memory behavior.

The strain maintained after unloading and the residual strain of each cycle were used to calculate the fixity (Rf) and recovery (Rr) ratios, which are indicated in the following equations:

$$R_f = \frac{\varepsilon_u}{\varepsilon_m} \, x \, 100\% \tag{2}$$

$$R_r = \frac{\varepsilon_m - \varepsilon_p}{\varepsilon_m} \, x \, 100\% \tag{3}$$

where ε_m is the maximum strain in the cycle (100%), ε_u is the residual strain after unloading and ε_p is the residual strain after recovery.

To evaluate the dependence of the shape recovery with the number of cycles, this parameter was also evaluated as:

$$R_r(N) = \frac{\varepsilon_m - \varepsilon_p(N)}{\varepsilon_m - \varepsilon_p(N-1)} x100\% \tag{4}$$

where $\varepsilon_p(N)$ represents the residual strain after heating in the Nth cycle.

Additionally, a dynamic mechanical analyzer (TA Instruments, RSA III) was used to determine the effect of recovery time on the shape memory behavior of the samples.

RESULTS AND DISCUSSION

Fourier Transform Infrared (FTIR)

FTIR spectroscopic analyses were carried out to insure that adequate time was given for the completion of the reaction between the diisocyanate (TDI or MDI) and the long chain polyol (PTMG 2000 or PTMG 2900) in the first step of the polymerization. In Figure II-5, the IR spectra of the TDI/PTMG 2000 and MDI/PTMG 2000 reactions are shown. The peak that occurs at 2275cm^{-1} corresponds to the isocyanate group. This peak was examined in order to observe the reaction between the diisocyanate group, –NCO, and the hydroxyl group, –OH. As can be seen in Figure II-5 a and b, the peak at 2270 cm^{-1} is decreasing with time. This indicates that the reaction between the isocyanate and the polyol is proceeding. It is expected that approximately 50% of the isocyanate groups will react with the PTMG 2900 in the first step of the reaction leaving the prepolymer with terminal isocyanate groups, and leaving the the remaining 50% to react during the second step of the reaction. This is observed in the FTIR spectra. After the addition of the BD, the isocyanate peak has an absorbance of zero which indicates that the isocyanate has completely reacted. The reactions between MDI and PTMG 2900 and TDI and PTMG 2900 follow similar trends.
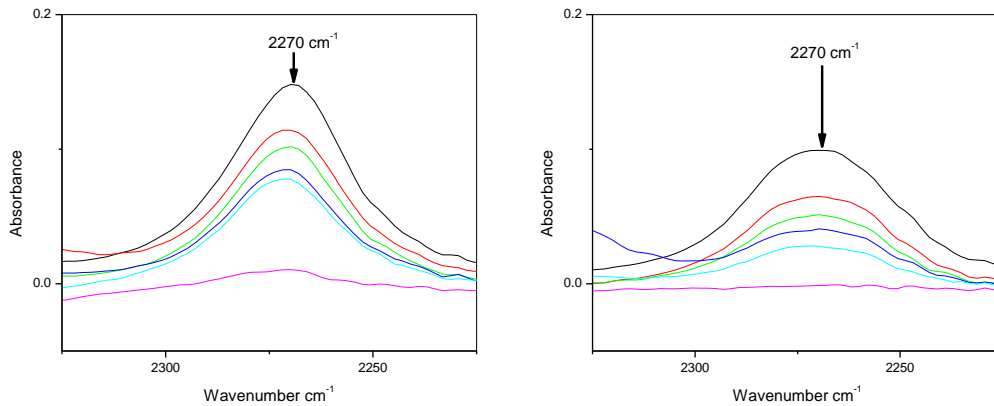
Figure II-5. FTIR spectroscopic analysis of reaction between a)TDI and PTMG 2000 and b) MDI and PTMG 2000 over a 45 minute period.

Molecular Mass Evaluation

The molecular masses of the prepared thermoplastic shape memory polyurethanes were determined using gel permeation/size exclusion chromatography. The measured M_n (g/mol) and polydispersity index (PDI) are summarized in Table II-2. As observed in the table, M_n values for synthesized polyurethanes of known chemical structure possess values that are similar to that of commercially available polyurethane (Irogran PS455-203, Huntsman, USA). The PDI values are acceptable for polymers produced using a condensation reaction. These values are in the range for M_n values reported elsewhere in literature [Chun et al., 2007; Lee et al., 2001; Takahashi et al., 1996].

Sample	M_n (g/mol)	PDI
Commercial PU	27009	1.62
MDI 2000/32	24257	2.01
MDI 2000/23	24943	1.97
MDI 2900/32	19267	1.46
TDI 2000/32	14687	1.73
TDI 2900/32	18641	2.72

Table II-2. Molecular weight and polydispersity for shape memory polyurethane samples.

Rheological Characterization

Rheological characterization was performed to determine the melting transition temperature of the shape memory polyurethane samples. For further testing of the viscoelastic response of the samples, which was performed in the molten state, it was important to determine the correct temperature at which to perform the tests. From Figure II-6 a, the TDI system was determined to be in the molten state at 180°C. For the MDI system, a temperature of 220°C was used for testing although it appears that the sample was not completely melted. The storage modulus shown in the graphs is 3 orders of magnitude higher than that of the typical melted sample, which indicates that some partial crosslinking is present in the MDI network. Higher temperatures were not used to avoid degradation of the samples.
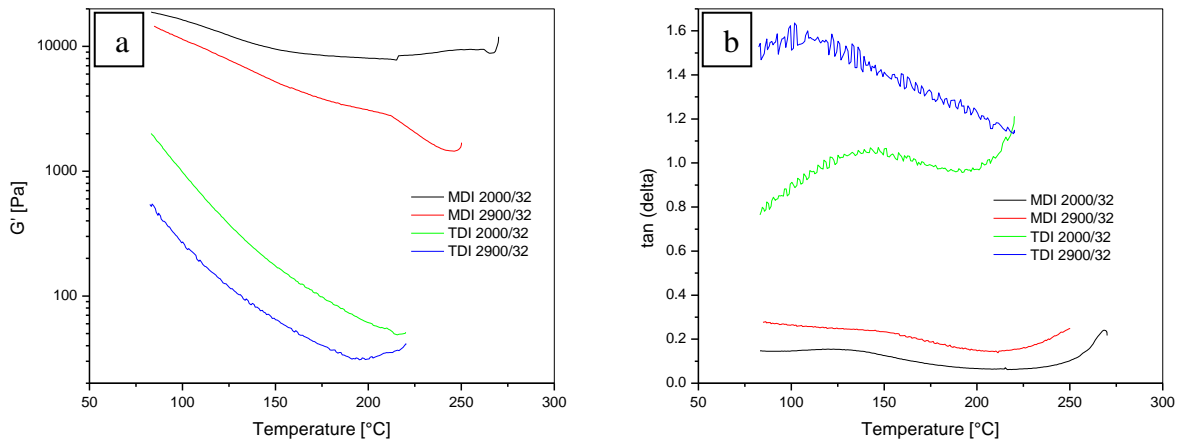
Figure II-6. Rheological results for segmented shape memory polyurethanes: a) G' versus temperature and b) tan(delta) versus temperature.

Thermal Characterization

Segmented copolymers exhibiting shape memory effect can be characterized not only by micro-phase separation but also by the ability of the soft segments to crystallize at room temperature [Li et al., 1996]. The effects of polymer structure and the crystallization temperatures of the soft segments were investigated by modulated differential scanning calorimetry (DSC). Similar to conventional DSC, modulated DSC measures the difference in heat flow between the sample and inert reference as a function of time and temperature. However, in modulated DSC a sinusoidal modulation (oscillation) is used in addition to the conventional linear heating ramp to yield a heating profile in which the temperature increases with time but nonlinearly. The effect is that of two experiments in which the sample is subjected to not only a linear heat rate but also a sinusoidal heat rate. Generally, shape memory polyurethanes show two clear melting peaks. One melting peak, which occurs around ambient conditions, corresponds to the melting of the soft segments (T_{mSS}) while the other, which corresponds to the melting of the hard segments (T_{mHS}), occurs at a much higher temperatures. During this study, it was found that a molecular

rearrangement occurs in the first thermal cycle. For this reason, focus was directed to the second thermal cycle for the observation of transition temperatures.

Effect of Hard Segment Content

Modulated DSC results observed for the transition temperatures related to the soft segments are presented in Table II-3. Results for the melting transitions were obtained from the reversible heat flow while those for crystallization were obtained from the total heat flow. During the first heating, melting of the hard segments was only exhibited for samples containing greater than or equal to 32 wt% hard segment content. The hard segment melting transitions for the MDI 2000 system containing 32, 39, and 45 wt% hard segment content occurred at 172, 175, and 185°C, respectively. The MDI 2900/32 sample exhibited a hard segment melting transition, which occurred at approximately 200°C. It has been reported in literature that segmented shape memory polyurethanes with low amounts of hard segment percentage usually do not exhibit hard segment transitions [Ji et al., 2007; Cho et al., 2004].

	Run 1			Run 2			
Sample Designation	T_m SS [°C]	ΔH_m SS (J/g)	ΔH_m (J/g SS)	T_m SS [°C]	ΔH_m SS (J/g)	T_c SS [°C]	ΔH_c SS (J/g)
PU Matrix	23.11	5.17	*	*	*	*	*
MDI 2000/45	5.98	4.61	8.38	19.69	42.76	-11.32	15.56
MDI 2000/39	5.25	8.42	13.80	18.01	43.41	-25.27	4.42
MDI 2000/32	6.83	6.23	10.21	15.81	27.85	-16.48	19.86
MDI 2000/23	7.49	21.04	34.49	*	*	*	*
MDI 2900/32	14.79	61.13	100.21	24.19	87.12	-6.4	32.83
TDI 2000/32	*	*	*	18.6	46.13	-22.95	17.31
TDI 2900/32	17.85	0.48	0.79	23.23	46.05	-9.04	27.49

Table II-3. Melting temperature (T_m), enthalpy of melting ($\Delta H_{melting}$), and enthalpy of crystallization (ΔH_c) of shape memory polyurethane soft segments. * indicates a transition was not observed.

During the first heating cycle, the MDI 2000 polyurethane system exhibits a decrease in the enthalpy of melting as the hard segment content is increased. This behavior has been reported [Lee et al., 2001] for a polyurethane system containing MDI, PTMG 1800, and BD. A smaller enthalpy of melting for the sample with the highest percentage of hard segment content suggests that it is possible to achieve more ordered packing of the hard segment. Restricted alignment of the hard segment chains would occur at higher hard segment contents due to the short, less flexible BD which is the main component of the soft segment [Auad et al., 2009; Lee et al., 2001]. In similar studies it has been found that MDI/BD hard segment glass transitions in polyurethanes with poly (tetramethylene oxide) or polypropylene oxide soft segments are usually not clearly observable, as is the case with the currently studied polyurethane system. This indicates that a significant portion of the soft segment is amorphous [Xu et al., 2008]. In the second heating, it is clearly observed that the melting temperature of the soft segments increases with increasing hard segment content, which shows that better phase separation is achieved with increasing hard segment content.

Effect of Soft Segment Length

The influence of soft segment length, from PTMG 2000 to PTMG 2900, on the thermal properties of the MDI polyurethane system with 32 wt% hard segments was evaluated (see Table II-4). The DSC scanning curves from the second thermal cycle of the prepared polyurethane films with different soft segment lengths (SS) and hard segment lengths (HS) are presented in Figure II-7. When the soft segment length is increased but the hard segment content is held constant, an increase in the melting temperature, crystallization temperature, enthalpy of melting, and enthalpy of crystallization occurs. Additionally, a more substantial increase occurs in the second heating. Also, as previously stated, samples composed of MDI/PTMG 2900 exhibit a melting transition for the hard segments that occurs at approximately 200°C. This effect was previously discussed for the MDI system whereby the length of the chains impacts the ordering and crystallinity of the polyurethane systems. As the length of the soft segment increases, the chains become more flexible which allows for an increase in crystallinity and better phase separation of the hard and soft segments, which leads to the visibility of the hard segment melting transition.
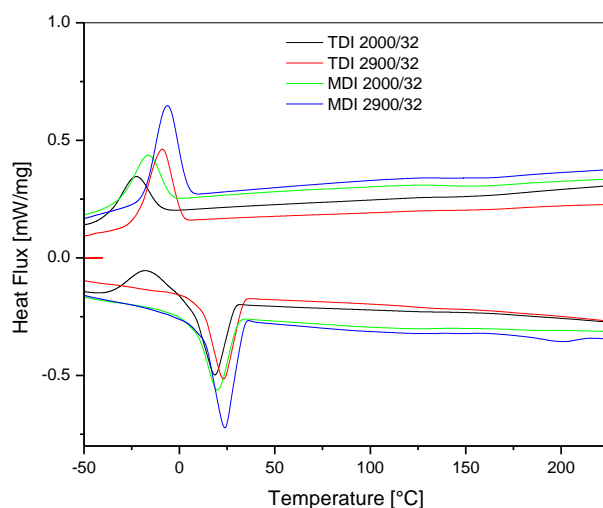
Figure II-7. Second thermal cycle of segmented shape memory polyurethane samples.

42

Sample Designation	Run 1			Run 2			
	T_m SS [°C]	ΔH_m SS (J/g)	ΔH_m (J/g SS)	T_m SS [°C]	ΔH_m SS (J/g)	T_c SS [°C]	ΔH_c SS (J/g)
MDI 2000/32	6.83	6.23	10.21	15.81	27.85	-16.48	19.86
MDI 2900/32	14.79	61.13	100.21	24.19	87.12	-6.4	32.83
TDI 2000/32	*	*	*	18.6	46.13	-22.95	17.31
TDI 2900/32	17.85	0.48	0.79	23.23	46.05	-9.04	27.49

Table II-4. Comparison of the thermal transitions of polyurethanes with constant hard segment content but varying soft segment length. * indicates that a transition was not observed.

In this study, the TDI 2000/32 polyurethane system exhibited no clear endotherms during the first heating step but upon cooling, a crystallization peak was formed. During the second run, a clear, low-temperature melting peak is observed and attributed to the melting of the soft segment domains. The associated cooling process now exhibits a crystallization peak that appears at a higher temperature and an increase in the enthalpy of crystallization (ΔH_c) is observed. This indicates that the heating/cooling process aids in crystal development, leading to the formation of more perfect crystalline regions (increased crystals with higher melting and crystallization temperatures and a narrow distribution of crystal sizes). Alternatively, packing disorder in the hard segments or release of residual strain could be aided by the temperature scanning which has often been observed [Petrovic et al., 2004]. The TDI 2900/32 polyurethane system performs similarly with the main difference being that upon the first heating, a low temperature melting peak is observed which is associated to the melting of the soft segments. In the TDI 2900/32 polyurethane system, the same trend is shown from the initial heating to the second heating as with the TDI 2000/32 polyurethane system: the melting temperature of the soft segments increases as do the enthalpy of melting ($\Delta H_{melting}$) and the temperature of crystallization increases as well as the enthalpy of crystallization (ΔH_c). Additionally, increasing the soft segment length in this system from PTMG 2000 to PTMG 2900 but leaving the hard segment content constant

creates an increase in the melting temperature of the soft segments and an increase in the crystallization temperature due to the additional orientation and crystallization of the soft segments that is achieved.

Degradation Characterization

Thermal gravimetric analysis was performed to evaluate the nature of degradation of solid polyurethane films with different formulations in an inert atmosphere. Shape memory polyurethane usually exhibits a three stage weight loss. The first stage, results from the evaporation of residual water. The decomposition of the urethane bonds of the hard segments, which begins at around 250°C, is responsible for the second stage. In the third and final stage, decomposition of the soft segments occurs [Yeh et al., 2008]. The hard segment is responsible for the thermal degradation whereas the soft segment accounts for the apparent weight loss [Tien & Wei, 2002]. For samples composed of MDI, BD, and PTMG, the decomposition is initiated from MDI-BD. Next, oxidation of the β-carbon next to the ether bond of the soft segments occurs. This oxidation breaks the C–O bond and unzips the molecular chain [Tien & Wei, 2002]. This behavior is exhibited in the synthesized shape memory polyurethanes. In Table II-5, the percent weight loss at increasing temperatures can be observed. The initial weight loss below 200°C is very low. As the temperature is increased to 300°C a relatively small reduction in the weight is observed, which relates to the degradation of the hard segments. However, at a temperature of 400°C, a substantial decrease in the weight is visible, due to degradation of the soft segments.

Sample	% Weight Loss at 200°C	% Weight Loss at 300°C	% Weight Loss at 400°C
MDI 2000/32	0.73	6.03	42.64
MDI 2900/32	0.84	8.42	42.56
TDI 2000/32	0.53	14.45	48.12
TDI 2900/32	2.22	21.93	51.07

Table II-5. % Weight loss of polyurethane films at designated temperatures.

The curves for the degradation of segmented shape memory polyurethanes with MDI hard segment composition are shown in Figure II-8. Although MDI is the most widely used diisocyanate for polyurethane preparation, it is susceptible to thermal degradation and oxidative degradation which leads to discoloring, which limits the applications. From the graph, it is clear that the length of the soft segment influences polymer degradation. Polyurethane synthesized with soft segment lengths of PTMG 2000 experience less degradation than those with soft segments composed of PTMG 2900.
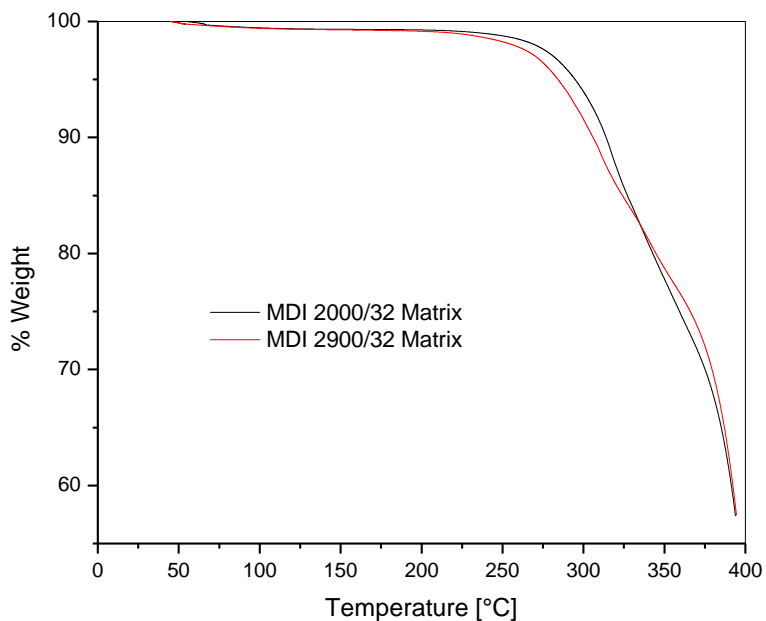
Figure II-8. Degradation of segmented polyurethane with MDI hard segment composition.

The curves for the degradation of shape memory polyurethane with TDI hard segment composition are shown below in Figure II-9. By comparing the values listed in Table II-4 above and the curves for the degradation of samples with MDI hard segment composition versus those with TDI, it is clear that the type of diisocyanate has a significant impact on degradation behavior as has previously been reported in other studies [Shieh et al., 1999]. Polyurethane samples with hard segments composed of TDI experience much greater levels of degradation than those composed of MDI. This is due to the molecular structure of the diisocyanates, which was previously discussed. Additionally, differences in the interactions, such as hydrogen bonding, dipole-dipole interactions, and Van der Waals forces, between the polymer systems may be responsible. The effect of soft segment length on the degradation behavior is also visible in samples possessing TDI hard segment composition. Similar to the MDI system, samples containing soft segment lengths composed of PTMG 2900 exhibit a much higher degree of

degradation at 300°C than those composed of PTMG 2000 due to better regularity of the polymer network which correlates to the increase in enthalpy of melting observed in the DSC experiments.
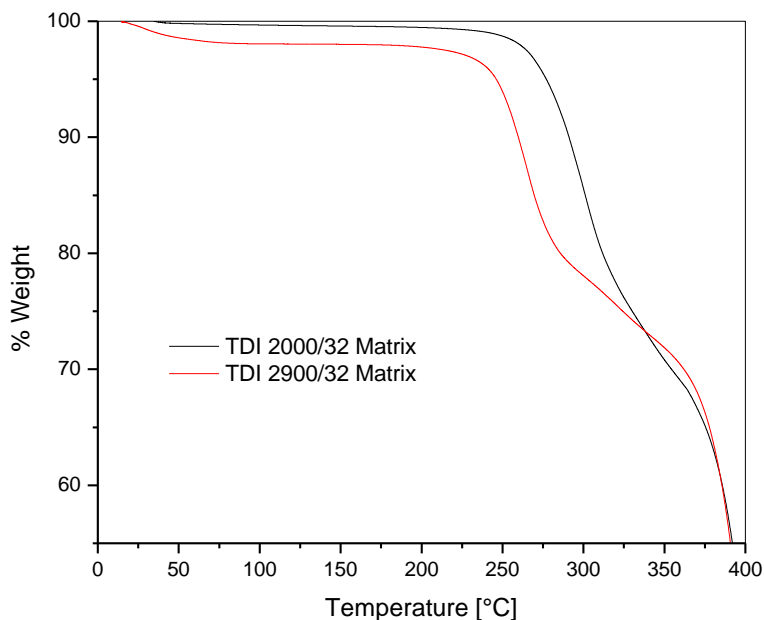
Figure II-9. Degradation of segmented polyurethane with TDI hard segment composition.

Morphology (SEM and AFM)

In order to observe the morphology of the segmented shape memory polyurethane samples, scanning electron microscopy and atomic force microscopy were utilized. Scanning electron micrographs of the shape memory polyurethane films composed of MDI hard segments are shown below in Figure II-10 a and b. The micrographs correspond to the fragile fractured cross section surface of freshly broken samples.

From Figure II-10 a, it is impossible to differentiate the micro-phase domains of the hard segments for the MDI 2000/32 from the micrograph. However, the micro-phase separation can

47

be differentiated in the MDI 2900/32 sample (Figure II-10 b). From these micrographs, it can be assumed that the MDI 2900/32 sample possesses a greater degree of phase separation between the hard and soft segments in comparison to the MDI 2000/32 sample. It is expected that a greater degree of micro-phase separation will significantly influence the properties of the sample creating an increase in modulus and strength as well as a change in the thermal transitions of the polyurethane.
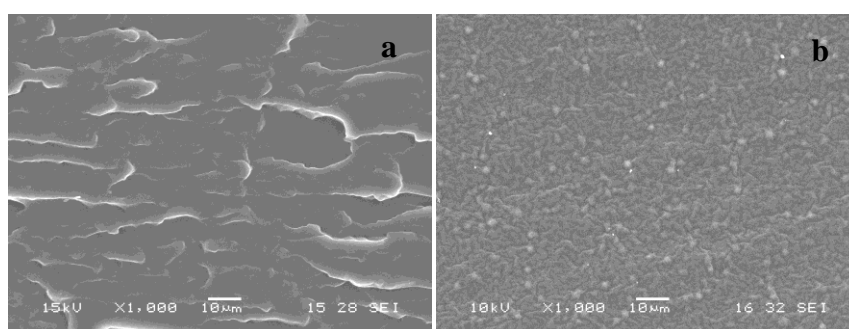
Figure II-10. Scanning electron micrographs of cryo-fractured shape memory polyurethane samples with MDI hard segments: a) MDI 2000/32, b) MDI 2900/32.

Tapping mode AFM amplitude images of the solid MDI system polyurethane films are presented in Figure II-11 a and b. In these images, the hard and soft segments are visible. The phase segregation of the soft and hard segments is obvious. The image for the MDI 2900/32 sample corresponds to the SEM image in that the phases are distinguishable. However, the MDI 2000/32 sample exhibits similar phase segregation that was not previously visible using the SEM. The properties of this system are greatly influenced by the degree of phase separation that exists between the two phases. This also confirms the conclusion drawn from the DSC experimental results that an increase in the length of the soft segments leads to an increase in

phase separation and an increase in the melting temperature and enthalpy of melting for the soft segments.
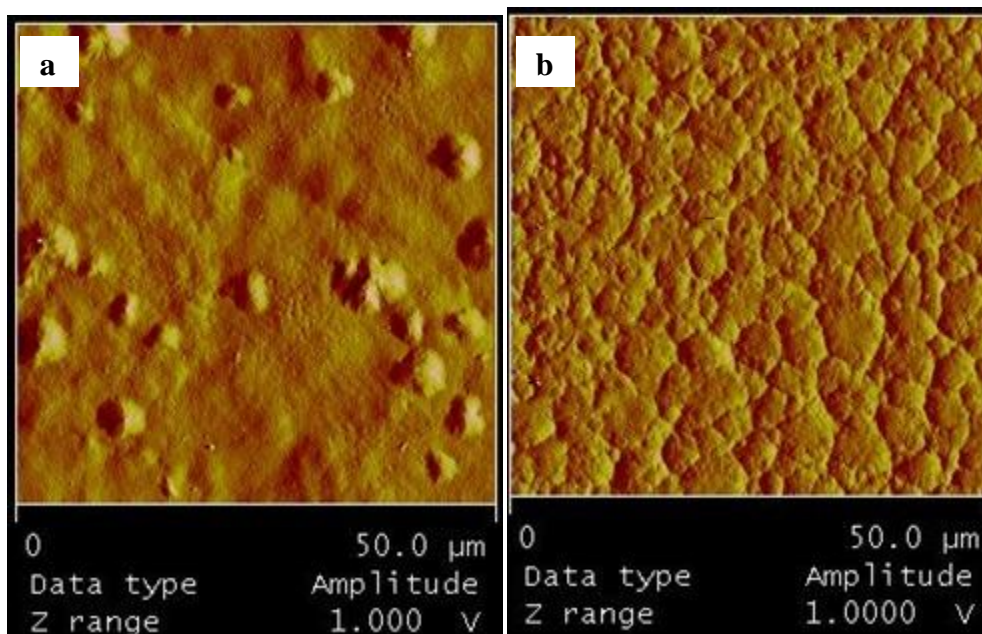
Figure II-11. Tapping mode AFM images of a) MDI 2000/32 and b) MDI 2900/32.

Figure II-12 a and b shows the micrographs for the TDI 2000/32, and TDI 2900/32 samples. Similar to the MDI 2000/32 sample, it is impossible to discern micro-phase separation of the soft and hard segments. This morphology can be attributed both to the structure of the isocyanate, which was previously discussed, and to the length of the soft segments. Due to the substitution of the –NCO groups in the structure of TDI, it is more difficult for the hard segments to organize. When the soft segment length increases, organization and crystallization of the hard segments becomes increasingly difficult. While the TDI system does not experience the increased phase separation of the MDI system, it does exhibit an increase in the melting temperature and enthalpy of melting of the soft segments during the DSC, which suggests phase separation is existent. At

lower hard segment contents, the micro-phase separation is difficult to observe. Comparable

behavior has been observed by Merline et al. in shape memory polyurethanes prepared from poly

(tetramethylene oxide) (PTMO), tolylene diisocyanate (TDI), and 1, 4 butanediol where it was

found that the SEM did not differentiate micro-phase domains of the hard segment but did

exhibit phase miscibilization as the hard segment content of the polyurethane was increased

above 33 wt% [Merline et al., 2007].
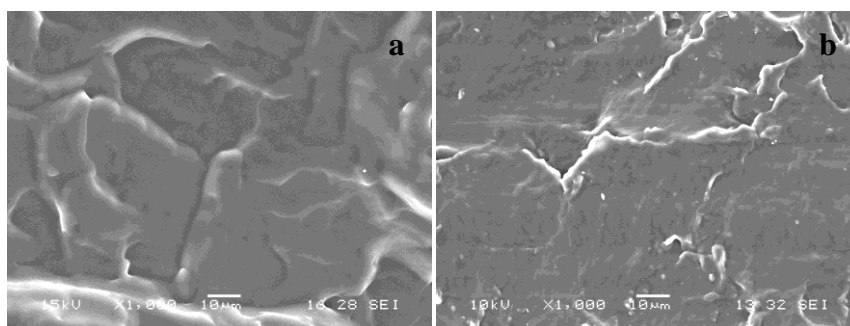
Figure II-12. SEM micrographs of cryo-fractured shape memory polyurethane samples: a) TDI
2000/32; b) TDI 2900/32.

The amplitude image of the TDI 2900/32 sample is shown below in Figure II-13. It was not

possible to obtain an image of the TDI 2000/32 sample. This sample was completely

transparent, indicating no phase separation and making it impossible to obtain an image. The

TDI 2900/32 sample did, however, show some features. It is important to note that these

features are not inherent to the polyurethane structure but are due to bubbles in the sample which

are the result of solvent evaporation. The TDI 2900/32 sample image and the inability to obtain

an image for the TDI 2000/32 sample corresponds with the SEM images in which no phase

separation is visible in the fractured film samples.
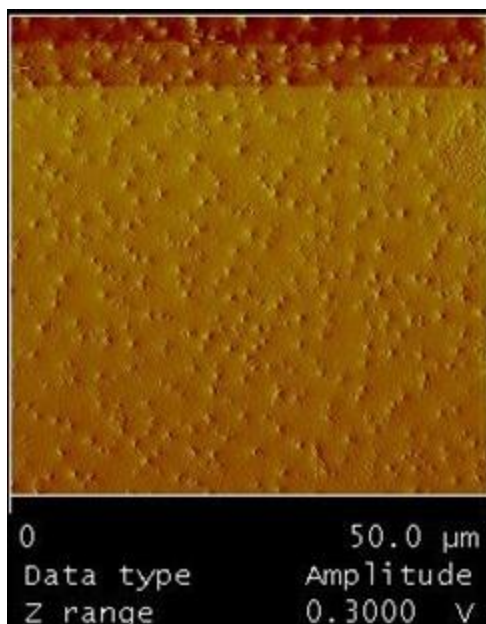
Figure II-13. AFM amplitude image of the TDI 2900/32 sample.

Mechanical Characterization

The mechanical properties of shape memory polyurethanes with varying hard segment concentration and composition and soft segment lengths were investigated by tensile testing at room temperature. The samples showed the expected elastomeric behavior. The Young's modulus (E), tensile strength (σ_y), and elongation at break (ε_b) were determined using ASTM D 1708. The results for the average of five samples and the standard deviations are shown below in Table II-6. As the stress is increased, plastic deformation occurs. Stress is redistributed by deformation and reorganization of the soft segments and the stress-strain curve deviates from the Hookean behavior, since stress redistribution by deformation and reorganization of the hard segments occurs. Eventually, the stress becomes so great that the polymer can no longer bear the load and the sample breaks. A representative stress versus strain curve for this behavior is shown below in Figure II-14.
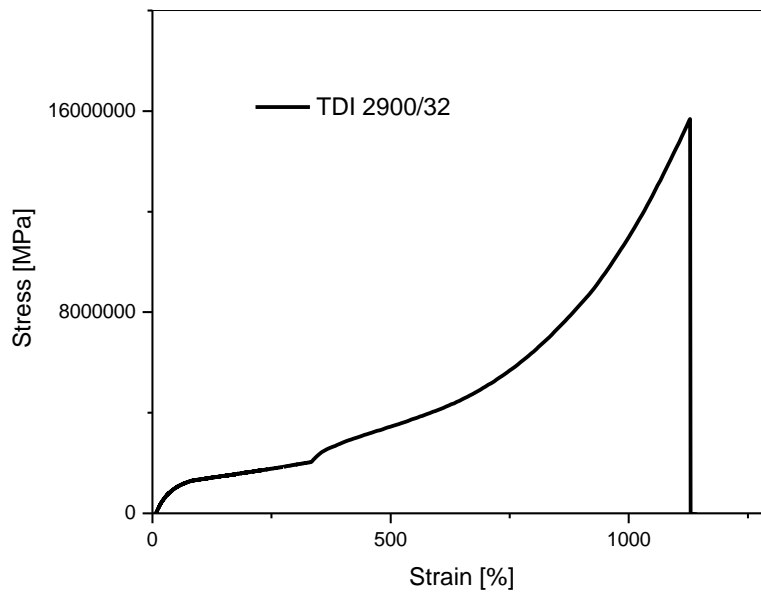
Figure II-14. Representative stress versus strain curve exhibiting the elastomeric behavior.

Effect of Hard Segment Content

In the MDI 2000 system, samples with lower percentages of hard segments exhibit a lower modulus but a much higher elongation at break. This behavior has been reported in other studies and is the result of the higher proportion of PTMG units which have a higher molecular mass and impart an enhanced flexibility and in turn are responsible for the higher elongation [Merline et al., 2007]. The Young's modulus of the MDI 2000 polyurethane system increases with an increase in hard segment content. The hard segment domains act as reinforcement for the soft matrix formed by the soft segments [Sheth et al., 2005]. The elongation at break for this system is very high for samples containing low hard segment content (MDI 2000/23) and decreases considerably as the hard segment concentration increases. This behavior was studied by Versteegen et al. and attributed to the reorganization and ease of deformation of the thin crystalline lamellae which leads to a more uniform stress distribution over the soft segments

[Versteegen et al., 2006]. However, if a higher hard segment content is present, there is more mobility restriction imposed on the material which leads to a decrease in the elongation at break.

Effect of Hard Segment Composition

To study the effect of the hard segment composition, the MDI and TDI systems were compared. The chemical structures of MDI and TDI were shown previously in Figure II-3. The structure of the isocyanate has a great impact on the regularity, orientation, and ability to organize in regular crystal domains. All of these factors influence the mechanical properties of the polyurethane systems. The 2, 4 substitution of the isocyanate groups in the structure of the TDI lead to a more irregular structure than the symmetrical 4, 4 substitution of MDI, which leads to a slightly bent structure that is capable of forming more regular crystalline regions in comparison to TDI. This structural influence leads polyurethanes with TDI hard segments to exhibit lower modulus with less crystallinity which in turn leads to a higher elongation at break in comparison to the MDI system.

The influence of the isocyanate structure has been studied using MDI, a bent structure, versus 1, 4-phenyldiisocyanate (PDI), a planar structure. This study found that the planar structure of PDI, pictured in Figure II-15 c, produced segmented polyurethanes with superior mechanical performance to polyurethanes produced with MDI, Figure II-15 a, due to stronger interactions between the hard segments which led to higher crystallinity of the hard segments and increased phase separation [Yang et al., 2003]. Similarly, in this study, it is expected that the mechanical properties of the MDI are higher than those of TDI, Figure II-15 b, due to the influence of the diisocyanate structure. In general, polyurethane systems incorporating hard segments composed

of MDI are harder and stiffer in comparison to those using TDI [Thomson, 2004]. Additionally,

MDI is most commonly used in the production of segmented shape memory polyurethanes due

to its symmetric structure [Shieh et al., 1999].
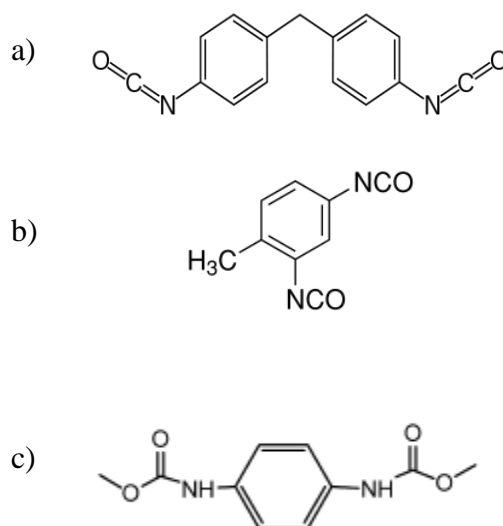
Figure II-15. Chemical structure of a) methylenedi-p-phenyl diisocyanate (MDI), b) tolylene 2, 4 diisocyanate (TDI), and c) 1, 4-phenyldiisocyanate (PDI).

Effect of Soft Segment Length

The effect of soft segment length on the mechanical properties was observed by comparing the

MDI 2000/32 to MDI 2900/32 polyurethane samples and the TDI 2000/32 to TDI 2900/32

samples. For the MDI system, the increase of the soft segment length produces a marked

increase in the Young's modulus and elongation at break and a slight increase in the tensile

strength. The TDI system follows the same trend with an increase in soft segment length leading

to a substantial increase in Young's modulus and elongation at break and a slight increase in the

tensile strength. The increase in length impacts the ability of the samples to phase separate and

crystallize. As previously discussed in the thermal characterization, samples possessing longer

soft segments lengths are more flexible and can crystallize more readily. The soft segment

length also directly affects the ultimate deformation at break, with longer soft segment lengths

leading to higher deformation.

Overall, several important trends were observed. The increase of soft segment length leads to

increased elongation at break. Samples with hard segments composed of MDI exhibit higher

modulus and lower elongation at break opposed to samples with TDI hard segments that posses

lower modulus but a much higher elongation at break.

	E [MPa]	σ_y [MPa]	ε_b [%]
Commercial PU Matrix	8.70 ± 1.425	1.51 ± 0.15	1664.07 ± 49.43
MDI 2000/45	37.00 ± 0.49	2.89 ± 0.20	203.0 ± 65.0
MDI 2000/39	15.70 ± 0.49	2.01 ± 0.12	473.00
MDI 2000/32	17.59 ± 0.57	4.19 ± 0.094	206.0 ± 27.10
MDI 2000/23	4.53 ± 0.32	1.08 ± 0.22	2165.00
MDI 2900/32	43.67 ± 3.15	5.95 ± 0.52	751.50 ± 39.30
TDI 2000/32	$0.74 \pm .056$	0.31 ± 0.031	891.80 ± 58.70
TDI 2900/32	4.67 ± 0.52	0.62 ± 0.056	1150.60 ± 140.00

Table II-6. Tensile properties of the shape memory polyurethanes

Shape Memory Behavior (SMB)

One of the most important features of shape memory materials is their ability to recover their

original dimensions upon application of an external force after deformation. During the

evaluation of shape memory behavior, deformation is the driving force for both the temporary

shape and the shape recovery [Kim et al., 1996]. Fixity is responsible for freezing the molecular

segmental motion of the soft segment phase in order to maintain a temporary shape while

recovery involves the reactivation of the mobility of the molecular segments necessary to obtain the original shape [Kim et al., 1996; Tobushi et al., 1998]. In this study, shape memory behavior was evaluated through a series of cyclic thermo-mechanical tests. Additionally, the recovery behavior over time was evaluated using dynamic mechanical analysis.

Figure II-16 shows the stress versus strain curves of the thermal cycles for the TDI 2900/32 matrix. The TDI 2900/32 matrix was chosen as the model for the study of the experimental parameters' impact on shape memory behavior testing results. This sample is representative of the behavior of all the synthesized segmented shape memory polyurethane samples. From the graph, it is clear that the first cycle is distinct from the remaining cycles. This is due to the inherent nature of thermoplastic elastomers. Complete elastic recovery is rarely observed; usually, some tensile set after elongation occurs. This is due to irreversible changes in the morphology of the material during deformation. After the material has been plastically deformed, the initial modulus of the second cycle will be lower compared to the initial modulus in the first or original cycle. Strain-induced crystallization has been shown to increase the tensile set [Versteegen et al., 2006]. This behavior is also exhibited in the mechanical testing performed using dynamic mechanical tensile testing.

56
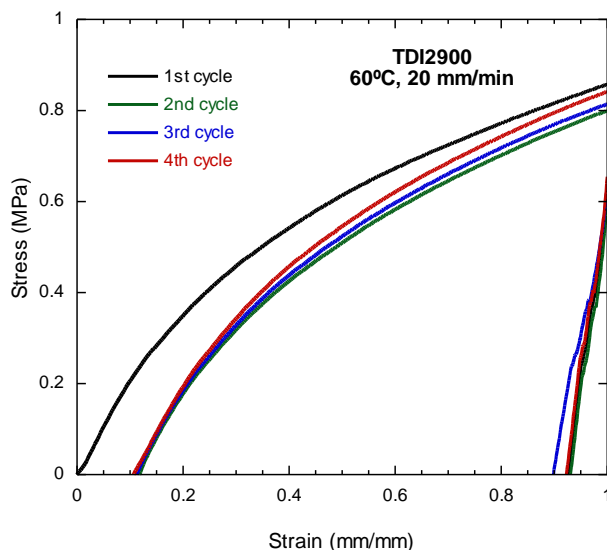
Figure II-16. Shape memory behavior cycles for TDI 2900/32 tested at a condition temperature of 60°C with a deformation rate of 20 mm/min and a maximum deformation of 100%.

When segmented shape memory polyurethanes are deformed in the temperature range between the melting temperature of the soft segments (~15°C) and the melting temperature of the hard segments (~175°C), and then subsequently cooled below the melting temperature of the soft segments under a fixed maximum strain, the deformed shape becomes fixed due to the freezing of the micro-Brownian motion. Rubber elasticity was observed in the temperature range between the melting temperature of the soft segments and that of the hard segments due to the micro-Brownian motion of the soft segments and the restricted molecular motion due to the crystalline frozen phase. Application of an external stress to the segmented polyurethane creates preferential extension of the soft segments in the direction of the applied stress between the fixed hard segment domains. However, a small recovery may occur after unloading, causing the maximum deformation to not be fully retained (which is reflected in the fixity values). Upon reheating to a temperature between the melting temperature of the soft segments and the melting

temperature of the hard segments, partially recovery of the original length is achieved due to the elastic energy stored during deformation.

In order to achieve effective shape memory behavior, the hard segments must retain their inter- or intra-polymer chain attractions, such as hydrogen bonding, dipole-dipole interactions, or physical crosslinking, while the soft segments should remain free to absorb external stress by unfolding and extending their molecular chains [Auad et al., 2009; Cho et al., 2004; Lee et al., 2001; Ratna & Karger-Kocsis, 2008]. If the stress destroys the interactions among the hard segments, shape memory will be lost and the recovery of the original shape will be impossible. Control of hard and soft segment composition is of the upmost importance in order to satisfy the conditions required for shape memory applications [Ratna & Karger-Kocsis, 2008].

Due to the large impact of structure and morphology on the properties of segmented shape memory polyurethanes and the large number of variables involved in the testing of shape memory behavior, it is important to understand the effects of different testing parameters in order to determine the optimum conditions. During this portion of the work, the influence of chemical structure, hard segment composition and soft segment length, on the shape memory behavior was studied. Additionally, the effects of the conditioning temperature, deformation rate, and maximum strain were evaluated.

As previously discussed, the stress versus strain behavior of the first cycle was distinct from the behavior in subsequent cycles. Therefore, the shape recovery was calculated with respect to the deformations of the previous cycle. It was noticed, however, that after the first cycle the

remaining cycles (cycles 2-4) exhibit similar behavior. It should be mentioned, however, that in some cases, additional testing of more than 4 cycles was performed (up to as many as 12 cycles) with repeatable results. This suggests that after the first deformation, which produces some reordering of the phase distribution, the behavior is almost that of an ideal elastic network with deformation which is almost completely reversible [Li et al., 1996].

Effect of Conditioning Temperature

The first experimental testing parameter to be evaluated was the effect of the conditioning temperature. In order to observe the effects, the TDI 2900/32 matrix was subjected to thermo-mechanical cycling using a maximum deformation of 100% and deformation speeds of 20 mm/min. Conditioning temperatures of 40, 60, and 80°C were evaluated. The results can be seen in Table II-7. From the data, it is clear that the fixity remains largely unaffected by the conditioning temperature; however, the recovery increases with temperature. Fixity is mainly a function of the soft segment domains while recovery is dependent on the hard segment domains. The increase in recovery can be attributed to the increased chain mobility of the soft segments which occurs with the increase in temperature making it easier for the hard segments to recover the original shape. However, the increase in chain mobility of the soft segments due to an increase in temperature does not appear to have a significant impact on the shape fixity.

TDI 2900/32 20 mm/min $\varepsilon_m = 100\%$	T [ºC]	1st cycle [%]	2nd cycle [%]	3rd cycle [%]	4th cycle [%]
Fixity	40	87.71±3.44	88.06±4.73	89.88±4.92	87.96±7.13
	60	90.80±2.54	91.26±2.46	88.84±1.36	90.58±2.40
	80	88.98±1.73	90.44±2.26	88.88±3.28	91.48±3.29
Recovery	40	80.12±10.58	74.68±5.20	76.24±4.12	76.22±5.06
	60	86.30±2.74	84.82±5.57	83.84±7.98	82.84±11.26
	80	92.36±2.21	84.90±5.80	81.82±6.99	76.90±8.51

Table II-7. Effect of conditioning temperature on shape memory behavior.

In order to further explore the effect of conditioning temperature on the shape recovery, the TDI 2900/32 sample was tested using a dynamic mechanical analyzer. Standard tensile tests were run at temperatures of 40, 60, and 80°C. The samples were strained to a maximum deformation of 300% at a strain rate of 20 mm/min, unloaded, allowed to recover for 10 minutes, and subsequently re-strained to 300% to evaluate the recovery. The results are shown in Figure II-17. Similar to the shape memory behavior testing, the samples exhibited an increase in recovery with an increase in conditioning temperature.
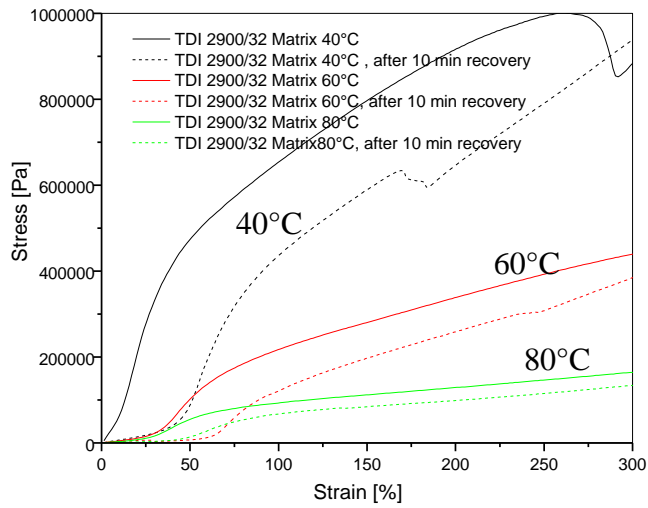
Figure II-17. Effect of recovery temperature evaluated using dynamic mechanical analysis. Dash line represents the second run, which was performed after a 10 minute recovery period.

In order to evaluate the actual percentage increase in recovery as conditioning temperature was increased, the point where the slope of the curves intersected the x-axis was determined for both the initial and recovery runs. The difference in these values was taken to be the percent recovery. As seen in Figure II-18, the percent recovery increases substantially with an increase in conditioning temperature.
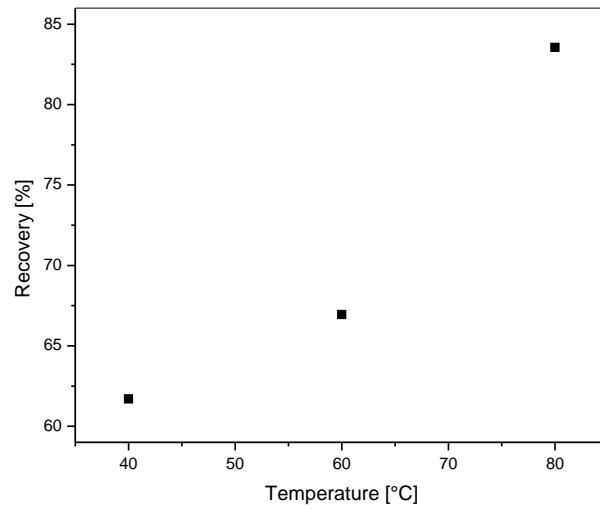
Figure II-18. Percent shape recovery with increasing temperature for the TDI 2900/32 sample.

Effect of Strain Rate

The next experimental testing parameter to be evaluated was the effect of the strain rate. In order to study this testing parameter, the TDI 2900/32 sample was tested at a temperature of 40°C and a maximum deformation of 100%. Strain rates, or loading rates, of 10, 20, and 30 mm/min were examined. The results are shown in Table II-8. In the range of strain rates studied, there is not a significant impact on the shape fixity and recovery of the TDI 2900/32 samples.

TDI 2900/32 $T = 40°C$ $\varepsilon_m=100\%$	ε rate (mm/min)	1st cycle [%]	2nd cycle [%]	3rd cycle [%]	4th cycle [%]
Fixity	10	88.44	75.87	80.7	84.7
	20	87.71±3.44	88.06±4.73	89.88±4.92	87.96±7.13
	30	83.83±0.71	78.78±3.87	87.52±2.50	85.18±3.71
Recovery	10	91.04	88.01	86.84	85.08
	20	80.12±10.58	74.68±5.20	76.24±4.12	76.22±5.06
	30	92.06±0.20	89.94±0.48	84.32±4.81	81.14±5.18

Table II-8. Effect of strain rate.

In order to determine whether strain rate has an impact on recovery, a dynamic mechanical analyzer in tensile mode was used to study the effect of much higher strain rates. The TDI 2900/32 samples were strained to a maximum deformation of 300% at a temperature of 40°C with strain rates of 20, 40, and 80 mm/min. The curves of stress versus strain are shown in Figure II-19. The values for modulus from the initial run and the recovery run are listed in Table II-9. From the values, it is obvious that modulus increases with an increase in strain rate. By increasing the strain rate from 20 to 80 mm/min, the modulus more than doubles. The increase in strain rate induces an increase in orientation of the polymer chains which leads to an increase in Young's Modulus.
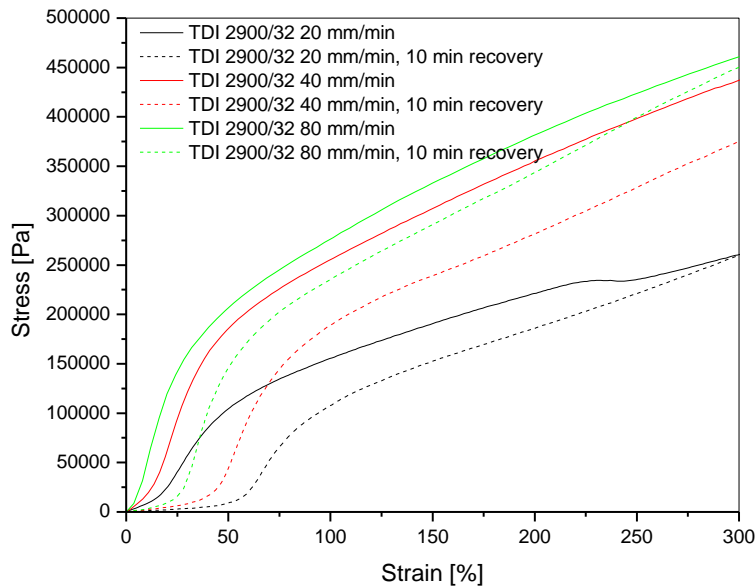
Figure II-19. Effect of strain rate on recovery evaluated using dynamic mechanical analysis.

As expected, the percent shape recovery of the samples increased with an increase in the strain rate. As previously discussed, the recovery is largely controlled by the hard segments. When much faster strain rates are utilized, orientation or alignment of the hard segments takes place much more quickly. This leads to not only an increase in the recovery, as can be seen in Figure II-20, but is also seen in the values for the modulus, Table II-9, which double when the strain rate is increased from 20 to 40 mm/min and nearly triple when the rate is increased from 20 to 80 mm/min. This increase in modulus is also expected due to the hard segments acting as reinforcements as previously discussed in the mechanical characterization.
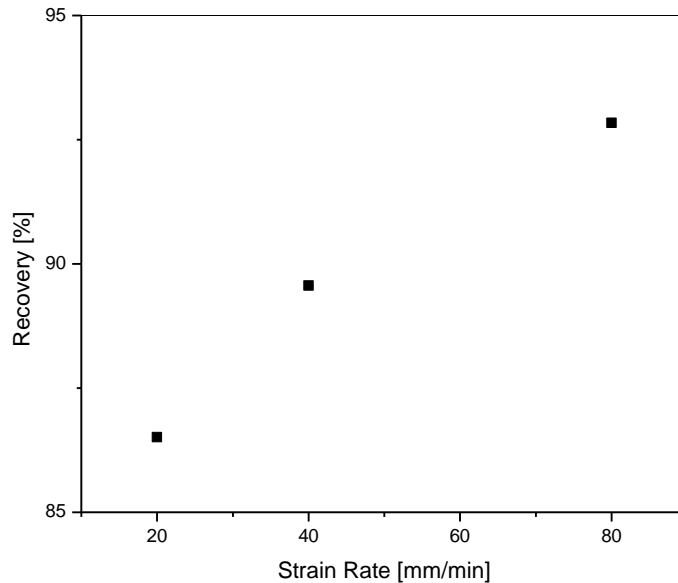
Figure II-20. Effect of strain rate on percent recovery for the TDI 2900/32 sample at 40°C with a 10 minute recovery.

	Strain Rate [mm/min]	Modulus [Pa]	Recovery Modulus [MPa]
TDI 2900/32, 40°C, 10min recovery	20	0.33	0.33
	40	0.61	0.46
	80	0.82	0.67

Table II-9. Effect of strain rate on modulus.

Effect of Maximum Deformation

Finally, the effect of maximum deformation on shape memory behavior was evaluated. Tests were performed on the TDI 2900/32 sample at a temperature of 40°C and a strain rate of 20 mm/min. Maximum deformations of 100% and 200% were evaluated. The results are shown in Table II-10. As expected, shape fixity and recovery both experience an increase with an increase in maximum deformation. During the loading of the sample, the molecular structure is aligned which increases the crystallinity of the soft and hard segment domains of the segmented shape memory polyurethane. By increasing the maximum deformation, the sample is becoming more crystalline due to the additional area, created during deformation, for alignment. An increase in crystallinity of the two phases leads to an increase in both shape fixity and recovery. Similar behavior was reported in the literature [Gunes et al., 2008].

TDI 2900/32 T = 40°C 20mm/min	ε (%)	1st cycle [%]	2nd cycle [%]	3rd cycle [%]	4th cycle [%]
Fixity	100	87.71±3.44	88.06±4.73	89.88±4.92	87.96±7.13
	200	94.80±2.26	94.15±0.495	94.29±0.976	94.87±1.17
Recovery	100	80.12±10.58	74.68±5.20	76.24±4.12	76.22±5.06
	200	87.27±3.49	84.74±3.28	84.67±3.32	84.35±3.012

Table II-10. Effect of maximum deformation.

Effect of Recovery Time

The TDI 2900 sample was strained to a maximum deformation of 100% using a strain rate of 20 mm/min at 40°C. The sample was then allowed to recover for 5, 10, or 20 minutes prior to performing the second cycle. The stress versus strain curves obtained at different recovery times are shown below in Figure II-21. The effect of an increase in recovery time is hard to observe

from the graphs due to the slight variation in initial modulus of the TDI 2900/32 samples tested. So, Figure II-22 shows the values that were found for the percent recovery of the samples. In order to determine these values, the intersection of the X-axis for each of the curves was determined. The value for the initial test was then subtracted from the value for the second test. From Figure II-22, it is clear that percent recovery increases almost linearly with the increase in recovery time. This result was expected. As the time allowed for recovery is increased, the hard segments have more time to recover the original shape.
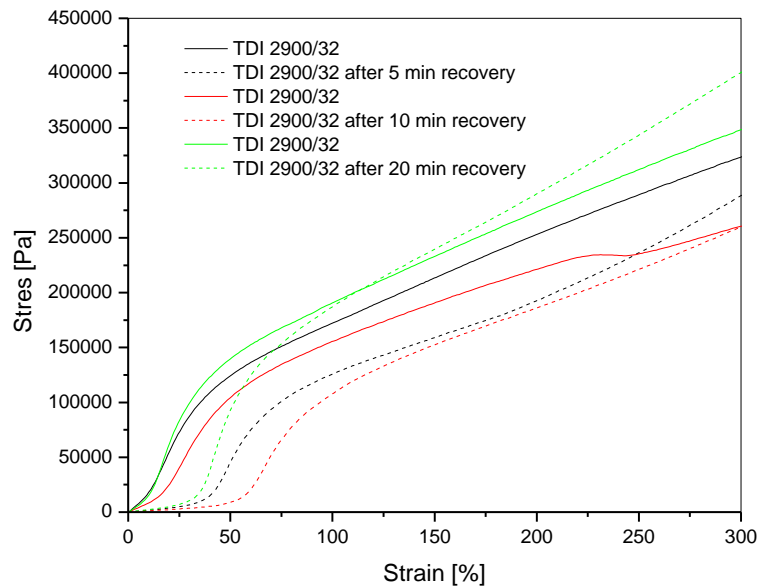
Figure II-21. Effect of recovery time.
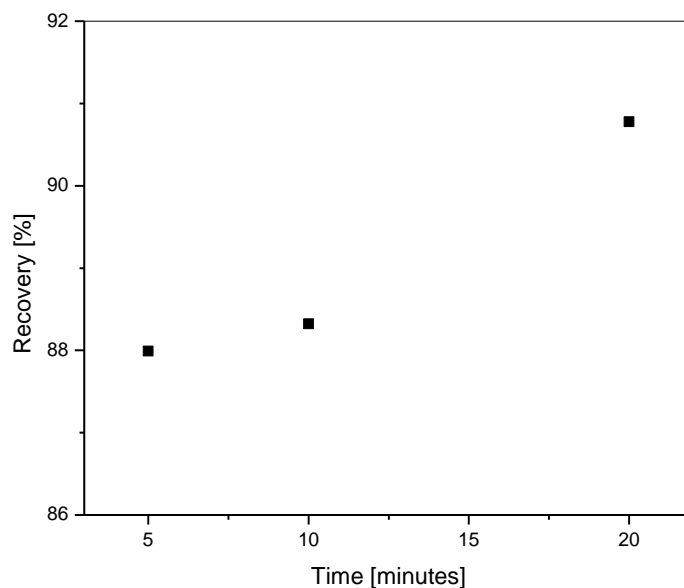
Figure II-22. Percent shape recovery with increasing time.

Effect of Chemical Structure

In this section, we will first study the influence of soft segment length on shape memory behavior and then evaluate the effect of hard segment composition (MDI versus TDI). First, the influence of soft segment length on the shape memory behavior of the MDI system was studied. Table II-11 lists the results for fixity and recovery of the MDI system. Thermo-mechanical tests were performed at a temperature of 60°C with a deformation rate of 20 mm/min and a maximum deformation of 100%. As expected, the fixity increased with an increase in soft segment length. As previously discussed, the MDI 2900/32 system possesses better phase separation. This was apparent in the observed melting transition of the hard segments from the differential scanning calorimeter as well as in the observed phase separation in the scanning electron micrographs. Better phase separation leads to an increase in fixity and recover. Additionally, the increased length of the soft segments aids in fixity.

67

MDI 2000/32 $\varepsilon_m = 100\%$ 20mm/min	T [°C]	1st cycle [%]	2nd cycle [%]	3rd cycle [%]	4th cycle [%]
Fixity	60	73.63±5.08	74.80±0.11	74.66±3.54	71.78±2.20
Recovery	60	83.68±2.37	82.84±2.30	81.02±0.93	78.66±6.02

MDI 2900/32 $\varepsilon_m = 100\%$ 20mm/min	T [°C]	1st cycle [%]	2nd cycle [%]	3rd cycle [%]	4th cycle [%]
Fixity	60	86.95±2.20	87.33±0.55	86.22±0.08	87.52±1.36
Recovery	60	85.32±0.45	84.00±1.87	83.06±2.74	81.90±1.65

Table II-11. Effect of soft segment length on the fixity and recovery of the MDI system.

Effect of Soft Segment Length

The influence of soft segment length on the shape memory behavior of the TDI system was studied next. Table II-12 lists the results for fixity and recovery of the TDI system. Shape memory behavior testing was performed at 40 and 60°C with a deformation rate of 20 mm/min and a maximum deformation of 100%. With the TDI system, a more complex behavior occurs. The hard segment domains are not effectively hydrogen bonded due to the substitution of the –NCO groups in the isocyanate structure. Additionally, the hard segments are much shorter than those of the MDI samples which make it increasingly difficult for the TDI hard segments to recover the longer soft segment chains. It is observed, however, that increasing the conditioning temperature from 40 to 60°C creates an increase in fixity and recovery. Once again, this is due to the increased chain mobility which allows for greater recovery by the hard segments and greater fixity by the soft segments.

TDI 2000/32 $\varepsilon_m = 100\%$ 20mm/min	T [°C]	1st cycle [%]	2nd cycle [%]	3rd cycle [%]	4th cycle [%]
Fixity	40	91.14±4.84	95.24±0.96	92.64±4.98	93.10±1.84
	60	93.02±2.80	91.40±0.91	90.73±0.89	92.02±1.73
Recovery	40	94.50±3.08	89.48±2.71	89.88±4.012	85.92±6.90
	60	90.24±0.23	90.46±1.16	90.28±3.28	91.44±1.98

TDI 2900/32 $\varepsilon_m = 100\%$ 20mm/min	T [°C]	1st cycle [%]	2nd cycle [%]	3rd cycle [%]	4th cycle [%]
Fixity	40	87.71±3.44	88.06±4.73	89.88±4.92	87.96±7.13
	60	90.80±2.54	91.26±2.46	88.84±1.36	90.58±2.40
Recovery	40	80.12±10.58	74.68±5.20	76.24±4.12	76.22±5.06
	60	86.30±2.74	84.82±5.57	83.84±7.98	82.84±11.26

Table II-12. Effect of soft segment length on the fixity and recovery of the TDI system.

The effect of soft segment length was studied additionally using the dynamic mechanical analyzer in tensile mode. Samples were strained to a maximum deformation of 300% using a deformation rate of 20 mm/min and conditioning temperatures of 40 and 60°C. After 10 minutes, the recovery was evaluated by performing a second run. From Figure II-23 it is clear that the TDI 2000/32 samples experience better shape recovery. This is further supported by the values for modulus which are shown in Table II-13. As previously discussed, higher modulus indicates the effectiveness of the hard segments. TDI 2000/32 samples possess more effective hard segments that are more capable of recovering the short soft segment length and therefore, exhibit better shape recovery than those of the TDI 2900/32 samples, which have lower modulus and recovery.
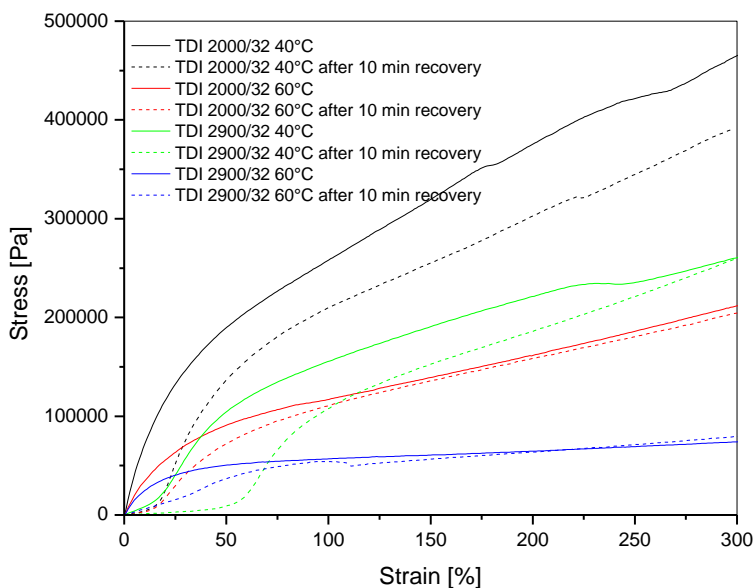
Figure II-23. Comparison of shape recovery for TDI 2000/32 versus TDI 2900/32.

	Temperature [°C]	Modulus [Pa]	Recovery Modulus [MPa]
TDI 2000/32	40	0.86	0.56
	60	0.40	0.26
TDI 2900/32	40	0.28	0.34
	60	0.32	0.09

Table II-13. Modulus values for the TDI system at 40 and 60°C.

Effect of Hard Segment Composition

The results for samples conditioned at 60°C from Tables II-11 and II-12 were compared to

evaluate the effect of hard segment composition on the shape memory behavior. The overall

structure of samples prepared from MDI is more rigid and consequently less capable of shape

recovery. This behavior was reported to be linked to microphase separation and density of

physical crosslinks affecting the dynamic properties of the segmented shape memory

70

polyurethanes [Lee et al., 2001]. Also, the larger size of the hard segment domains in the MDI system allow for recovery of much longer soft segment chains as opposed to TDI which has difficulty recovering the shape when longer soft segment chains are utilized.

Tensile tests were performed on the MDI 2900/32 and TDI 2900/32 samples using a dynamic mechanical analyzer. The samples were tested at 60°C to a maximum deformation of 100% using a strain rate of 20 mm/min. Recovery was evaluated after 10 minutes. The stress versus strain curves are shown in Figure II-24. From the curves, the different behavior of the systems is evident. While the MDI system has a much higher Young's modulus, it exhibits a reduction of shape memory behavior in comparison to the TDI 2900/32 system.
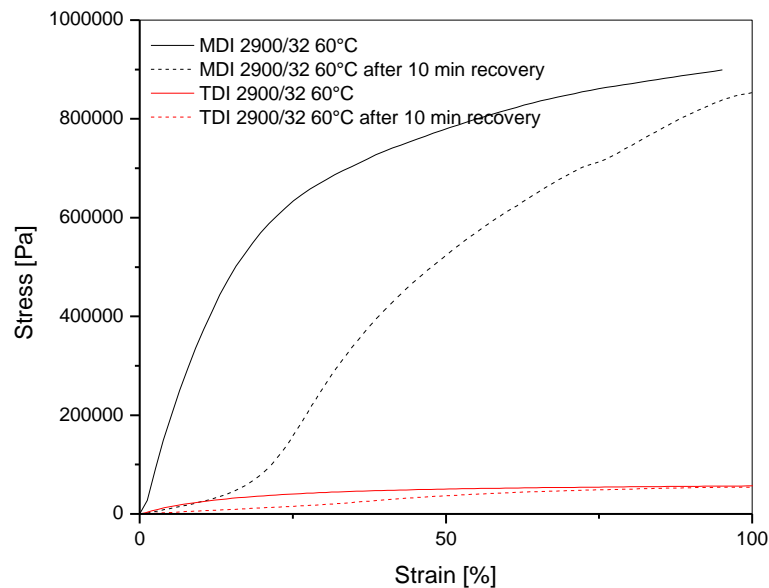
Figure II-24. Comparison of MDI 2900/32 versus TDI 2900/32 using the DMA.

As a final remark, the effect of segmented shape memory polyurethane chemical structure (hard segment composition and soft segment length) obviously influences the material properties and

transition temperatures which in turn effect the hard segment structure, phase segregation, and ordering. This subsequently determines the shape memory behavior of the materials [Lee et al., 2004].

CONCLUSIONS

Segmented shape memory polyurethanes with a controlled chemical structure were synthesized by controlling the molar ratio of the reactants. These samples were thoroughly characterized in order to determine the impact that hard segment content, hard segment composition, and soft segment length make on the final polymer properties. It was observed that samples with 32 wt% hard segment content exhibit the best combination of mechanical, thermal, and shape memory properties. For this reason and their similarity to the commercial polyurethane sample, samples containing 32 wt% were chosen as the focus of the remainder of this research with particular emphasis on the TDI 2900/32 system.

It was found that the hard segment composition has a great impact on the mechanical and thermal properties due in large part to the structure of the isocyanate utilized which has a substantial impact on the phase separation and crystallinity of the hard segments. The soft segment length significantly influenced the ultimate deformation at break for both polymer systems studied. The thermal properties were also influenced due to the increase in length of the soft segments.

Both of the synthesized systems exhibited shape memory behavior. The evaluation of the influence of testing parameters exhibited the importance of choosing shape memory testing

parameters similar to those of the end use application. Changing the shape memory behavior testing parameters significantly affects the test results. Additionally, from the study of chemical structure, it is evident that in order to achieve shape memory behavior the following must be present: phase separation of the hard and soft segments, crystallinity of the soft segments for fixity, and effective hard segments for recovery. Dynamic mechanical analysis was used to further reinforce the findings in the shape memory behavior testing and to study the impact of recovery time, which was observed to be a significant factor in shape recovery.

The thermal, mechanical, and shape memory properties of the segmented shape memory polyurethane can be greatly influenced by the chemical structure and the experimental variables such as maximum deformation, strain rate, and conditioning temperature. Therefore, careful consideration should be given to the end use application so that the polymer may be engineered to achieve the desired properties.

REFERENCES

1. Ahn, T. O.; Choi, I. S.; Jeong, H. M.; Cho, K. Thermal and Mechanical Properties of Thermoplastic Polyurethane Elastomers from Different Polymerization Methods. *Polymer International*, **2007**, *31*(4), pp 329-333.

2. Aneja, A.; Wilkes, G. L. A Systematic Series of 'Model' PTMO Based Segmented Polyurethanes Reinvestigated Using Atomic Force Microscopy. *Polymer*, **2003**, *44,* pp 7221-7228.

3. Auad, M. L.; Mosiewicki, M. A.; Richardson, T.; Aranguren, M. I.; Marcovich, N. E. Tailored Shape Memory Polyurethane Reinforced with Microcrystalline Cellulose Nanofibers. Accepted for publication in *Journal of Applied Polymer Science*, **2009**.

4. Chen, S.; Hu, J.; Liu, Y.; Liem, H.; Zhu, Y.; Meng, Q. Effect of Molecular Weight on Shape Memory Behavior in Polyurethane Films. *Polymer International*, **2007**, *56*, pp 1128-1134.

5. Cho, J. W.; Jung, Y. C.; Chung, Y.; Chun, B. C. Improved Mechanical Properties of Shape-Memory Polyurethane Block Copolymers through the Control of the Soft-Segment Arrangement. *Journal of Applied Polymer Science*, **2004**, *93*, pp 2410–2415.

6. Chun, B. C.; Cho, T. K.; Chung, Y. Blocking of Soft Segments with Different Chain Lengths and Its Impact on the Shape Memory Property of Polyurethane Copolymer. *Journal of Applied Polymer Science*, **2007**, *103*, pp 1435-1441.

7. Gunes, I. S.; Cao, F.; Jana, S. C. Evaluation of Nanoparticulate Fillers for Development of Shape Memory Polyurethane Nanocomposites. *Polymer*, **2008**, *49*, pp 2223-2234.

8. Jeong, H. M.; Lee, J. B.; Lee, S. Y.; Kim, B. K. Shape Memory Polyurethane Containing Mesogenic Moiety. *Journal of Materials Science*, **2000**, *35*, pp 279-283.

9. Ji, F. L.; Hu, J. L.; Li, T. C.; Wong, Y. W. Morphology and Shape Memory Effect of Segmented Polyurethanes. Part I. With Crystalline Reversible Phase. *Polymer*, **2007**, *48*, pp 5133-5145.

10. Kim, B. K.; Lee, S. Y.; Xu, M. Polyurethanes Having Shape Memory Effects. *Polymer*, **1996**, *37*, pp 5781-5793.

11. Kim, B. K.; Lee, S. Y.; Lee, J. S.; Baek, S. H.; Choi, Y. J.; Lee, J. O.; Xu, M. Polyurethane Ionomers Having Shape Memory Effects". *Polymer*, **1998**, *39*, pp 2803-2808.

12. Lee, B. S.; Chun, B. C.; Chung, Y.; Sul, K. I.; Cho, J.W. Structure and Thermomechanical Properties of Polyurethane Block Copolymers with Shape Memory Effect. *Macromolecules*, **2001**, *34*, pp 6431-6437.

13. Lee, S. H.; Kim, J. W.; Kim, B. K. Shape Memory Polyurethanes Having Crosslinks in Soft and Hard Segments. *Smart Materials and Structures,* **2004**, *13,* pp 1345-1350.

14. Lin, J. R.; Chen, L. W. Study on Shape-Memory Behavior of Polyether-Based Polyurethanes. I. Influence of the Hard-Segment Content. *Journal of Applied Polymer Science*, **1998**, *69*, pp 1563-1574.

15. Lin, J. R.; Chen, W. Study on Shape-Memory Behavior of Polyether-Based Polyurethanes. II. Influence of Soft-Segment Molecular Weight. *Journal of Applied Polymer Science*, **1998**, *69*, pp 1575-1586.

16. Li, F.; Hou, J.; Zhu, W.; Zhang, X.; Xu, M.; Luo, X.; Ma, D.; Kim, B. K. Crystallinity and Morphology of Segmented Polyurethanes with Different Soft Segment Length. *Journal of Applied Polymer Science*, **1996**, *62*, pp 631-638.

17. Li, F.; Zhang, X.; Hou, J.; Xu, M.; Luo, X.; Ma, D.; Kim, B. K. Studies on Thermally Stimulated Shape Memory Effect of Segmented Polyurethanes. *Journal of Applied Polymer Science*, **1996***, 64*, pp 1511-1516.

18. Liu, C.; Qin, H.; Mather, P. T. Review of Progress in Shape Memory Polymers. *Journal Mater. Chem.*, **2007**, *17*, pp 1543-1558.

19. Maiti, P.; Radhakrishnan, G.; Aruna, P.; Ghosh, G. Novel Polyurethane Gels: The Effect of Structure on Gelation. *Macromol. Symp.*, **2006**, *241*, pp 51-59.

20. Merline, J. D.; Reghunadhan Nair, C. P.; Gouri, C.; Bandyopadhyay, G. G.; Ninan, K. N. Polyether Polyurethanes: Synthesis, Characterization, and Thermoresponsive Shape Memory Properties. *Journal of Applied Polymer Science*, **2007***, 107,* pp 4082-4092.

21. Mondal, S.; Hu, J. L. Shape Memory Study of Thermoplastic Segmented Polyurethane: Influence of Hard Segment. *Polymer-Plastics Technology and Engineering,* **2007**, *46*, pp 939-942.

22. Petrovic, Z. S.; Cho, Y. J.; Javni, I.; Magonov, S.; Yerina, N.; Schaefer, D. W.; Ilavsky, J.; Waddon, A. Effect of Silica Nanoparticles on Morphology of Segmented Polyurethanes. *Polymer,* **2004**, *45*(12), pp 4285-4295.

23. Ratna, D.; Karger-Kocsis, J. Recent Advances in Shape Memory Polymers and Composites: A Review. *J Mater Sci.*, **2008**, *43*, pp 254-269.

24. Sheth, J. P.; Klinedinst, D. B.; Pechar, T. W.; Wilkes, G. L.; Yilgor, E.; Yilgor, I. Time-Dependent Morphology Development in a Segmented Polyurethane with Monodisperse Hard Segments Based on 1, 4- phenylene diisocyanate. *Macromolecules*, **2005**, *38 (24)*, pp 10074-10079.

25. Shieh, Y.; Chen, H.; Liu, K.; Twu, Y. Thermal Degradation of MDI-Based Segmented Polyurethanes. *Journal of Polymer Science*, **1999**, *37,* pp 4126-4134.

26. Takahashi, T.; Hayashi, N.; Hayashi, S. Structure and Properties of Shape-Memory Polyurethane Block Copolymers. *Journal of Applied Polymer Science*, **1996**, *60*, pp 1061-1069.

27. Tien, Y. I.; Wei, K. H. The Effect of Nano-sized Silicate Layers from Montmorillonite on Glass Transition, Dynamic Mechanical, and Thermal Degradation Properties of Segmented Polyurethanes. *Journal of Applied Polymer Science*, 86: 1741-1748 (2002).

28. Thomson, T. *Polyurethanes as Specialty Chemicals: Principles and Applications.* CRC Press: Boca Raton, FL, 2004.

29. Tobushi, H.; Hashimoto, T.; Ito, N. *J Intell. Mat. Syst. Struct.*, **1998**, *9*, pp 127-135.

30. Versteegen, R. M.; Kleppinger, R.; Sijbesma, R. P.; Meijer, E. W. Properties and Morphology of Segmented Copoly(ether urea)s With Uniform Hard Segments. *Macromolecules*, **2006**, *39*, pp 772-783.

31. Xu, Y.; Petrovic, Z.; Das, S.; Wilkes, G. L. Morphology and Properties of Thermoplastic Polyurethanes with Dangling Chains in Ricinoleate-Based Soft Segments". *Polymer*, **2008**, *49*, pp 4248–4258.

32. Yang, J. H.; Chun, B. C.; Chung, Y.; Cho, J. H. Comparison of Thermal/Mechanical Properties and Shape Memory Effect of Polyurethane Block-Copolymers with Planar or Bent Shape of Hard Segment. *Polymer*, **2003**, *44*, pp 3251-3258.

33. Yeh, J.; Yao, C.; Hsieh, C.; Yang, H.; Wu, C. Preparation and Properties of Amino-Terminated Anionic Waterborne-Polyurethane-Silica Hybrid Materials through a Sol-Gel Process in the Absence of an External Catalyst. *European Polymer Journal*, **2008**, *44*, pp 2777-2783.

CHAPTER III.

EFFECT OF AGING AND THERMAL TREATMENT

INTRODUCTION

Polyurethane block copolymers play an important role in the area of shape memory polymers. Transitions from the glassy state to the rubbery state in the soft segment phases and the phase separation between the hard and soft segments of the polymer itself are responsible for polyurethane's shape memory behavior [Cho et al., 2004]. Due to the importance of chemical structure for shape memory behavior, researchers have focused on the microphase and macrophase separation behavior and the corresponding impact on structural and physical properties. Additionally, the properties of segmented polyurethanes have been observed to be highly time dependent [Tey et al., 2006]. Moreover, in addition to the chemical structure and composition of the polymer molecules, the shape recovery behavior of the specimens may be influenced by their processing conditions during preparation [Li et al., 1997].

Researchers have shown that amorphous solids are not thermodynamically stable at temperatures below their transition temperature [Simon, 1930; Kovacs, 1963]. Instability occurs when this state is not in equilibrium. Studies of glassy materials have shown that a slow process occurs in which an attempt to reach and establish equilibrium is made. During this approach towards equilibrium, many properties of the material are affected. As these properties change with time, the material is said to undergo physical aging [Struik, 1978]. The physical aging phenomenon

77

encompasses a wide range of behaviors, all of which include an observed change in a polymer property as a function of storage time, at constant temperature and zero stress, and with no other influence from external conditions [Hutchinson, 1995]. Physical aging is distinguished from chemical or biological aging, which involve permanent modification of the chemical or physical structure, because it involves only reversible changes in properties [Hutchinson, 1995]. During the aging process, a gradual continuation of the glass form sets in around the glass transition temperature of the polymer. This impacts the temperature dependent properties that often change drastically at or around the transition temperature. Properties will change in the same direction as during cooling through the glass transition range. Therefore, the material becomes stiffer, experiences decreased damping, and creep and stress relaxation rates [Struik, 1978].

Since the aging process affects many polymer properties, it is very important to understand for controlling polymer properties for use in practical applications [Struik, 1978; Li et al., 1997]. Thus, this portion of the work explores the aging of segmented polyurethanes as well as the effect of thermal treatment on the final morphology, thermal and mechanical properties of polyurethane. It is hypothesized that the properties will be influenced by both thermal treatment and aging.

MATERIALS & METHODS

Two series of linear, thermoplastic polyurethanes with 32 wt% hard segment content were prepared as outlined in Chapter II. Upon completion of film preparation, samples were characterized both with and without thermal treatment. Samples designated as "no thermal treatment" were tested at ambient conditions while samples designated as "with thermal

78

treatment" were first conditioned to 80°C for three hours in a convection oven and then allowed to cool in the oven for 2 hours prior to characterization. The morphology and thermal and mechanical properties of all samples were evaluated.

TECHNIQUES

Atomic force microscopy (AFM), differential scanning calorimetry (DSC), and tensile measurements were performed as outlined in Chapter II.

Atomic Force Microscopy (AFM)

As outlined in Chapter II, atomic force microscopy (AFM; Veeco Instruments Inc., Dimension 3100) in tapping mode was used to evaluate sample morphology. Sample preparation was previously discussed. In order to evaluate the effects of time/aging on sample morphology, images were initially taken at ambient conditions immediately following their preparation. This was designated as time zero. Samples were then stored at -20°C between subsequent viewings.

RESULTS AND DISCUSSION

TDI System

Annealing

An annealing treatment was performed on the TDI system at an intermediate temperature between the crystallization and melting temperatures ($T_{annealing}$ = 0 or 5°C). Annealing is the use of a heat treatment to alter a material's morphology and properties. When the polymer is heated above a transition temperature for an arbitrary amount of time and then allowed to gradually cool, the internal stress of the material is removed. The annealing treatment was performed

using a differential scanning calorimeter. The samples were first heated from room temperature to 180°C at a rate of 10°C/min. They were then cooled from 180°C to -50°C at 10°C/min. Next, they were heated from -50°C to 0°C (for TDI 2000/32 samples) or 5°C (for TDI 2900/32 samples). Samples were held at the annealing temperature ($T_{annealing}$) for the selected amount of time. Finally, they were heated from the $T_{annealing}$ to 180°C. The results for annealing times ranging from 0 to 120 minutes are shown in Table III-1.

Annealing Time [min]	$T_{crystallization}$ SS [ºC]	$\Delta H_{crystallization}$ SS [J/g]	$T_{melting}$ SS [ºC]	$\Delta H_{melting}$ SS[J/g]
0	-15.86	-30.11	23.94	35.74
30	-19.97	-29.01	25.09	42.30
60	-18.04	-29.90	23.95	45.07
120	-17.18	-29.58	23.95	45.16

Table III-1. Effects of annealing time on melting and crystallization transitions of the TDI 2900/32 system.

From the annealing results, it can be seen that the melting temperature ($T_{melting}$ SS) does not change with annealing, indicating that the crystals are not perfected. However, the enthalpy of melting ($\Delta H_{melting}$ SS) increases with annealing time which indicates that the amount of crystals is increasing. This confirms that initial phase separation is incomplete immediately after film forming. Figure III-1 shows further evidence of these results. From this graph it is clear that the enthalpy of melting reaches a plateau at approximately 60 minutes. This indicates that the TDI 2900/32 samples experience a very short aging period.
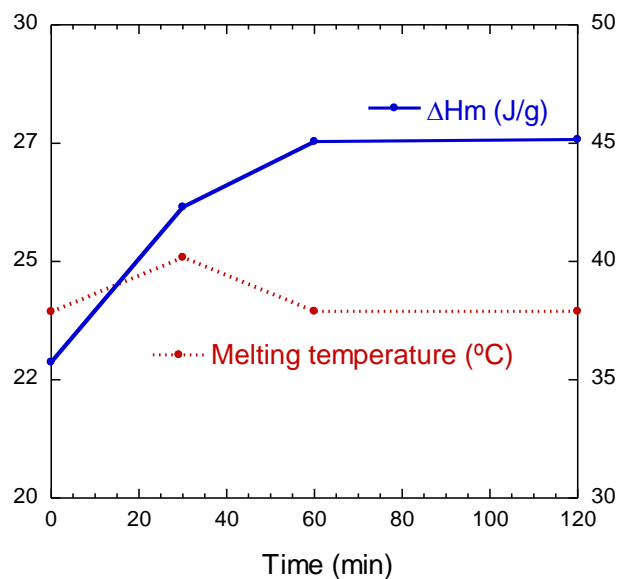
Figure III-1. Effect of annealing time on the melting temperature and enthalpy of melting for the TDI 2900/32 system.

Annealing results for the TDI 2000/32 system are shown in Table III-2. With this system two things were noticed: the enthalpy of melting of the soft segments increases from 0 to 60 minutes and if the annealing is performed to 180°C instead of 280°C no transitions are observed. It is unknown whether the enthalpy of melting continues to increase as the annealing time is increased above 60 minutes. Also, the behavior exhibited in the annealing testing is similar to the DSC results, which will be discussed later in the chapter, in which no thermal treatments are present for samples that are not first subjected to a thermal treatment.

Annealing Time [min]	$T_{crystallization}$ SS [ºC]	$\Delta H_{crystallization}$ SS [J/g]	$T_{melting}$ SS [ºC]	$\Delta H_{melting}$ SS[J/g]
0	No crystallization was noticed		19.1	16.23
60			20.13	34.96

Table III-2. Effects of annealing time on melting and crystallization transitions of the TDI 2000/32 system.

Mechanical Properties

The mechanical properties for the TDI 2000/32 system both with and without thermal treatment are shown below in Table III-3. The properties for all samples tested are relatively constant over the time studied (80 days) with the values obtained immediately following sample preparation showing no significant change as the sample is aged. As previously discussed, the aging period for the TDI system is very short so there were no visible changes expected in the time period studied due to the polymer samples reaching an equilibrium so soon after sample completion.

TDI 2000/32	E [MPa]		σ_y [MPa]		ε_b [%]	
Days	No Thermal Treatment	With Thermal Treatment	No Thermal Treatment	With Thermal Treatment	No Thermal Treatment	With Thermal Treatment
0	0.7 ± 0.06	1.0 ± 0.2	0.3 ± 0.03	0.4 ± 0.07	891.8 ± 58.7	849.6 ± 111.0
6	0.9 ± 0.2	1.2 ± 0.3	0.4 ± 0.04	0.5 ± 0.05	543.9 ± 53.8	672.3 ± 33.0
80	1.0 ± 0.05	1.5 ± 0.4	0.4 ± 0.03	0.6 ± 0.05	865.5 ± 77.4	492.1 ± 36.2

Table III-3. Tensile properties as a function of time for TDI 2000/32 samples.

The TDI 2900/32 system showed similar behavior to the TDI 2000/32 system. The mechanical properties, shown in Table III-4, exhibited no significant changes and remained relatively constant over the 80 day time period studied.

TDI 2900/32	E [MPa]		σy [MPa]		εb [%]	
Days	No Thermal Treatment	With Thermal Treatment	No Thermal Treatment	With Thermal Treatment	No Thermal Treatment	With Thermal Treatment
0	4.68±0.52	5.06±0.20	0.62±0.056	1.03±0.21	1150.6±140.0	1202.7±52.2
6	2.56±0.19	4.98±0.68	1.03±0.078	1.15±0.040	1257.36±140.2	1214.0±175.8
80	3.80±0.10	4.74±0.68	1.01±0.21	1.46±0.25	959.5±227.1	770.2±459.8

Table III-4. Tensile properties as a function of time for TDI 2900/32 samples.

The constancy of the tensile properties supports the annealing findings that the samples reach equilibrium in a very short period of time. Aging has very little effect on the mechanical properties of the TDI system.

Morphology

Tapping mode AFM was used to study the evolution of the polymer structure over time. Attempts were made to take images of the TDI 2000/32 samples prior to conditioning at -20°C. However, no images were obtainable. The sample was completely clear which suggests that no phase separation is present in the sample immediately following its preparation. The image taken 2 days after the sample was prepared, shown in Figure III-2, however, shows that crystalline regions are developing over time. When the development of a crystalline structure occurs so does phase separation and the ability to obtain AFM images.
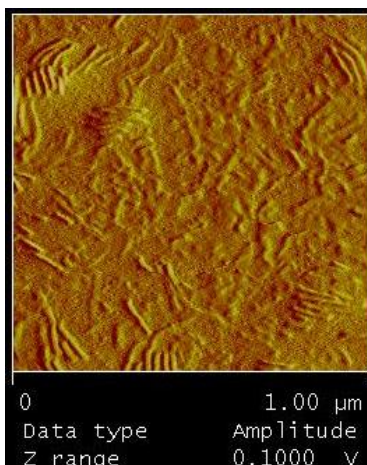
Figure III-2. TDI 2000/32 sample morphology at 2 days after sample preparation.

The TDI 2900/32 system showed similar behavior to that of the TDI 2000/32 system. The images obtained at time Day 0, Day 1, and Day 2, are shown in Figures III-3 a, b, and c, respectively. The main difference is that an image was obtained for time= Day 0, prior to sample conditioning at -20°C. While the image does exhibit a phase separated structure, there were bubbles present in the sample that were visible to the naked eye. It is believed that the structures that are visible in the AFM images are these bubbles, which are attributed to the solvent evaporation during the sample preparation. When subsequent images were taken of the TDI 2900/32 system after conditioning at -20°C, a structure very similar to that present in the TDI 2000/32 system develops.
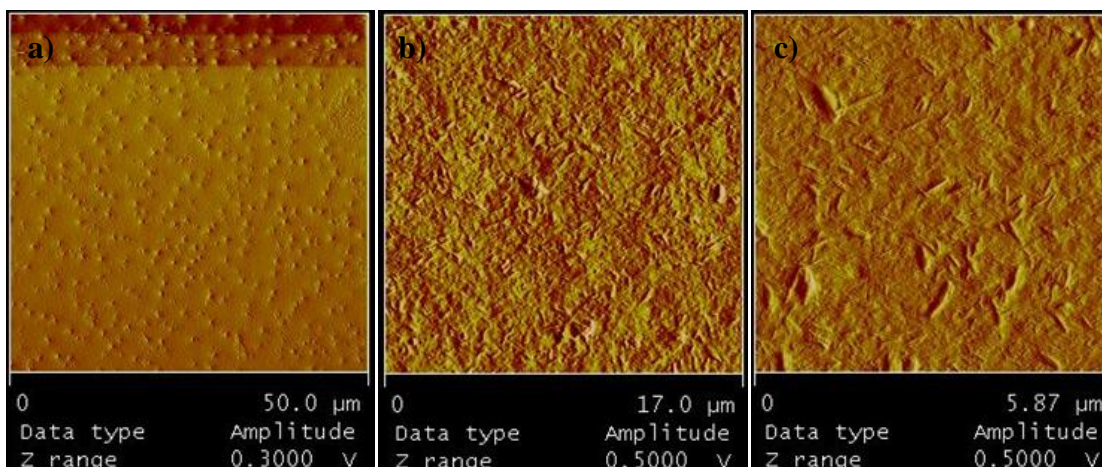
Figure III-3. TDI 2900/32 sample morphology at times a) Day 0, b) Day 1, and c) Day 2.

From the atomic force micrographs presented for the TDI 2000/32 and TDI 2900/32 samples, the combined effect of aging and thermal effects are obvious. Aging at a low temperature allows for organization and development of a crystalline structure within the samples. This structure will have a substantial impact on the thermal and mechanical properties of the samples.

Thermal Properties (DSC)

In order to further evaluate the development of organizational order of crystalline domains within the polymer structure, DSC was used. DSC indicates the degree of organizational order of crystalline domains through the melting behavior of the crystalline phase and the interaction between the hard and soft segments [Petrovic, 2004]. Since the molecular rearrangement that occurs in the samples is the focus of this study, the thermal transitions obtained during the first thermal cycle were evaluated.

The thermal transitions for the soft segments of the TDI 2000/32 system are shown in Table III-5. Transitions were only observed for the TDI 2000/32 samples with no thermal treatment. No

transitions, melting or crystallization, appeared in the first run for samples that had been subjected to thermal treatment prior to testing. The morphology of the TDI 2000/32 system exhibited little to no phase separation. The DSC results further reinforce this conclusion. Additionally, the lack of transitions for the samples that were subjected to thermal treatment suggests that the thermal treatment is effective in erasing the thermal history of the material.

TDI 2000/32 No Thermal Treatment	Run 1			
	Tm SS [°C]	ΔH [J/g]	Tc SS [°C]	ΔH [J/g]
Day 0			-27.9	5.57
Day 6			-28.92	3.59
Day 80			-29.28	5.546

Table III-5. Thermal transitions of the TDI 2000/32 system.

The DSC results for the TDI 2900/32 system are shown in Table III-6. Samples tested periodically over the 80 day period studied, show constant transition temperatures. As expected, the effect of aging has very little impact on these samples due to the short time required to reach equilibrium.

TDI 2900/32 No Thermal Treatment	Run 1			
	Tm SS [°C]	ΔH [J/g]	Tc SS [°C]	ΔH [J/g]
Day 0			-12.98	26.82
Day 6			-7.63	31.81
Day 80			-14.7	27.8

Table III-6. Thermal transitions of the TDI 2900/32 system.

The thermal transitions for TDI 2900/32 samples that were subjected to thermal treatment are in the same range as those that were not. The values are shown in Table III-7.

TDI 2900/32 With Thermal Treatment	Run 1			
	Tm SS [°C]	ΔH [J/g]	Tc SS [°C]	ΔH [J/g]
Day 0			-9.71	30.21
Day 6			-13.6	26.14
Day 80			-15.68	28.03

Table III-7. Transitions of the TDI 2900/32 system after subjecting to thermal treatment.

MDI System

Mechanical Properties

The tensile properties for the MDI 2000/32 system both with and without thermal treatment are shown in Table III-8. Most samples exhibit a decrease of the modulus and strength in the first 20 days of observation. After this the values reach a plateau and remain relatively constant. The thermal treatment appears to be effective in creating stability of the properties during the first 20 days. After this time, the yield stress and elongation at break remain relatively constant for the remainder of the study. It is important to note, however, that thermal treatment leads to decreased mechanical properties. This effect is expected as thermal treatment leads to more mobility of the soft segments. The contamination of the hard segments with soft segments reduces the hard segment interactions, which leads to a decrease in modulus and strength.

MDI 2000/32	E [MPa]		σ_y [MPa]		ε_b [%]	
Days	No Thermal Treatment	With Thermal Treatment	No Thermal Treatment	With Thermal Treatment	No Thermal Treatment	With Thermal Treatment
0	17.59±5.68	14.90±1.34	4.20±0.09	3.98±0.11	206.0±27.0	133.9±58.8
6	17.33±1.20	13.80±0.52	5.01±0.20	3.95±0.30	608.0±49.5	376.1±62.1
21	16.02±0.49	9.51±0.87	2.20±0.10	1.90±0.20	109.0±36.8	137.6±39.0
35	16.05±1.29	11.88±1.16	2.29±0.09	2.09±0.09	149.1±8.8	165.4±3.1
83	20.57±1.50	13.40±4.07	2.00±0.20	2.01±0.11	109.9±1.0	113.0±7.0

Table III-8. Tensile properties as a function of time for MDI 2000/32 samples.

The tensile properties of the MDI 2900/32 system exhibit behavior similar to that of the MDI 2000/32 system. The mechanical properties are reported in Table III-9. From the table, it is evident that the Young's modulus (E), strength (σ_y), and the deformation at break (ε_b) experience a decrease within the first 20 days. After this time, the properties reach a plateau and the properties remain fairly constant. The effect of thermal treatment on this system is much clearer. From the results, it is obvious that the thermal treatment significantly affects the modulus of the system, with thermally treated samples exhibiting a much lower modulus. Due to the longer length of the short segments, a more pronounced difference is expected for the same reason listed in the MDI 2000/32 system. The additional length of the soft segments, which are now a longer length, produces the decrease in modulus. However, it should be noticed that the thermal treatment has a more significant influence on the elongation at break of this system, with the values decreasing approximately 50% during the study.

MDI 2900/32	E [MPa]		σ_y [MPa]		ε_b [%]	
Days	No Thermal Treatment	With Thermal Treatment	No Thermal Treatment	With Thermal Treatment	No Thermal Treatment	With Thermal Treatment
0	43.68±3.15	13.29±1.56	5.95±0.52	5.21±0.73	751.6±39.3	755.6±39.1
6	23.60±14.5	12.58±1.16	5.99±0.32	4.10±0.07	896.4±52.6	950.1±56.7
21	16.22±4.23	10.53±2.06	2.49±0.55	1.74±0.15	486.1±41.6	432.5±68.4
35	19.53±1.24	10.61±1.64	3.13±0.29	1.82±0.12	535.4±36.5	364.1±86.4
83	26.84±5.20	10.23±1.85	4.28±0.31	1.77±0.03	523.0±106.4	357.6±125.5

Table III-9. Tensile properties as a function of time for MDI 2900/32 samples.

From the mechanical properties, it is clear that the time required to reach equilibrium is much longer than in the TDI system. Additionally, the structure of polyurethanes constructed with hard segments of MDI or TDI produces a large difference in not only the mechanical properties of the polymer itself, but also a difference in the way samples react to aging and thermal treatment.

Morphology (AFM)

Tapping mode AFM amplitude images of the solid MDI 2000/32 polyurethane films taken immediately following sample preparation and 3 days after sample preparation are presented in Figure III-4 a) and b), respectively. In these images, the phase segregation of the hard and soft segments is clearly visible. However, it is difficult to determine if any evolution of the samples is occurring during the time evaluated.
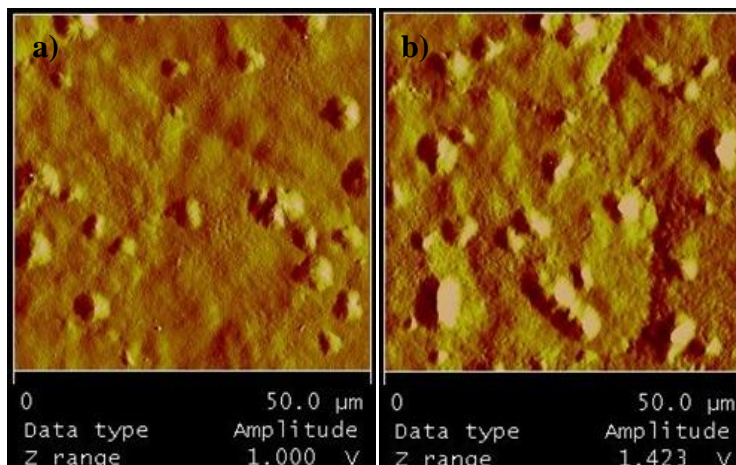
Figure III-4. MDI 2000/32 sample morphology at time a) Day 0 and b) Day 3.

The images for the MDI 2900/32 samples immediately following sample preparation and 3 days later are shown in Figure III-5 a) and b). Phase separation of the hard and soft segments is clearly visible at Day 0. Once again, the changes during the time evaluated are not significant enough to observe.
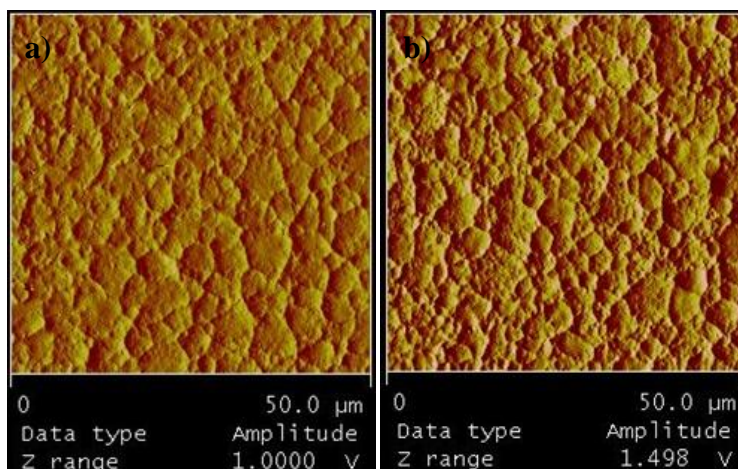
Figure III-5. MDI 2900/32 sample morphology at time a) Day 0 and b) Day 3.

The effect of aging on the polymer morphology is less noticeable in the MDI system is less than in the TDI system. This does not mean that there is no impact but merely that the changes are

minute during the short time period in which polymer morphology was observed. It should be noted, however, that the MDI system has a much less active structure at room temperature due to the to the structure of the diisocyanates, which was previously discussed in Chapter II, and the length of the soft segments, which effects the polymer's mobility and ability to crystallize. This decreased activity of the structure leads to a much longer aging period to reach equilibrium in the MDI system, which was also observed in the mechanical properties, and leads to the expected result of less observation of aging impact during a very short time period.

Thermal Properties

DSC was used to further investigate the crystal structure of the MDI system. First, the MDI 2000/32 samples with no thermal treatment were evaluated. Once again, the focus was on thermal transitions occurring in the first DSC cycle. The thermal transitions are shown in Table III-10. Transitions for both melting and crystallization of the soft segments were observed. This corresponds to the AFM images which show clear phase separation in the polymer morphology. While the melting transitions do not exhibit a clear trend, it is clear from the increase of the crystallization transition of the soft segments that as the polymer ages increased crystallization of the soft segments is occurring.

MDI 2000/32 No Thermal Treatment	Run 1			
	Tm SS [°C]	ΔH [J/g]	Tc SS [°C]	ΔH [J/g]
Day 0	12.54	27.16	-12.82	25.75
Day 6	11.51	43.55	-10.44	30.39
Day 21	13.75	32.45	-13.81	25.12
Day 35	11.35	41.71	-13.87	22.17
Day 83	9.56	25.18	-17.32	22.92

Table III-10. Thermal transitions of the MDI 2000/32 system.

MDI 2000/32 samples subjected to thermal treatment also exhibited thermal transitions in the first DSC cycle. The values for these transitions are listed in Table III-11. The thermal transitions of heat treated samples exhibit a trend similar to the mechanical properties. The melting and crystallization temperatures of the soft segments exhibit a decrease until day 21. After this, the values remain relatively constant. This indicates that the heat treatment is effective in reducing the internal stress of the polymer chains.

MDI 2000/32 With Thermal Treatment	Run 1			
	Tm SS [°C]	ΔH [J/g]	Tc SS [°C]	ΔH [J/g]
Day 0	11.38	26.57	-14.28	26.72
Day 6	10.46	35.58	-12.05	28.54
Day 21	9.89	21.6	-14.0	25.63
Day 35	14.2	38.84	-13.99	23.96
Day 83	11.5	25.85	-15.17	24.08

Table III-11. Thermal transitions for MDI 2000/32 samples with thermal treatment.

Next, the crystalline structure of the MDI 2900 system was evaluated using DSC. This system also exhibited a phase separated structure when viewed using AFM. During DSC, this sample exhibited transitions for the melting and crystallization of the soft segments and also crystallization of the hard segments, which was not exhibited in the other polyurethane systems. Due to the observance of the crystallization of the hard segments, it can be concluded that the degree of phase separation in the MDI 2900/32 system is higher than that in the other systems. Samples from the MDI 2900/32 system behave similarly to that of the MDI 2000/32 system. From the data for samples with no thermal treatment, Table III-12, there is once again no visible trend in the values.

MDI 2900/32 No Thermal Treatment	Run 1					
	Tm SS [°C]	ΔH [J/g]	Tc HS [°C]	ΔH [J/g]	Tc SS [°C]	ΔH [J/g]
Day 0	14.79	62.60	*	*	-1.60	36.81
Day 6	15.96	41.83	167.03	1.99	-1.14	35.67
Day 21	18.77	52.16	166.93	2.60	-0.75	40.15
Day 35	18.13	46.39	166.18	2.09	-2.07	35.48
Day 83	17.74	42.64	166.06	2.31	-2.13	37.95

Table III-12. Thermal transitions for MDI 2900/32 samples with no thermal treatment.
* indicates that no transition was observed.

Thermal treatment of the MDI 2900/32 system, Table III-13, creates a similar decrease in the melting transition temperature of the soft segments over the period of time studied. Additionally, the crystallization temperature of the soft segments moves to a lower temperature. The crystallization temperature of the hard segments, however, seems to be unaffected. These results are expected. As previously observed, samples with no thermal treatment experience an increase in melting temperature over the aging period examined. The decrease in soft segment melting

temperature exhibited by samples which have been subjected to thermal treatment is due to the mobility of the polymer chains, which is enhanced by the thermal treatment prior to DSC experiments. Additionally, the temperature of the thermal treatment, 80°C, is not high enough to impact the soft segments so, similar to the samples with no thermal treatment, no changes are observed in these transitions as a result of the thermal treatment.

MDI 2900/32 With Thermal Treatment	Run 1					
	Tm SS [°C]	ΔH SS [J/g]	Tc HS [°C]	ΔH_c HS [J/g]	Tc SS [°C]	ΔH_c SS [J/g]
Day 0	15.77	63.12	165.97	1.97	-0.27	41.31
Day 6	16.21	60.30	168.94	2.46	-0.08	38.49
Day 21	14.66	41.03	168.25	2.01	-1.30	37.14
Day 35	13.76	45.17	165.40	1.99	-2.58	37.47
Day 83	11.29	29.59	165.05	2.20	-2.76	38.07

Table III-13. Thermal transitions of the MDI 2900/32 system after thermal treatment.

The MDI system has a more regular, oriented structure. This structure, which can be viewed in the AFM and is exhibited in the thermal transitions gained from the DSC, leads to increased phase separation and decreased activity or mobility of the structure at room temperature. Additionally, thermal treatment is effective in influencing polymer properties.

CONCLUSIONS

The effects of aging and thermal treatment on the morphology and thermal and mechanical properties of synthesized linear, thermoplastic polyurethanes were studied. It was found that a very short period of time (approximately 1 hour) is required to reach equilibrium for samples with hard segments composed of TDI. However, samples with hard segments composed of MDI

take much longer to reach equilibrium (approximately 20 days). The use of thermal treatment was effective in the MDI system but showed little effect in on the TDI system. The properties and morphology of the polymers were affected by the age and thermal history of the samples. From this study, the impact of the age of the polymer on its properties was recognized. From this point on in the research, it was recognized that the results of polyurethane characterization were highly time dependent.

REFERENCES

1. Cho, J. W.; Jung, Y. C.; Chung, Y-C.; Chun, B. C. Improved Mechanical Properties of Shape-Memory Polyurethane Block Copolymers through the Control of the Soft-Segment Arrangement. *Journal of Applied Polymer Science*, **2004**, *93*, pp 2410–2415.

2. Crawford, D. M.; Bass, R. G.; Haas, T. W. Strain Effects on Thermal Transitions and Mechanical Properties of Thermoplastic Polyurethane Elastomers. *Thermochimica Acta*, **1998**, *323*, pp 53-63.

3. Hutchinson, J. M. Physical Aging of Polymers. *Prog. Polym. Sci.,* **1995***, 20*, pp 703-760.

4. Kovacs, A. J. Glass Transition in Amorphous Polymers. A Phenomenological Study. *Fortschr. Hochpolym. Forsch.*, **1963**, *3*, pp 394-507.

5. Li, F.; Zhang, X.; Hou, J.; Xu, M.; Luo, X.; Ma, D.; Kim, B. K. Studies on Thermally Stimulated Shape Memory Effect of Segmented Polyurethanes. *J Appl Poly Sci*, **1997**, *64*, pp 1511-1516.

6. Petrovic, Z. S.; Cho, Y. J.; Javni, I.; Magonov, S.; Yerina, N.; Schaefer, D. W.; Ilavsky, J.; Waddon, A. Effect of Silica Nanoparticles on Morphology of Segmented Polyurethanes. *Polymer*, **2004**, *45*(12), pp 4285-4295.

7. Simon, F. *Ergeb. exakt. Naturwiss,* **1930**, *9*, pp 222–274.

8. Struik, L. C. E. *Physical Aging in Amorphous Polymers and Other Materials*, 2nd ed., Elsevier: Amsterdam, 1978.

9. Tey, J. N.; Soutar, A. M.; Mhaisalkar, S. G.; Yu, H.; Hew, K. M. Mechanical Properties of UV-Curable Polyurethane Acrylate Used in Packaging of MEMS Devices. *Thin Solid Films*, **2006**, *504*, pp 384-390.

CHAPTER IV.

PREPARATION OF NANOREINFORCEMENTS

INTRODUCTION

A composite is a material that is composed of two or more different materials in order to blend/combine the best properties of each of the constituents. Similarly, a polymer nanocomposite is also composed of two materials: one being a continuous polymeric material, which may be a thermoset, thermoplastic, or elastomer, and the other being a discontinuous reinforcing material in the nanoscopic range (one of the characteristic dimensions should be in the nanometer range). This reinforcing material is known by a variety of different names such as nanoreinforcement, nanofiller, or nanoparticle [Koo, 2006]. Even though nanocomposites have been in existence for centuries, they were not recognized until modern characterization techniques evolved. In fact, the term nanocomposite was not coined until 1986 [Twardowski, 2007]. Research articles involving nanocomposites have appeared in a wide variety of journals and now journals and books are being dedicated totally to the subject [Paul & Robeson, 2008]. Within the field, many diverse topics exist such as composite reinforcement, barrier properties, flame resistance, cosmetic applications, bactericidal properties, and biomedical applications [Twardowski, 2007; Njuguna et al., 2008].

Traditional, macroscale composites require more than 40 wt% reinforcement to induce a considerable increase in properties. Nanocomposites, however, exhibit property enhancements

97

with as little as 0.5wt% reinforcement [Wouterson et al., 2007]. Property enhancements using reinforcements in the range of micrometers include increases in thermal stability, stiffness, and strength of the employed polymer matrix [Angelovici et al., 1998; Kazanci, 2004]. However, utilization of reinforcements with such a large size does have its drawbacks. Reductions in strain to failure, impact strength, and fracture toughness are often observed [Friedrich et al., 2005]. Due to their high aspect ratio (ratio of length to diameter), nanoparticle incorporation offers a way to achieve the same property enhancements without many of the drawbacks witnessed from microreinforcements. Even nanocomposite materials with particle sizes exceeding 20 nanometers have exhibited the ability to increase properties over neat polymer matrices [Friedrich et al., 2005].

As previously discussed, shape memory polyurethanes exhibit disadvantages of lower strength and stiffness, which limits their application. The use of nanofillers in a shape memory polyurethane matrix has been widely investigated as a way to overcome these disadvantages and to increase the application areas of the polymer [Ratna & Karger-Kocsis, 2008]. Due to the wide variety of available nanofillers and their vastly different properties, it is important to choose a nanofiller/polymer system that fits the desired end use. Nanofillers possess many advantages. However, as with any material there are disadvantages. While the focus of this research is the enhancement of the mechanical, thermal, and shape memory properties, it is important to note that selection of the correct nanofiller for a composite system can also lead to improvements in barrier properties, flame retardant properties, dimensional stability, thermal conductivity, chemical resistance, and ablation resistance. For example, silicon carbide (SiC) was shown to produce an increase in micro-hardness and modulus [Gall et al., 2002], exfoliated nanoclays have

been studied for barrier and flame retardant applications [Choi et al., 2006; Pluta et al., 2002], and carbon nanotubes are being researched for their conductive properties [Baibarac & Gomez-Romero, 2006]. Additionally, the use of conductive nanofillers in segmented shape memory polyurethanes may lead to alternate pathways for shape memory actuation. The major disadvantages associated with the use of nanofillers come with dispersion and processability [Koo, 2006]. Of course, the main advantage lies in the nanocomposite system itself. Nanocomposites offer the ability to construct lighter, stronger, and thinner structures. The ability of polymer nanocomposites to produce these structures is already being achieved in many commercial applications [Njuguna et al., 2008].

The nanoreinforcements chosen for investigation during this research are cellulose nanofibers (CNF), conductive cellulose nanofibers (C-CNF), and carbon nanotubes (CNT). Cellulose, a natural and biodegradable nanofiller which constitutes the primary structural material in a wide variety of plant life, is one of nature's most abundant materials [Eichhorn & Young 2001]. Natural nanofillers offer many advantages over conventional reinforcement materials. They are low in cost and density, have high specific properties, are non-abrasive, and are a renewable and biodegradable resource [Zadorecki & Michell 1989; Boldizar et al., 1987; George et al., 2001]. They are readily available and are comparable to other reinforcing materials for property enhancements. There are disadvantages, however, such as incompatibility with hydrophobic polymer matrices and aggregation during processing.

Cellulose fibers are composed of assemblies of microfibrils, which form slender and nearly endless rods [Mark, 1980; Marchessault & Sundarrjan, 1983]. Hydrogen bonding is responsible for the attraction that these nano/micro crystals possess. Upon exposure to strong acids, the

microfibrils are degraded into microcrystals that are similar in structure to the parent microfibril but with shorter lengths ranging from a few hundred nanometers to a few microns. However, depending on the treatment efficiency, some association between crystals may remain and has been reported by other authors [Ebeling et al., 1999]. Additionally, cellulose possesses polar groups that can interact with SMPu. The structure of cellulose is shown in Figure IV-1.
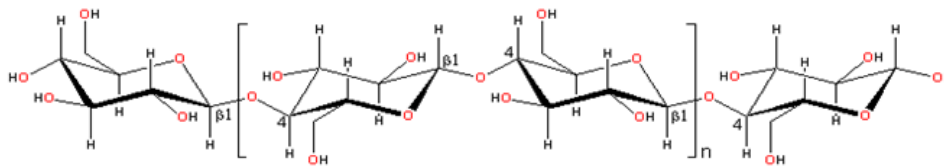
Figure IV-I. Chemical structure of cellulose.

During polyurethane synthesis it is possible for the –OH group of cellulose to co-react with the polyurethane. This interaction leads to strong interfacial adhesion that is necessary for property enhancement in nanocomposites. During this portion of the work, cellulose nanofibers will be achieved through acid hydrolysis of microcrystalline cellulose. This treatment will aid in achieving stable suspensions of cellulose crystals in an organic polar solvent, dimethylformamide (DMF), for incorporation into a polymer matrix. This portion of the work is closely related to that of Dufresne and coworkers, who attempted to incorporate cellulose crystals into polymeric matrices [Favier et al., 1995; Dufresne and Vignon, 1998; Dufresne and Cavaille, 1999; Neus Angles and Dufresne, 2000].

Cellulose nanofibers coated with polyaniline, in order to achieve conductive cellulose nanofibers (C-CNF), presents a new approach to creating conductive polymers through the use of nanoreinforcement. Polyaniline was chosen for this application due to its good environmental

100

stability, low cost, and easy polymerization. Conducting polymers have gained attention due to the possibility of commercial applications. However, conductive polymers present a challenge for applications due to their low mechanical properties [Malmonge et al., 2001]. In this research, a way to overcome this challenge will be investigated. By coating a nanoreinforcement, such as CNF, with polyaniline, and then creating a nanocomposite, it is expected that a non-conductive polymer will not only gain the conductive properties of the polyaniline but will also experience an increase in mechanical properties due to the nanoreinforcement material. Additionally, the use of electrically conductive cellulose opens the door to a new pathway for actuation of shape memory polyurethanes. Electrical conduction of the nanoreinforcements may be used to induce the shape memory effect in the polyurethane matrix.

The use of synthetic carbon nanotubes as a nanoreinforcement presents another challenge. While carbon nanotubes possess a number of advantages, such as excellent mechanical properties, increased electrostatic discharge, chemical stability, low density, and conductivity, their poor surface reactivity and high aspect ratio create dispersion problems in nanocomposites [Chen et al.,2006; Auad et al., 2009]. Synthetic CNT are generally incompatible with organic molecules, including polymers. Entanglements are usually encountered due to the extremely high aspect ratio and can cause difficulty when preparing CNT nanocomposites [Ajayan et al., 2000; Zhou et al., 2003; Cadek et al., 2004; Andrews et al., 2002; Sun et al., 2002]. For this reason, several researchers have focused on surface functionalization of CNT to aid in nanofiller dispersion [Auad et al., 2006; Cui et al., 2003; Gong et al., 2000]. During these studies, functionalization methods have been described including covalent bonding methods in which carboxyl groups on the CNT surface are converted to organic groups in order to improve the surface group reaction

efficiency between the CNT and the SMPu [Auad et al., 2006]. This research will study the synthesis, modification, and characterization of nanofillers as a means to overcome the challenges associated with dispersion and agglomeration.

MATERIALS

Microcrystalline cellulose powder (MCC; Avicel PH-101 MCC, FMC Biopolymer, Philadelphia, PA) was selected as the raw material for obtaining cellulose nanocrystals.

In order to obtain conductive cellulose nanofibers, aniline, ammonium peroxydisulfate (APS), hydrochloric acid (HCL), *p*-toluenesulfonic acid (*p*TSA), sulphonated lignin acid (SLA), dodecylbenzenesulfonic acid (DBSA), ammonium hydroxide (NH_4OH), and sulfuric acid were purchased from Sigma-Aldrich and used without treatment.

Multi-walled carbon nanotubes (Shengzhen Nanotech Port Co., China) were used after corresponding chemical modifications. Technical specifications for the multi-walled carbon nanotubes are a diameter range of 40-60nm, length range of 5-15µm and purity of 95%. The functionalization of the multi-walled carbon nanotubes utilized sulfuric acid (H_2SO_4), 70% HNO_3, acetone, and methylenedi-p-phenyl diisocyanate (MDI), which were purchased from Sigma-Aldrich and used without treatment.

METHODS

Cellulose Nanofibers (CNF)

Cellulose nanofibers (CNF) were obtained by subjecting MCC to acid hydrolysis in a concentrated sulfuric acid solution (64wt% sulfuric acid in deionized water). The ratio of MCC to sulfuric acid solution was 1:8.75 g/ml. The treatment was performed at 45°C under strong stirring for 2 hours. To aid in dispersion, the solution was subjected to a 10 min ultrasonic treatment (Ultrasonik 250, NEY). The solution was then diluted with an equal volume of water and washed repeatedly. Centrifugation (12000 rpm, 10 min) was used to separate MCC from the aqueous solution. This process was performed until a pH of 5 was obtained. The final suspension was freeze-dried and stored in a dessicator to avoid moisture absorption from the air.

Conductive Cellulose Nanocrystals (C-CNF)

Conductive cellulose crystals were prepared by through *in situ* polymerization. Aniline was dissolved (0.15 v/v%) in an aqueous solution of HCl (1.0 M). Then, 67 ml of the aniline solution was gently added to 50 ml of the CNF suspension (1 wt/vol %), Finally, 50 ml of a solution of ammonium persulfate (APS) in aqueous HCl (0.25 g of APS in 50 ml of the 1.0 M HCl solution) was added for carrying out the aniline polymerization. The reaction was monitored by open circuit potential using platinum and saturated - calomel electrodes. A schematic of the set up used for the open circuit potential (Voc) measurements taken during the polymerization is shown below in Figure IV-2. During the final stage the mixture took the characteristic dark green color, which corresponds to the emeraldine oxidation state of the conductive polyaniline. The resulting coated cellulose was washed repeatedly and finally dialyzed [Mattoso et al., 2009].
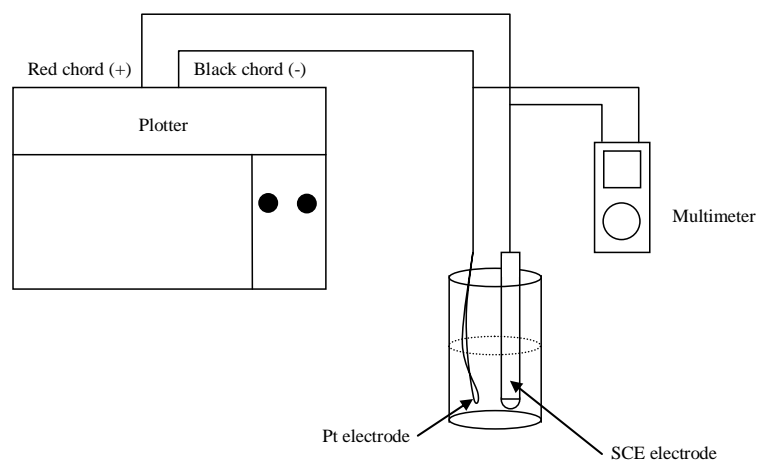
Figure IV-2. Schematic representation of the set up used for open circuit potential (Voc) measurements during polymerization of aniline.

Carbon Nanotubes (CNT)

As-received multi-walled carbon nanotubes (MWNTs) were purified and acidified by means of ultrasonication in concentrated acid solution (3:1 H_2SO_4/70% HNO_3) for 1 h at room temperature. After exhaustive washing, drying and grinding, carbon nanotubes were re-dispersed in acetone for reaction with excess methylenedi-p-phenyl diisocyanate (MDI). The solution containing CNTs and MDI was refluxed and sonicated. The sample was thoroughly washed to remove excess MDI. The resulting modified carbon nanotubes, CNT-MDI, were stored in a desiccator to avoid moisture. The reaction steps are shown in Figure IV-3. Functionalized CNTs provide bonding sites to the polymer matrix so that the load can be transferred to the nanotubes to prevent separation between the polymer surface and nanotubes. Interfacial adhesion of nanoreinforcements in the polymer matrix is important for achieving improved mechanical and thermal properties.
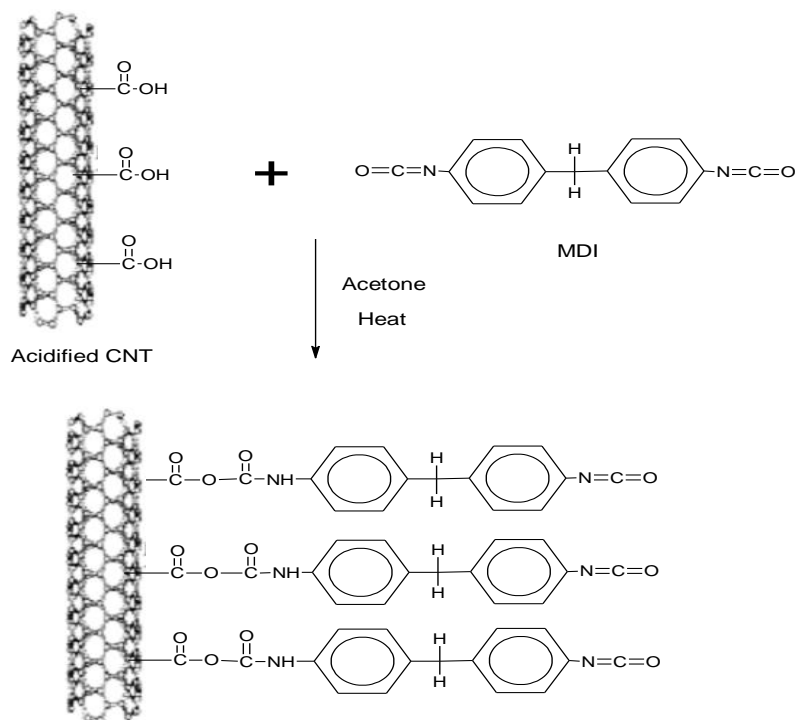
Figure IV-3. The reaction between isocyanate groups and the carboxyl groups on CNTs surface.

TECHNIQUES

Fourier Transform Infrared (FTIR)

Fourier Transform Infrared (FTIR; Nicolet 6700) equipped with an attenuated total reflectance (ATR) stage was used to verify that the –OH groups present in cellulose are available for and participating in the reaction with a polyurethane system.

X-Ray Diffraction

In order to determine the effectiveness of acid hydrolysis in the degradation of the amorphous regions of the cellulose, X-ray diffraction (Philips X-Ray diffractometer Model PW 1830 with Ni-filtered CuKα radiation at 40kV and 30mA) was used. Cellulose prior to and post hydrolysis

were analyzed. Samples were scanned from 2θ=5 to 60° in steps of 0.02°. The resultant peaks of the spectra were deconvoluted using Origin^{TM} software and the areas under the peaks were calculated. The ratio of the area of the crystal peaks to the sum of crystal and background areas was considered the degree of crystallinity.

Scanning Electron Microscopy (SEM)

A scanning electron microscope (Philips model SEM 505) was used to observe the hydrolyzed cellulose fibers (CNF), the conductive cellulose nanofibers (C-CNF), and the functionalized carbon nanotubes (CNT).

Thermal Gravimetric Analysis (TGA)

Thermal gravimetric analysis (TGA; TA Instruments Q500) was employed to observe the degradation behavior of the CNF, C-CNF, and the CNTs. CNF and C-CNF were evaluated from room temperature to 400°C and the CNTs were evaluated from room temperature to 600°C. A heating rate of 10°C/min was used. The enclosure was purged with dry nitrogen.

RESULTS AND DISCUSSION

Cellulose Nanofibers (CNF)

The cellulose nanofibers were evaluated to determine the effectiveness of the acid hydrolysis treatment in degrading the amorphous regions of the cellulose. The crystalline peaks observed in the X-ray diffraction analysis of the post acid hydrolysis MCC show an increased area over cellulose which has not been subjected to treatment. As can be seen in Figure IV-4 below, crystallinity increased from 56% (pre-hydrolysis) to 67% (post hydrolysis). These values are in

the same range as values provided elsewhere in literature for vegetable source cellulose [Eichorn & Young, 2001; Ardizzone et al., 1991; Fink, 1999; Marcovich et al., 2006]. Additionally, this result was expected as the amorphous regions of the MCC are more easily susceptible to acid attack.
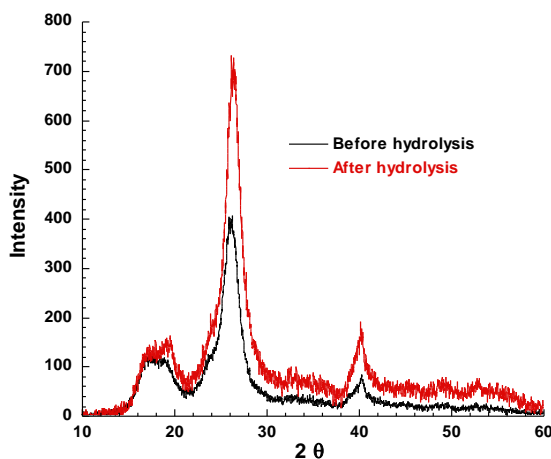
Figure IV-4. X-ray diffraction analysis of pre and post acid hydrolysis MCC.

Morphology

Optical microscopy of the pre-hydrolysis MCC exhibits large agglomerates, which are formed by strong hydrogen bonding, of up to 30µm in size [Marcovich et al., 2002]. Additionally, scanning electron microscopy of the post hydrolysis MCC showed cellulose crystals with diameters of significantly smaller size, in the range of 50-100nm with an average aspect ratio above 50. The optical and scanning electron micrographs can be seen below in Figure IV-5 a and b.
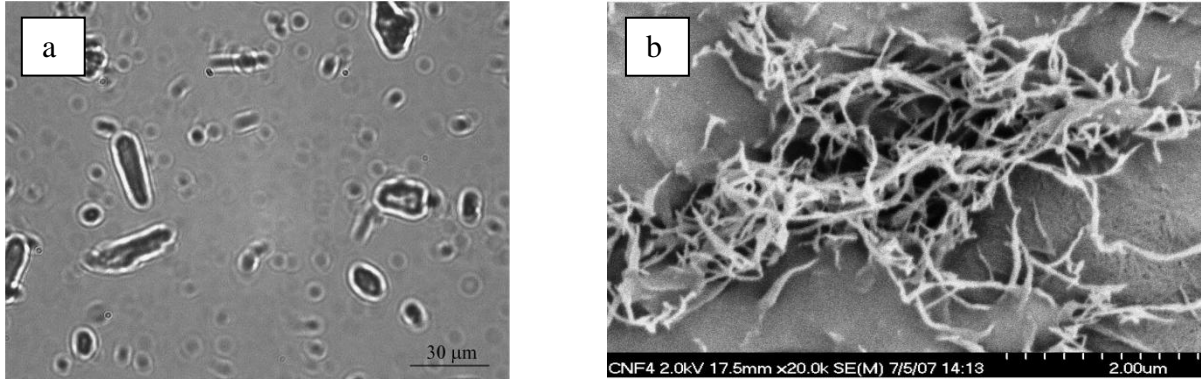
Figure IV-5. Micrographs of pre and post hydrolysis cellulose; a) Optical micrograph of pre-hydrolysis cellulose, b) Scanning electron micrograph of post-hydrolysis cellulose.

Degradation Characterization

Thermal gravimetric analysis was performed to evaluate the nature of degradation of the selected nanofillers in an inert atmosphere. Figure IV-6 shows the degradation behavior of the CNF. The weight loss curve of the neat microcrystalline cellulose shows just one peak corresponding to the thermal degradation of cellulose. The maximum degradation rate occurs at 313°C.
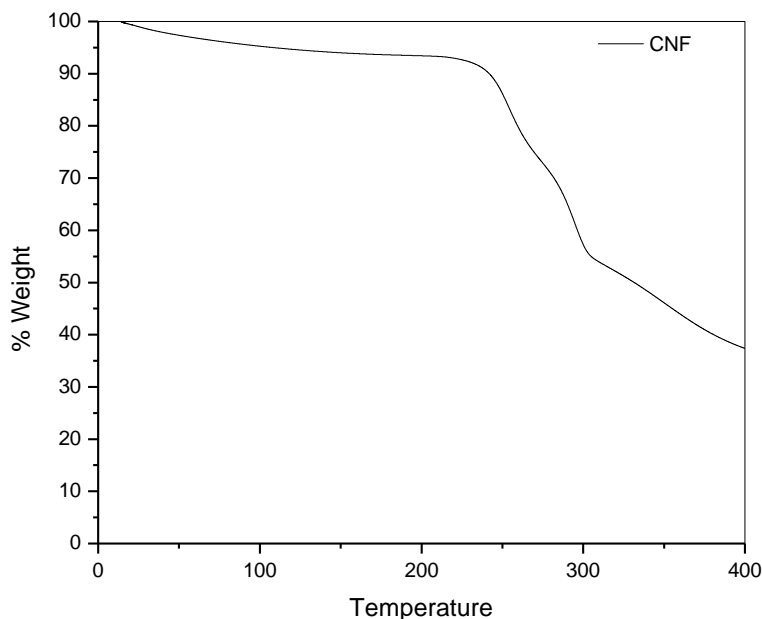
Figure IV-6. Degradation of CNF.

Reaction Evaluation

The chemical reaction that occurs during curing between the –OH groups of cellulose and the isocyanate groups is responsible for the formation of strong matrix-reinforcement adhesion in a polyurethane system. To confirm that the reaction takes place, excess MDI was mixed with hydrolyzed cellulose nanocrystals and heated at 70°C. After curing for 1 hour under pressure, samples were milled and analyzed using Fourier Transform Infrared (FTIR) spectroscopy. The results are shown below in Figure IV-7. Curve 1 (Figure IV-7) shows the spectra of the hydrolyzed cellulose. Curve 2 corresponds to the reacted sample after a wash was performed with toluene to remove the unreacted MDI. Curve 3 represents the spectra of the MDI and the hydrolyzed cellulose after curing. This curve exhibits a new peak at 1720cm^{-1}, which corresponds to the formation of urethane, as well as a peak at 2270cm^{-1}, which corresponds to

the isocyanate (MDI). The isocyanate peak at 2270cm^{-1} decreases from Curve 3 to Curve 2 indicating that MDI is removed but not completely eliminated. However, the urethane peak at 1720cm-1 is neither reduced nor eliminated by washing. The observations confirm that the hydrolyzed cellulose reacts with the isocyanate groups and are not removed by washing.
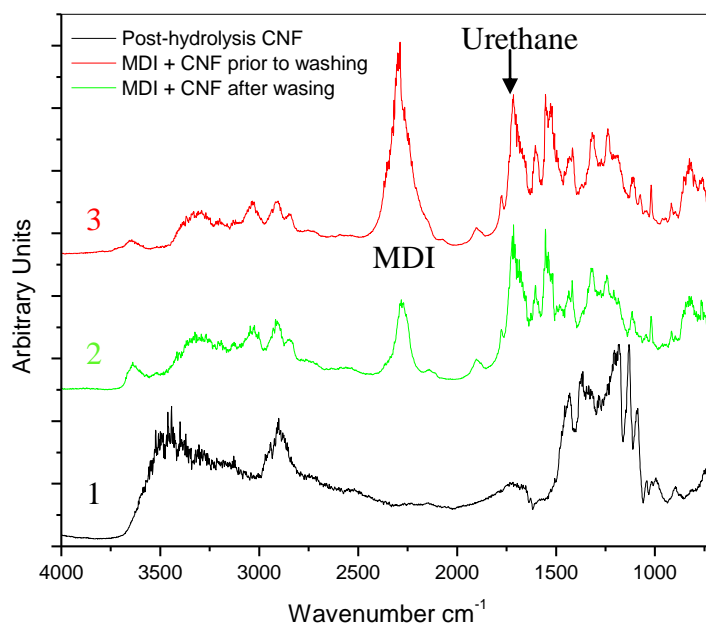
Figure IV-7. FTIR spectra of the hydrolyzed cellulose prior to and post reaction with MDI prepolymer: 1) hydrolyzed cellulose (CNF), 2) MDI reacted with CNF after washing with Toluene, 3) MDI reacted CNF

Conductive Cellulose Nanofibers (C-CNF)

Conductivity

The electrical resistivity of the C-CNF was found to be 5.3 10^5 Ω cm.

Morphology

The image below, Figure IV-8, shows cellulose nanofibers that have polyaniline grown on the surface (C-CNF). The C-CNF shown in the image were dried from an aqueous suspension. The fiber diameter does not appear to be substantially influenced by the polyaniline deposition. However, the fibers do appear to be aggregated. This is partially the result of the evaporation of the solvent before the microscopy analysis and also of the interlinking between fibrils caused by the polyaniline. The aggregation due to the polyaniline will play an important role in the use of the C-CNF as nanoreinforcement in polyurethane matrices.
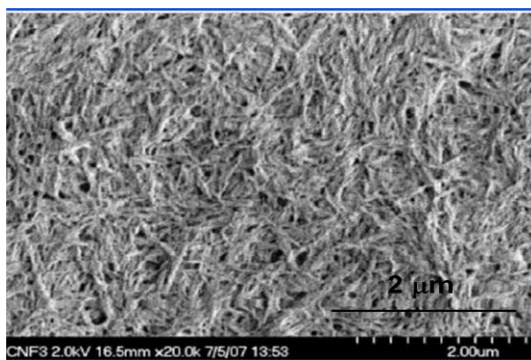
Figure IV-8. Cellulose nanofibers with polyaniline deposited on the surface (C-CNF).

Degradation Characterization

The degradation behavior of cellulose with polyaniline deposited on the surface can be seen below in Figure IV-9. From the graph, it is clear that the polyaniline has an impact on the degradation temperature of the cellulose nanofibers. Additionally, as the deposition time of the polyaniline onto the cellulose nanofiber surface is increased from 2 to 4 hours, degradation is noticed at a lower temperature. In other studies, the major weight losses of polyaniline have been observed at around 160°C and 450°C. The first decrease of mass in the polyaniline was

111

attributed to the removal of dopant molecules, HCl, and possible impurities, such as remaining monomers [Kim et al., 2001].
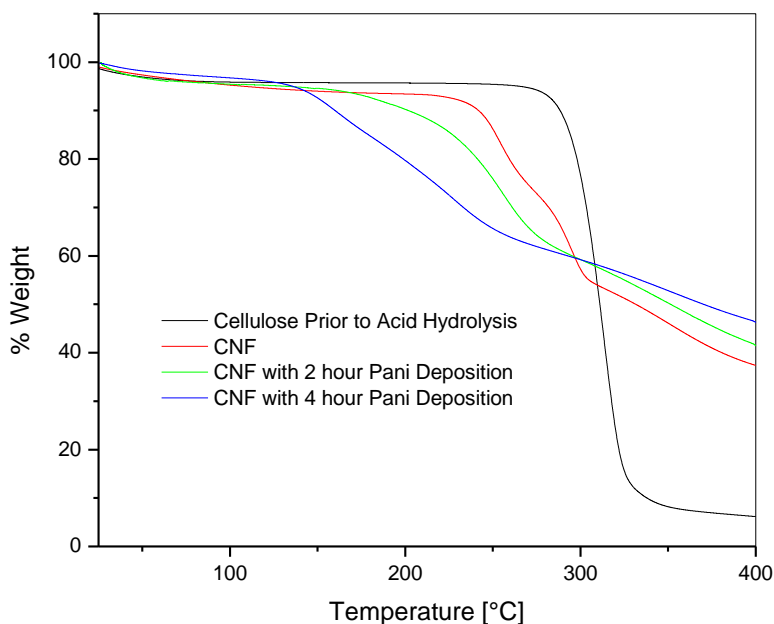
Figure IV-9. Degradation of conductive cellulose nanofibers (C-CNF).

Reaction Evaluation

Comparison of the FTIR spectra (Figure IV-10) of the cellulose nanocrystals before and after polyaniline growth show a new peak at 806 cm^{-1} in the spectrum of the modified CNF, which corresponds to the out of bending vibration of the C-H band of the benzene rings of the polyaniline. There is also a small new band at 1570 cm$^{-1,}$ which is assigned to the stretching vibration of the N in the quinoid moieties in the polyaniline chains [Stejskal et al., 2005].
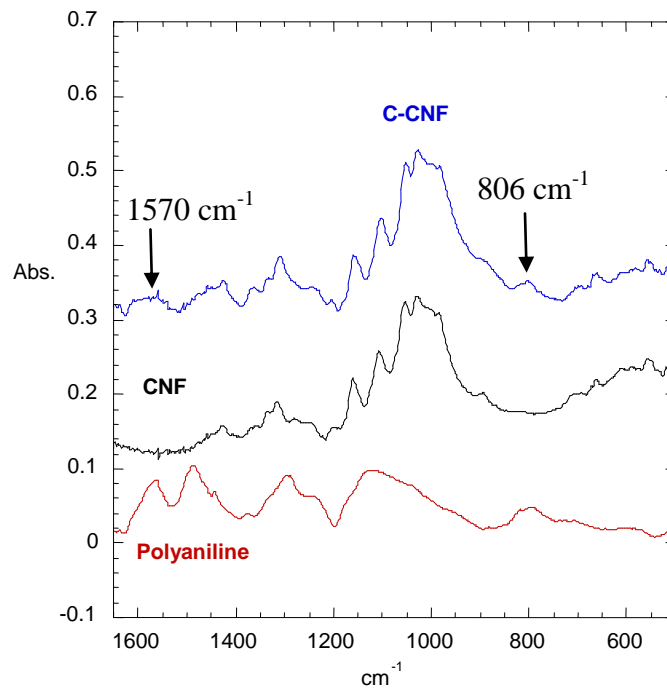
Figure IV-10. FTIR spectra of the cellulose nanocrystals before and after PANI growing. The spectra of homopolymerized PANI is included for comparison.

Carbon Nanotubes (CNT)

Morphology

In Figure IV-11, the structure of the carbon nanotubes prior to acidification and modification can be observed. The high aspect ratio of the pristine carbon nanotubes prior to acidification, which is visible in the scanning electron micrograph, leads to entanglements of the MWNTs and difficulty in dispersion.
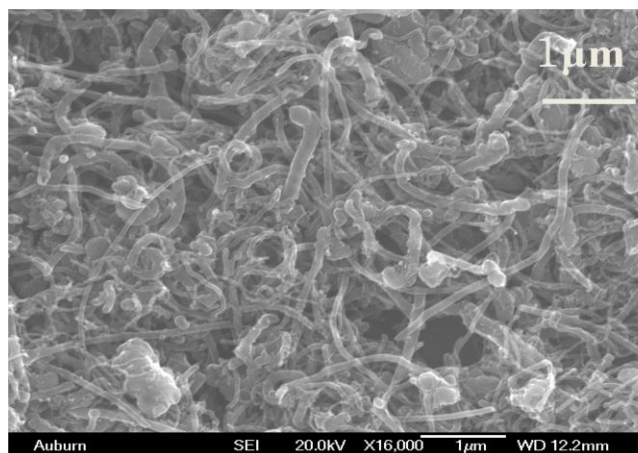
Figure IV-11. Unmodified multi-walled carbon nanotubes (MWNTs).

Degradation Characterization

Thermal gravimetric analysis was performed to evaluate the weight percentage of isocyanate

groups successfully attached to the surface of the MWNTs. The small amount of mass loss

(<1wt %) of the unmodified MWNTs observed in TGA, Figure IV-12, is attributed to the

presence of small amounts of amorphous carbon and impurities. The curves for the acidified

MWNTs show a continuous loss process for the range of analyzed temperatures. The results

show that the two step surface modification process was efficient with a significant mass fraction

of organic groups being successfully chemically bonded to the surface of the MWNTs. The

mass fraction of the organic groups eliminated at 600ºC was calculated. It was found that 30wt%

of isocyanate groups were attached to the surface of the MWNTs.
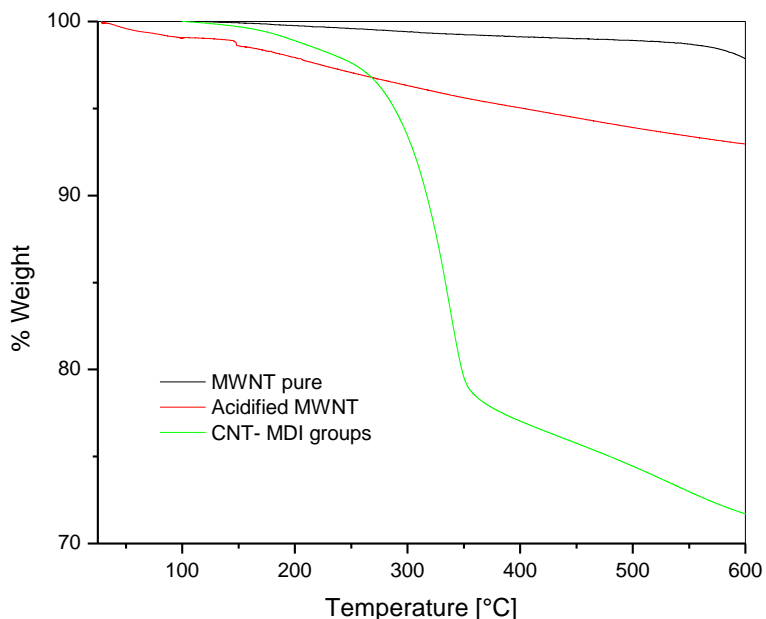
Figure IV-12. Comparative thermal gravimetric analysis of pure MWNTs, acidified MWNTs, and functionalized MWNTs (CNT-MDI).

CONCLUSIONS

During this portion of the research, nanofillers were selected and modified for use in polymer matrices. Cellulose nanofibers were chosen for their availability, low cost, and attractive properties. Their incompatibility was overcome through the use of acid hydrolysis to aid in dispersion. Similarly, conductive cellulose nanofibers (C-CNF) were modified in order to determine if it was possible to create a low cost, electrically conductive nanofiller from a renewable resource and to evaluate the effects of the modification on the structure of the cellulose. Multi-walled carbon nanotubes (MWNTs), chosen for their outstanding mechanical properties, were successfully acidified and functionalized with MDI groups in order to enhance dispersion and compatibility of the nanofiller with a polyurethane matrix.

REFERENCES

1. Ajayan, P. M.; Schadle, L. S.; Giannaris, C.; Rubio, A. Single-walled Carbon Nanotube-polymer Composites: Strength and Weakness. *Advanced Materials*, **2000**, *12* (10), pp 750-753.

2. Andrews, R.; Jacques, D.; Qian, D.; Rantell, T. Multi-wall Carbon Nanotubes: Synthesis and Application. *Accounts of Chemical Research*, **2002**, *35* (12), pp 1008-1017.

3. Angelovici, M. M.; Bryants, R. G.; Northam, G. B.; Roberts Jr, A. S. Carbon/Ceramic Microcomposites, Preparation and Properties. *Materials Letters*, **1998**, *36*, pp 254-265.

4. Neus Angles, M.; Dufresne, A. Plasticized Starch/Tunicin Whiskers Nanocomposites. 1. Structural Analysis. *Macromolecules*, **2000**, *33*, pp 8344-8353.

5. Ardizzone, S.; Dioguaardi, F. S.; Mussini, T.; Mussini, P. R.; Rondinini, S.; Verceli, B.; Vertova, A. *Cellulose*. **1991**, *6*, pp 59.

6. Auad, M. L.; Mosiewicki, M. A.; Uzunpinar, C.; Williams, R. J. J. *Composites in Science and Technology*, accepted for publication (2009).

7. Baibarac, M.; Gomez-Romero, P. Nanocomposites Based on Conducting Polymer and Carbon Nanotubes from Fancy Materials to Functional Applications. *Journal of Nanoscience and Nanotechnology*, **2006**, *6*, pp 1-14.

8. Boldizar, C.; Klason, J.; Kubat, P.; Na¨slund, P.; Saha, P. *International Journal Polym Mater*, **1987**, *11*, pp 229–62.

9. Cadek, M.; Coleman, J. N.; Ryan, K. P.; Nicolosi, V.; Bister, G.; Fonseca, A.; Nagy, J. B.; Szostak, K.; Beguin, F.; Blau, W. J. Reinforcement of Polymers with Carbon Nanotubes: the Role of Nanotube Surface Area. *Nano Letters,* **2004**, *4* (2), pp 353-356.

10. Chen, W.; Auad, M. L.; Williams, R. J. J.; Nutt, S. R. Improving the Dispersion and Flexural Strength of Multiwalled Carbon Nanotubes-Stiff Epoxy Composites Through β-hydroxyester Surface Functionalization Coupled with the Anionic Homopolymerization of the Epoxy Matrix. *European Polymer Journal*, **2006**, *42*, pp 2765-2772.

11. Choi, W. J.; Kim, H. J.; Yoon, K. H.; Kwon, O. H.; Hwang, C. I. *Journal Applied Polymer Science*, **2006**, *100*, pp 4875-4879.

12. Cui, S.; Canet, R.; Derre, A.; Couzi, M.; Delhaes, P. *Carbon*, **2003**, *41* (4), pp 797-809.

13. Dufresne, A.; Cavaille, J. Y. Nanocomposite Materials of Thermoplastic Polymers Reinforced by Polysaccharide. *ACS Symposium Series*, **1999**, *723*, pp 39-54.

14. Dufresne, A.; Vignon, M. Improvement of Starch Film Performances Using Cellulose Microfibrils. *Macromolecules*, **1998**, *31*, pp 2693-2696.

15. Ebeling, T.; Paillet, M.; Borsali, R.; Diat, O.; Dufresne, A.; Cavaille, J-Y.; Chanzy, H. Shear-Induced Orientation Phenomena in Suspensions of Cellulose Microcrystals Revealed by Small Angle X-ray Scattering. *Langmuir*, **1999**, *15*(19), pp 6123.

16. Eichhorn, S. J.; Young, R. J. *Cellulose*, **2001**, 8, pp 197.

17. Favier, V.; Canova, G. R.; Cavaille, J. Y.; Chanzy, H.; Dufresne, A.; Gauthier, C. Nanocomposite Materials From Latex and Cellulose Whiskers. *Polymers for Advanced Technologies*, **1995**, *6* (5), pp 351-355.

18. Friedrich, K.; Fakirov, S.; Zhang, Z. Eds. *Polymer Composites: from nano-to macro-scale.* Springer: New York, 2005.

19. Fink, H. P.; Walenta, E.; Kunze, J. *Papier*, **1999**, *53*, pp 534.

20. Gall, K.; Dunn, M. L.; Liu, Y.; Finch, D.; Lake, M.; Munshi, N.A. Shape Memory Polymer Nanocomposites. *Acta Materialia*, **2002**, *50*, pp 5115-5126.

21. George, J.; Sreekala, M. S.; Thomas, S. A Review on Interface Modification and Characterization of Natural Fiber Reinforced Plastic Composites. *Polymer Engineering and Science,* **2001**, *41* (9), pp 1471-1485.

22. Gong, X.; Liu, J.; Baskaran, S.; Voise, R. D.; Young, J. S. *Chemistry of Materials*, **2000**, *12* (4), pp 1049-1052.

23. Kazanci, M. Carbon Fiber Reinforced Microcomposites in Two Different Epoxies. *Polymer Testing*, **2004**, *23*, pp 747-753.

24. Ratna, D.; Karger-Kocsis, J. Recent Advances in Shape Memory Polymers and Composites: A Review. *J. Mater. Sci.*, **2008**, *43*, pp 254-269.

25. Kim, B.; Oh, S.; Han, M.; Im, S. Synthesis and Characterization of Nanoparticles in SDS Micellar Solutions. *Synthetic Metals*, **2001**, *122,* pp 297-304.

26. Koo, J. H. *Polymer Nanocomposites: Processing, characterization, and applications.* McGraw-Hill Professional: New York, 2006.

27. Malmonge, J. A.; Compoli, C. S.; Malmonge, L. F.; Kanda, D. H. F.; Mattoso, L. H. C.; Chierice, G. O. Effect of the Doping Medium on Blends of Polyurethane and Polyaniline. *Synthetic Metals*, **2001**, *119*, pp 87-88.

28. Marchessault, R. H.; Sundarrjan, P. R. In *Cellulose. The Polysaccharides*. Academic Press: New York, 1983; pp 11-95.

29. Marcovich, N. E.; Auad, M. L.; Bellesi, N. E.; Nutt, S. R.; Aranguren, M. I. Cellulose Micro/Nanocrystals Reinforced Polyurethane. *Journal of Materials Research,* **2006**, *21* (4), pp 870-881.

30. Mark, H. Fify Years of Cellulose Research. *Cellulose Chem Technol*, **1980**, *14*, pp 569–81.

31. Mattoso, L. H. C.; Medeiros, E. S.; Baker, D. A.; Avloni, J.; Wood, D. F.; Orts, W. J. Electrically Conductive Nanocomposites Made from Cellulose Nanofibrils and Polyaniline. *Journal of Nanoscience and Nanotechnology*, **2009**, *9,* pp 2917-2922.

32. Njuguna, J.; Pielichowski, K.; Desai, S. Nanofiller-reinforced Polymer Nancomposites. *Polymers for Advanced Technologies,* **2008**, *19*, pp 947-959.

33. Paul, D. R.; Robeson, L. M. Polymer Nanotechnology: Nanocomposites. *Polymer,* **2008**, *49*, pp 3187-3204.

34. Pluta, M.; Galeski, A.; Alexandre, M.; Paul, M. A.; Dubois, P. Polylactide/Montmorillonite Nanocomposites and Microcomposites Prepared by Melt Blending: Structure and Some Physical Properties. *Journal of Applied Polymer Science*, **2002**, *86* (6), pp 1497-1506.

35. Stejskal, A.; Trchova, M.; Sapurina, I. Flame-Retardant Effect of PANI Coating Deposited on Cellulose Fibers. *Journal of Applied Polymer Science*, **2005**, *98* (6), pp 2347–2354.

36. Sun, Y.; Fu, K.; Lin, Y.; Huang, W. *ACNFOUNTS of Chemical Research*, **2002**, *35* (12), pp 1096-1104.

37. Twardowski, T. E. *Introduction to Nanocomposite Materials: Properties, Processing, Characterization*. DesTech Publications, 2007.

38. Wouterson, E. M.; Boey, F. Y. C.; Wong, S.-C.; Chen, L.; Hu, X. Nano-Toughening Versus Micro-Toughening of Polymer Syntactic Foams. *Composites Science and Technology,* **2007,** *67*, pp 2924–2933.

39. Zadorecki, P.; Michell, A. J. Future Prospects for Wood Cellulose as Reinforcement in Organic Polymer Composites. *Polymer Composites*, **1989,** *10*, pp 69–77.

40. Zhou, J.; Kim, J. D.; Peng, H. Q.; Margrave, J. L.; Khabashesku, V. N.; Barrera, E.V. *Nano Letters*, 3 (8), pp 1107-1113.

CHAPTER V.

SEGMENTED SHAPE MEMORY POLYURETHANE/CELLULOSE NANOFIBER

NANOCOMPOSITES: CELLULOSE ADDITION DURING REACTION

INTRODUCTION

Recent environmental concerns have resulted in a push for biodegradable or recyclable materials constructed from renewable resources. Eco-design is a driving force behind the research and development of many new materials. Natural fibers have gained increasing attention as a replacement for many synthetic materials [George et al., 2001]. Since the mid-1990's, when Favier et al. reported the potential of cellulose nanofibrils in a copolymer acrylate latex film as an "all-organic" nanocomposite, several researchers have explored the use of natural cellulose nanofibrils as a replacement for clay and other nanoreinforcements [Orts et al., 2005; Favier et al., 1995; Dufresne et al., 2000; Paillet & Dufresne, 2001].

The purpose of this section of the work is to investigate the properties and shape memory potential of nanocomposites prepared by incorporation of cellulose nanofibers into the polyurethane matrix during the first step of the synthesis reaction. The chemical structure of linear polyurethanes was varied as outlined in Chapter II, in order to obtain matrices with different soft segment molecular weights and hard to soft segment ratios. The main goal was to

observe the effect of CNF incorporated during the synthesis reaction on the nanocomposite behavior.

MATERIALS AND METHODS

The materials and preparation of the segmented shape memory polyurethane matrices were detailed in Chapter II. The origin and preparation of the cellulose nanofibers (CNF) used for nanoreinforcement was detailed in Chapter IV.

Preparation of Nanocomposites

Cellulose nanofiber/segmented shape memory polyurethane nanocomposites were prepared by addition of a selected amount of hydrolyzed cellulose nanofibers in the first step of the reaction. The reinforcement was previously dispersed in DMF by ultrasonication and subsequently incorporated into the reaction. Films containing 0.1, 0.5, and 1.0 wt% of cellulose crystals were obtained. The final films were produced by casting the reaction mixture with the cellulose in an open mold and drying in a convection oven at 80°C for 24 hours.

TECHNIQUES

Differential scanning calorimetry (DSC), tensile measurements, scanning electron microscopy (SEM), and evaluation of shape memory behavior were performed following the procedures outlined in Chapter II.

RESULTS AND DISCUSSION

Thermal analysis (DSC)

The interactions between the nanofiller and the polymer on the nanocomposite behavior were investigated using thermal analysis. A summary of the transition temperatures and enthalpy of melting for the hard and soft segments is included in Table V-1. In the table, the enthalpy of melting in J/g of soft segments was calculated by dividing the observed enthalpy of melting (J/g) by the soft segment percent for each sample. This allowed for comparison of the enthalpy of melting between each sample.

Matrix	CNF Content [wt%]	Soft segments			Hard segments	
		$T_{melting}$ [°C]	$\Delta H_{melting}$ [J/g]	$\Delta H_{melting}$ [J/g SS]	$T_{melting}$ HS [°C]	$\Delta H_{melting}$ HS [J/g]
MDI 2000/45	0	5.98	4.61	8.38	185.36	9.53
	0.1	7.06	6.5	11.82	*	*
	0.5	9.64	15.16	27.56	*	*
	1.0	8.12	10.59	19.25	*	*
MDI 2000/39	0	5.25	8.42	14.03	178.7	5.61
	0.1	5.74	11.8	19.67	*	*
	0.5	8.17	13.99	23.32	*	*
	1.0	8.06	12.21	20.35	*	*
MDI 2000/32	0	6.83	6.23	9.16	172.75	2.23
	0.1	9.41	28.48	41.88	*	*
	0.5	11.62	26.51	38.99	*	*
	1.0	8.97	26.69	39.25	*	*
MDI 2000/23	0	7.49	21.04	27.3	*	*
	0.1	12.99	31.36	40.73	*	*
	0.5	11.31	31.35	40.71	*	*
	1.0	11.68	31.97	41.52	*	*

Table V-1. Thermal properties of the hard and soft segments in the SPU reinforced with different percentages of cellulose. * indicates that a transition was not observed.

The results for the MDI 2000/39 sample with varying concentrations of CNF show that the thermal behavior is significantly affected by small concentrations of CNF. The data shows that the addition of a small amount of CNF shifts the melting temperature of the soft segments upwards and increases the enthalpy of melting. This indicates that the cellulose favors the phase segregation of the polyurethane hard and soft segments. This effect reduces the interruption of soft segment crystallites by reducing order in the hard segments. Soft segment crystallites formed in the presence of the CNF reinforcement are more perfect and melt at higher temperatures than the unreinforced matrix. The segregation effect due to the cellulose addition is also present in MDI 2000/39 and MDI 2000/45, although in these cases the effect of the high concentration of HS interfering with the SS crystallization is more important.

As previously discussed in Chapter II, the melting endotherm corresponding to the hard segment phase in the neat polyurethane is small, but noticeable in all the samples, except for the sample with the lowest hard segment content (23% hard segment). The effect of adding cellulose nanocrystallites is the suppression of the endotherm. This suppression occurs because the polar nature of the cellulose crystals, which suggests a preferential association with the hard segments that are more polar than the PTMG soft segments. This association between the nanocellulose and the hard segments interferes with the hydrogen bonding that physically link hard segment together in crystalline domains, thus, preventing them from ordering. This effect has been reported previously in segmented polyurethane reinforced with clay nanoplatelets [Gregory, 2005]. In that case, the morphology study of the different neat PU and derived nanocomposites lead to the conclusion that the polar nanoparticles affected mostly the ordering of the hard segmented phase, and that the crystallization of the soft segment phase was favored through the

122

increased phase segregation.

Mechanical analysis

The mechanical properties of polyurethanes with different concentration of hard segment, length of soft segments and percentages of cellulose crystals were investigated by testing the composites at room temperature (25°C). As seen in Figure V-1, the stress versus strain curves exhibited typical elastomeric behavior. Stress increases linearly with the strain at very small deformations. Plastic deformation occurred as the stress was increased. At this stage, the stress-strain curve deviates considerably from the Hookean behavior, since stress is redistributed by deformation (fragmentation) and reorganization of the hard segments. Finally, the polymer cannot bear the load anymore, and the material breaks.
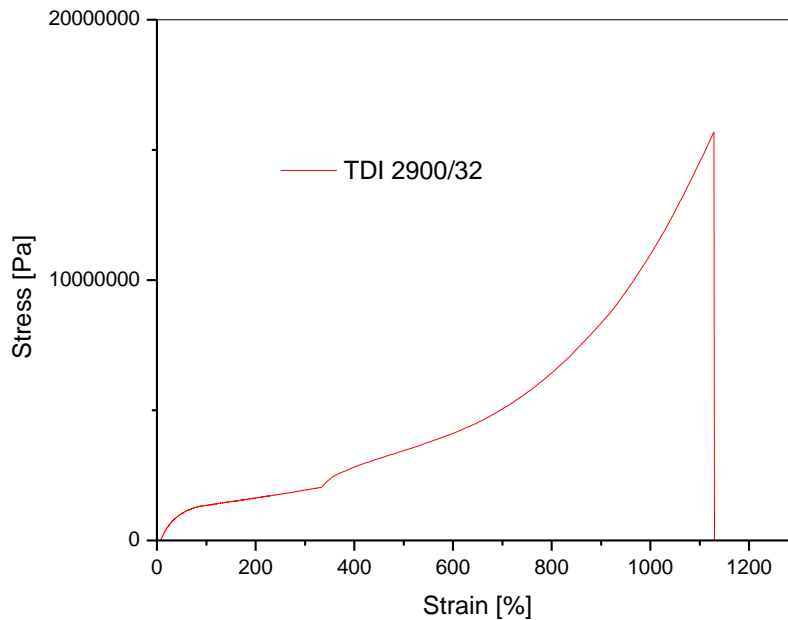
Figure V-1. Tensile stress versus strain curve for the segmented polyurethane with 32% hard segment content.

The values of the Young's modulus (E) and elongation at break (ε_b) are reported in Table V-2. The effect of soft segment length and hard segment content on the mechanical properties of the shape memory polyurethane matrices was previously discussed in Chapter II. The focus will be on the effect of cellulose nanofibers added during the reaction. When cellulose nanofibers are added during the first step of the polyurethane synthesis, there is the possibility of a reaction occurring between the soft segment chains and the CNF through the action of the diisocyanate. It is important to note that the values for the polyurethane matrices listed in this chapter vary from those previously reported in Chapter II. This is due to variations in room temperature when tensile testing was performed. Even a slight variation in the temperature creates a major impact in the tensile properties. This is because the soft segment transition is close to room temperature and the behavior will behave either as a glassy solid or a rubbery viscoelastic material depending on the temperature. This is visible in the DSC thermograph for the MDI 2000/32 sample shown in Figure V-2. Prior to the melting transition, which occurs at approximately 20°C, the material is in the glassy state. However, after this transition, the rubbery plateau, where the material is viscoelastic, can be seen.

	wt % CNF	E [MPa]	$\varepsilon_b[\%]$
MDI 2000/45	0	37.04 ± 1.13	203 ± 65
	0.5	26.14 ± 2.42	16 ± 2
	1	29.04 ± 4.93	37 ± 2
MDI 2000/39	0	15.71 ± 0.49	473
	0.5	21.67 ± 2.36	79 ± 8
	1.0	21.05 ± 5.30	114 ± 5
MDI 2000/32	0	9.60 ± 0.03	672
	0.5	14.31 ± 0.48	115 ± 21
	1.0	14.75 ± 0.78	68 ± 7
MDI 2000/23	0	4.54 ± 0.32	2165
	0.5	6.47 ± 0.80	261 ± 43
	1.0	6.56 ± 1.06	142 ± 28

Table V-2. Mechanical properties of MDI 2000 samples with CNF added during the first step of the reaction.
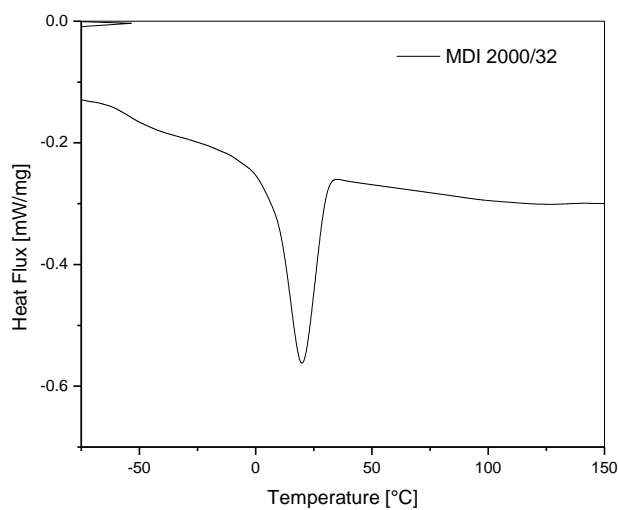
Figure V-2. DSC thermograph of the MDI 2000/32 sample exhibits the glassy state prior to the soft segment melting transition and the rubbery plateau after the transition.

From the DSC results, it is evident that the addition of cellulose during the first step of the reaction does not hinder the capability for crystallization of the soft segment chains. So, it can be inferred that low range spatial mobility of the chains is not compromised by the creation of these bonds. Additionally, the presence of cellulose nanofibers with abundant hydroxyl groups affects the ordering and grouping of the hard segments, which is based on hydrogen-bonding attractions. This observation is also supported by the DSC data which shows the disappearance of the hard segment melting peak after cellulose reaction. The mechanical properties of the nanocomposites respond to a balance of these two effects. While the addition of high modulus CNF to the polymer matrix increases the modulus of the elastomers, the CNF also simultaneously interfere with the formation of the hard segment domains, which leads to a reduction of the modulus. The analysis of the tensile test results for the MDI 2000 nanocomposites indicates that the presence of a small amount of CNF (0.5 wt%) produces a marked increase of the tensile modulus. Addition of greater amounts of CNF does not appear to have a significant impact on further increasing the previous result. The effect of adding rigid fibrils to the elastomer is the dominant effect. However, the MDI 2000/45 sample shows a reduction of the modulus when CNF is added to the polymer matrix. The interaction of the CNF with the hard segment reduces the ordering of the hard segments and CNF addition does not compensate or counteract for this change.

The addition of cellulose crystals also impacts the elongation at break of the samples. For the two samples with lower hard segment content (and lower modulus), the behavior is the expected for an elastomer reinforced with rigid particles, and thus, the higher the cellulose content, the lower the elongation at break. Just as with the variations in the modulus, the major change occurs

by addition of a minimum amount of cellulose. For the MDI 2000 samples with higher hard segment content, the effect of addition of rigid particles is accompanied by the disruption of the hard segment domains. The main effect is the reduction of elongation at break by incorporation of a minimum amount of cellulose. At 1 wt% of cellulose, the disruption of the hard segment domains can also favor the higher extensibility of the soft segment chains, leading to the increase of the deformation at break.

Morphology

Scanning electron micrographs of the cryo-fractured films, Figure V-3, illustrate the morphology of the unfilled segmented shape memory polyurethane films and the impact due to the presence of cellulose nanofibers. The fractured surface of the unfilled polyurethane matrix shows characteristic brittle marks and very little plastic deformation. In contrast, the sample with 1 wt% CNF exhibits a rougher fracture surface which suggests the activation of new and different energy dissipating mechanisms. The advancing cracks are deflected due to the presence of the rigid cellulose nanofibers, which generate a more tortuous crack path. Additionally, the image features are similar in the areas analyzed, indicating a homogeneous dispersion of cellulose nanofibers at the level observed by the scanning electron microscope.
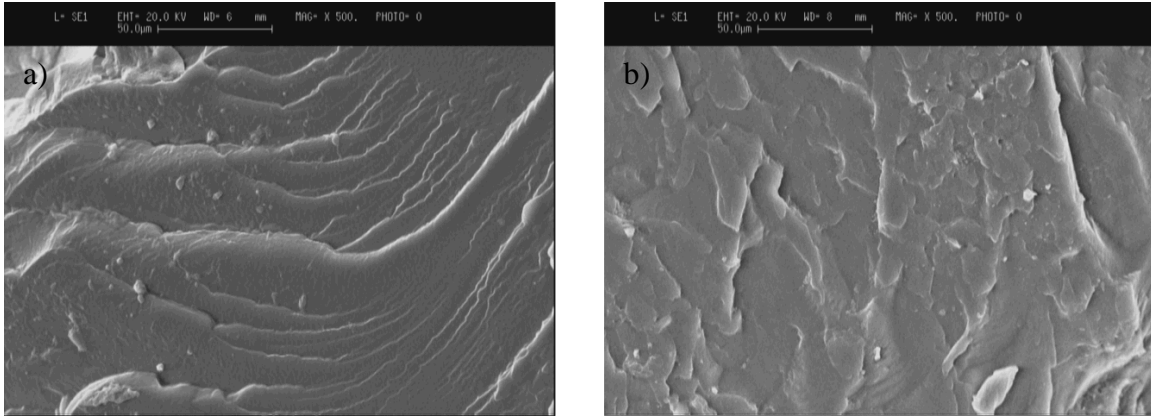
Figure V-3. SEM images of the MDI 2000/23 containing: a) 0 wt% and b) 1 wt% of CNF incorporated during the first step of the synthesis reaction.

Shape Memory Behavior (SMB)

Shape memory behavior was observed through a series of cyclic thermo-mechanical tests.

Shape memory behavior of the segmented shape memory polyurethane matrices was previously discussed in Chapter II. The effect of CNF added during the reaction on the shape memory behavior of the nanocomposite system was the focus of this portion of the work. Nanocomposites with CNF added during the first step of the synthesis reaction did not exhibit shape memory behavior. As previously indicated, cellulose can chemically react with the diisocyanate (MDI in this case), which strongly interferes with the formation of the hard segments. The excess interactions between the cellulose nanofibers and polyurethane chains results in structures that are not capable of showing shape memory behavior. At the high temperature part of the cycles (Temperature > Melting Temperature of Soft Segments (T_mSS; in this case a temperature of 45°C was used), the low ordered hard segment domains of the composites are easily perturbed by the imposed tensile loads and the material breaks at relatively low deformations.

Finally, it is clear from Chapter II that the segmented shape memory polyurethane structure (hard segment content and soft segment chain length) and the experimental testing parameters obviously have a large impact on the material properties, phase segregation, and phase ordering, which determine the shape memory response of the materials [Lee et al., 2004]. From this work, it becomes clear that not only the presence of cellulose nanofibers but also the time at which the cellulose nanofibers are added to the polymer matrix also has an effect on the shape memory behavior. As seen in Table V-3, CNF/PU nanocomposites in which the cellulose is incorporated after the reaction exhibit similar shape memory properties to the unfilled polyurethane matrix. This behavior will be the focus of the next chapter of this work.

Sample	Cellulose [wt%]		1st Cycle [%]	2nd Cycle [%]	3rd Cycle [%]
MDI 2000/39	0.0	R_f	84.6	67.9	81.6
		R_r	71.2	71.2	71.2
MDI 2000/32	0.0	R_f	62.9	61.8	70.5
		R_r	80.6	79.9	79.0
MDI 2000/23	0.0	R_f	53.8	55.8	51.3
		R_r	90.7	88.3	85.6
MDI 2000/23	1*	R_f	79.3	80.9	78.2
		R_r	82.1	80.2	80.0

Table V-3. Shape memory properties of the unfilled polyurethane matrix in comparison to a nanocomposites with 1 wt% CNF (notated 1*) incorporated after the reaction.

CONCLUSIONS

Segmented shape memory polyurethanes were synthesized through a two step polymerization. Small percentages of cellulose nanofibers were added during the first step of the polymerization

reaction. The incorporation of cellulose induced changes in the micro-structure of the polyurethanes, which affected the thermal, mechanical, and shape memory performance of the nanocomposites. In general, CNF favored the phase separation between the soft and hard domains, as exhibited by an upward shift in the melting temperatures of the crystalline phases and an increase in the Young's modulus and a decrease in the deformation at break.

The effect of the addition of cellulose nanofibers during the reaction on the nanocomposite properties was investigated. The incorporation of CNF during the polyurethane synthesis leads to nanocomposites with increased modulus, reduced deformability, and eliminated the shape memory behavior of the segmented polyurethanes. The shape memory behavior is a property that this research wishes to maintain. Therefore, addition of cellulose during the reaction is not desirable to obtain the desirable properties of the nanocomposite system.

REFERENCES

1. Dufresne, A. ; Dupeyre, D. ; Vignon, M. R. Cellulose Microfibrils from Potato Tuber Cells : Processing and Characterization of Starch-Cellulose Microfibril Composites. *Journal of Applied Polymer Science*, **2000**, *76*, pp 2080-2092.

2. Favier, V. ; Chanzy, H. ; Cavaille, J. Y. Polymer Nanocomposites Reinforced by Cellulose Whiskers. *Macromolecules*, **1995**, *28*, pp 6365-6367.

3. George, J. ; Sreekala, M. S. ; Thomas, S. A Review on Interface Modification and Characterization of Natural Fiber Reinforced Plastic Composites. *Polymer Engineering and Science*, **2001**, *41* (9), pp 1471-1485.

4. Gregory, S. P. Synthesis and Characterization of Silk-Inspired Thermoplastic Polyurethane Elastomers, PhD Thesis, Massachusetts Institute of Technology, Dept. of Chemical Engineering, USA (2005).

5. Kim, B. K.; Lee, S. Y.; Xu, M. Polyurethane Having Shape Memory Effect. *Polymer*, **1996**, *37* (26), pp 5781-5193.

6. Lee, S. H.; Kim, J. W.; Kim, B. K. Shape Memory Polyurethanes Having Crosslinks in Soft and Hard Segments. *Smart Mater. Struct.*, **2004**, *13* (6), pp 1345-1350.

7. Orts, W. J. ; Shey, J. ; Imam, S. H. ; Glenn, G. M. ; Guttman, M. E.; Revol, J-F. Application of Cellulose Microfibrils in Polymer Nanocomposites. *Journal of Polymers and the Environment*, **2005**, *13* (4), pp 301-306.

8. Paillet, M. ; Dufresne, A. Chitin Whisker Reinforced Thermplastic Nanocomposites. *Macromolecules*, **2001**, *34* (19), pp 6527-6530.

9. Sheth, J. P.; Klinedinst, D. B.; Pechar, T. W.; Wilkes, G. L.; Yilgor, E.; Yilgor, I. Time – dependent Morphology Development in a Segmented Polyurethane with Monodisperse Hard Segments Based on 1, 4- Phenylene Diisocyanate. *Macromolecules*, **2005**, *38* (24), pp 10074-10079.

CHAPTER VI.

SEGMENTED SHAPE MEMORY POLYURETHANE/CELLULOSE NANOFIBER

NANOCOMPOSITES: POST REACTION CELLULOSE ADDITION

INTRODUCTION

Eco-friendly polymer composites utilizing cellulose micro and nanofibrils have recently received attention due to the possibility of obtaining enhanced mechanical properties similar to those nanocomposites utilizing clay and synthetic nanofillers [Panaitescu et al., 2008; Orts et al., 2005].

This section of the work investigates the properties and shape memory potential of composites prepared by post synthesis incorporation of cellulose nanocrystals into a segmented polyurethane matrix. In order to obtain matrices with different soft segment molecular weights and hard to soft segment ratios, the chemical structure of linear polyurethanes was varied as outlined in Chapter II. The effect of post reaction addition of cellulose nanofibers to the segmented shape memory polyurethane matrix on the nanocomposite behavior was analyzed. The addition of cellulose added after the reaction is expected to have a different effect on the polymer matrix than cellulose added during the reaction due to the lack of interactions between the matrix and the nanoreinforcement material, as previously highlighted in Chapter V.

MATERIALS & METHODS

The materials used for preparation of the segmented shape memory polyurethane matrices were detailed in Chapter II. The origin and preparation of the cellulose nanofibers (CNF) used for nanoreinforcement was detailed in Chapter IV.

Preparation of Nanocomposites

Synthesized segmented shape memory polyurethanes with 32% hard segment content were dissolved in N,N-dimethylformamide (DMF). Solutions containing 30 wt% polyurethane were prepared. Cellulose nanofibers, which had been previously freeze dried, were dispersed in dry DMF using ultrasonic treatments. The CNF/DMF suspensions were subjected to ultrasonication until they became milky in color and the suspension remained stable. The coloration of the suspensions after ultrasonic treatment can be seen in Figure VI-1. The ultrasonic treatment time was approximately 12 minutes.
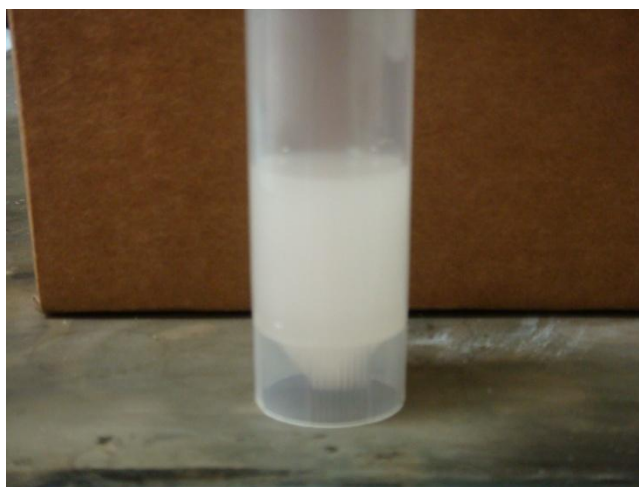
Figure VI-1. CNF/DMF suspension after ultrasonic treatment.

The CNF/DMF suspension was then incorporated into the dissolved polyurethane/DMF solution. A speedmixer (DAC 150) was used at 2000 rpm for 18 minutes to aid in dispersion. Reinforced polyurethane films containing 0, 0.5, 1.0, 1.5, and 2.0 wt % CNF were obtained by casting the mixture into an open Teflon® mold and drying in a convection oven at 80°C for 24 hours.

TECHNIQUES

Differential scanning calorimetry (DSC), scanning electron microscopy (SEM), thermal gravimetric analysis (TGA), tensile measurements, and evaluation of shape memory behavior were performed following the procedures outlined in Chapter II.

Rheological Characterization

Information regarding the percolation thresholds, or the connectivity, of the nanocomposites was obtained by rheological measurements of films in their molten state. This was previously determined to be 220°C for the MDI system and 180°C for the TDI system. A rheometer, TA instruments AR-G2, equipped with parallel plates (diameter = 25 mm) was used to register the viscoelastic response of the samples. The measurements were carried out in the linear viscoelastic region, which was determined by performing strain sweeps. Frequency sweeps were then performed using a strain of 1%.

RESULTS AND DISCUSSION

Rheological Characterization

Percolation, which is the study of connectivity in networks, is a very important concept in polymer nanocomposites. Rheological characterization is often used to examine the structural

transitions of polymer nanocomposites. Through percolation studies, the critical filler concentration value can be determined. Due to the structural transition that occurs, a sudden, expected change in the properties of polymer nanocomposites occurs beyond the critical filler concentration. Two critical concentrations, the first and second percolation thresholds, have been proposed in literature [Kotsilkova, 2007]. These parameters determine the qualitative and structural transitions of nanocomposites as nanofiller content increases. The first percolation threshold, known as flocculation, occurs at the critical concentration where fractal flocs are formed. The second percolation threshold, percolation, occurs when fractal flocs form a continuous structural network. Through observation of rheological properties of nanocomposite dispersions, a clear change in properties is exhibited with respect to both percolation thresholds. Below the first percolation threshold, or flocculation, solutions exhibit very little to no viscoelasticity. Dispersions in this concentration region exhibit rheological behavior very similar to the homopolymer. In the concentration range between the two percolation thresholds, the behavior becomes viscoelastic but still exhibits a largely liquid-like response. Above the second percolation threshold, however, the rheological behavior of the nanocomposite dispersion drastically changes. Nanocomposite solutions with critical concentration values above this range display the following characteristics: a secondary plateau of the storage modulus, dynamic modulus that exhibits a pseudo-solid like behavior, a sudden increase in the solution viscosity, and a yield stress [Kotsilkova, 2007]. The determination of the second percolation threshold, or percolation, was of interest in this study.

The rheology results of G' (storage modulus) versus frequency for the MDI systems are shown in Figure VI-2 a and b. In general, the MDI system exhibits similar behavior for soft segment

lengths of 2000 and 2900. The values of G' are very large and the slope of the G' versus frequency curves are very small at 220°C, which is characteristic of solid-like materials indicating that the samples may not have been in the molten state or samples in which partial crosslinking may have occurred. In this case, the latter is believed to be the cause. Similar behavior has been observed for ester based MDI/poly(oxytetramethylene adipate)/BD polyurethane matrices at 190°C [Han, 2007]. During this study, a similar upswing in the slope of G' was found when the temperature was increased above a certain critical temperature. It is possible that some degradation of the polymer matrix may be occurring or that insoluble gels might be forming during the dynamic frequency sweep experiments giving rise to an increase in G'. Since the temperature sweeps were performed to determine the melting temperature of the matrices and thermal analysis corresponded to a molten sample at 220°C, it can be assumed that the addition of CNF has a major impact on the storage modulus of the nanocomposites.
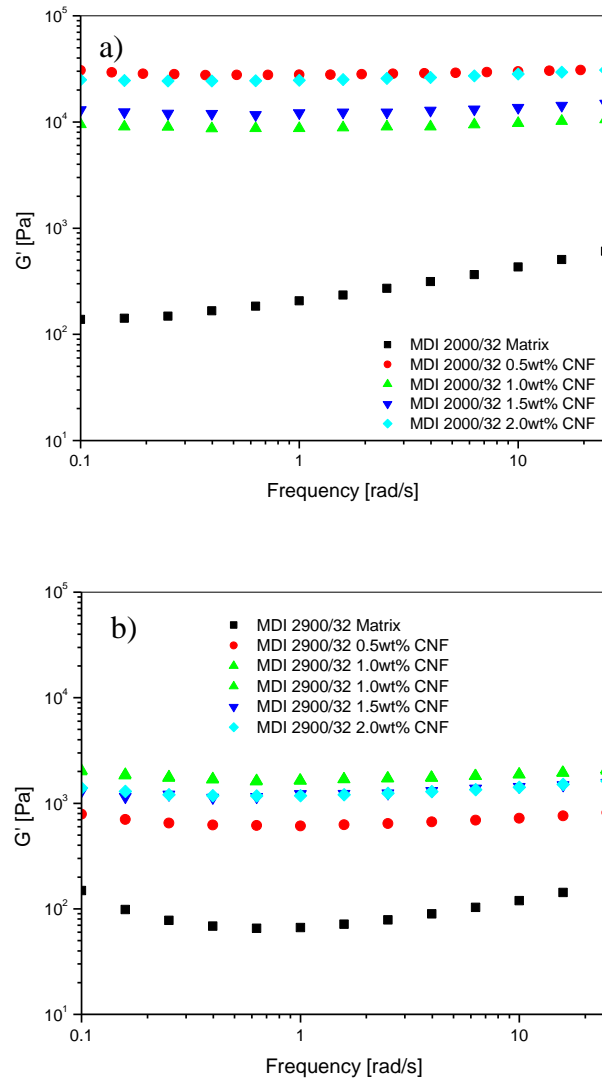
Figure VI-2. Storage modulus, G', versus frequency for a) MDI 2000/32 nanocomposites and b) MDI 2900/32 nancomposites.

In Figure VI-3 a and b, the rheological response of the TDI 2000/32 and TDI 2900/32 nanocomposites is presented as G', the storage modulus of the suspension, versus frequency. TDI nanocomposites with soft segment lengths of 2000 and 2900 exhibit similar behavior. The largest differences in the curves occur at low frequencies. The storage modulus of the nanocomposites increased with increasing CNF concentration. An equilibrium plateau occurred

at low frequencies for the sample containing only 1.0 wt% CNF. The behavior of the

nanocomposites clearly shifted from that of a Newtonian liquid to a viscoelastic solid with

increasing CNF concentration.
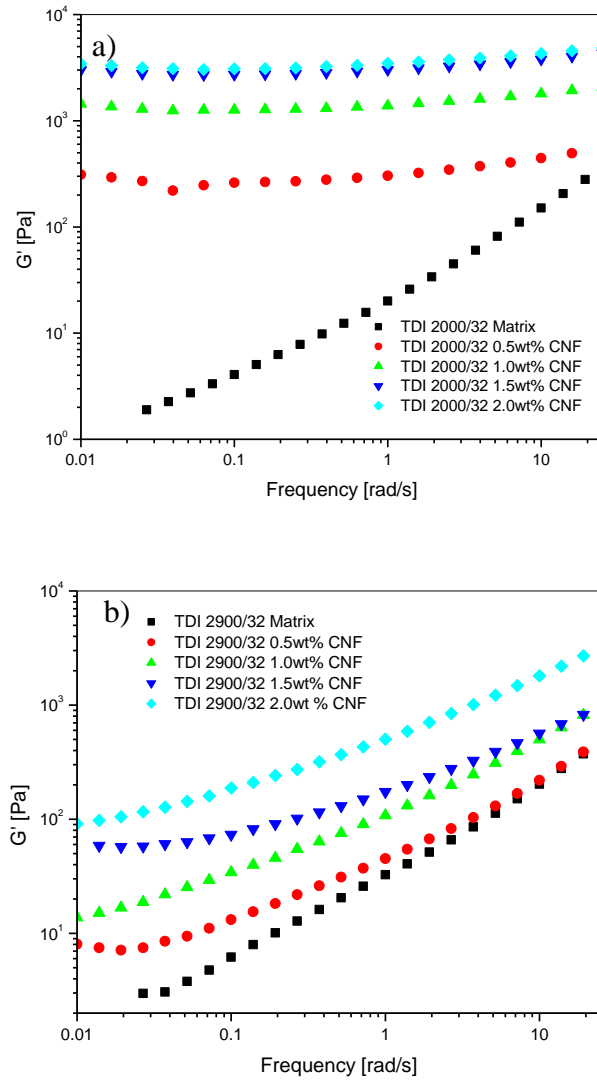
Figure VI-3. G' versus frequency for a) TDI 2000/32 nanocomposites and b) TDI 2900/32 nanocomposites.

The dynamic viscosity of the TDI 2900/32 nanocomposites plotted as a function of the frequency

for different CNF concentrations is shown in Figure VI-4.   The curve for the unfilled

polyurethane matrix remains relatively unchanged over the range of frequencies evaluated and the sample behaves as a Newtonian liquid. As cellulose nanofibers are added to the polyurethane matrix, the low-frequency viscosity increases. This is an indication of the non-Newtonian behavior introduced by the cellulose nanofibers. At approximately 1.0 wt% CNF concentration, the behavior exhibits a Newtonian plateau at low frequencies and shear thinning at higher frequencies. This plateau is attributed to the structure formed due to interactions between the individual nanofibers. At higher frequencies, this structure breaks down into individual nanofibers. This rheological behavior has been observed in other studies of liquid rubbers filled with carbon black or silica particles [Aranguren et al., 1992]. Addition of increasing amounts of CNF (2.0 wt%), a power law behavior was exhibited that extended over the entire frequency range studied. Similar behavior has been observed in nanocomposites constructed from CNF and a commercial polyurethane matrix [Marcovich et al., 2006].
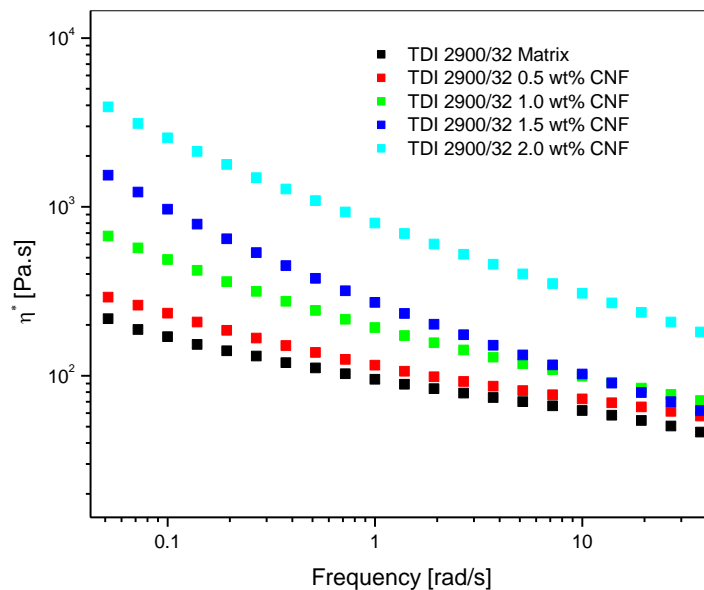
Figure VI-4. Dynamic viscosity versus frequency of the TDI 2900/32 nanocomposites.

139

Theoretical Determination of Percolation Threshold

A theoretical model was used to predict the percolation threshold of the polymer nanocomposites. The TDI 2900/32 system was selected for evaluation because it is in the liquid stage at high temperatures and does not exhibit the partial crosslinking that is visible in the MDI system.

The Einstein model has led to the derivation of many simple models for describing particle suspension viscosity. However, these models only take into account volume concentration of the particles and their aspect ratio (in the case of non-spherical particles) [Guth, 1945]. In these models, the hydrodynamic effects of the particles on the flow field are taken into account. The usual result is an increase in the viscosity with increasing particle concentration. Other models use formulas to predict an infinite viscosity of the suspension at maximum particle packing, which is experimentally determined to be 0.6-0.7 volume fraction for spheres [Krieger, 1972]. If particles have irregular forms, or rod shapes as is the case in the CNF/PU system, maximum packing is reduced. One of the equations that takes into account the aspect ratio of the particles is shown below [Guth, 1945; Payne & Whittaker 1972]:

$$\frac{\eta}{\eta_m} = 1 + 0.67\,\phi_f f + 1.62\,\phi_f^2 f^2 \tag{1}$$

where η is the suspension viscosity, η_m is the suspending media viscosity, Φ is the volume fraction of the particles, and f is the aspect ratio (Length/Diameter) of the fibers.

The above equation (1) was used to evaluate the obtained experimental data. The results of the predicted and experimental viscosities for the molten nanocomposites suspensions (expressed as $\frac{\eta}{\eta_m}$) are shown in Figure VI-5, which plots the η_r, reduced viscosity, versus the volume fraction of the fibers for different aspect ratios of the fibers, f. Artificial aspect ratios ranging from 10 to 200 were evaluated. From the plot, it appears that cellulose nanofibers with an aspect ratio of 150 most closely fit the obtained experimental data. During previous evaluation of the cellulose nanofibers by scanning electron microscopy in Chapter IV, an average aspect ratio of greater than 50 was found so there is some discrepancy in the measured aspect ratio and the aspect ratio determined using the model.
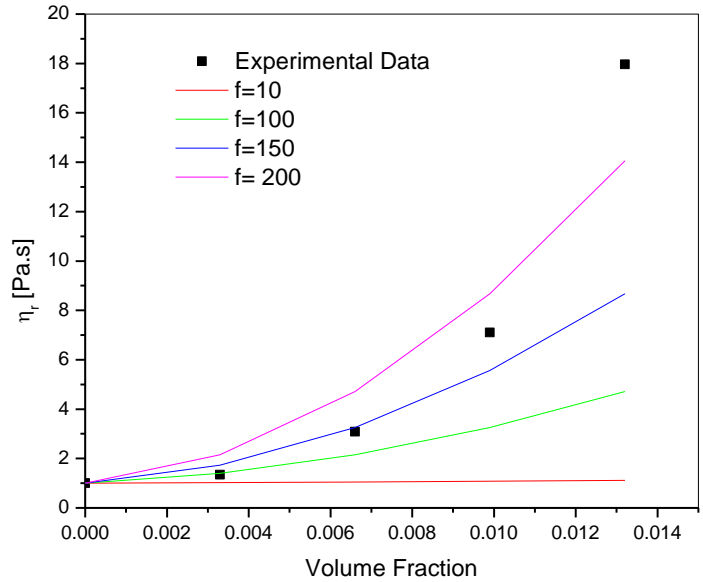
Figure VI-5. η_r versus volume fraction for the TDI 2900/32 nanocomposites.

Theoretical Model for Determination of the Concentration Percolation Threshold

The experimental results of the frequency sweeps were analyzed using a van Gurp-Palmen plot. This plot is useful for quickly identifying the range of concentrations where the liquid-solid

141

change occurs (percolation threshold). In this plot, Figure VI-6, the phase angle, δ, is plotted against the complex dynamic modulus, G*. The unfilled matrix, which exhibits Newtonian liquid behavior, is expected to be completely out of phase with respect to the sinusoidal strain input (δ ~ 90°). For the remaining nanocomposite samples, however, the expected viscoelastic behavior, in which the phase angle is much higher at higher frequencies but decreases at lower frequencies, is observed. The curve corresponding to 1 wt% CNF shows a large curvature that when extrapolated to a phase angle of 0° a non-zero G^* value is obtained, which is characteristic of the development of a 3D network formed by the nanofiller.
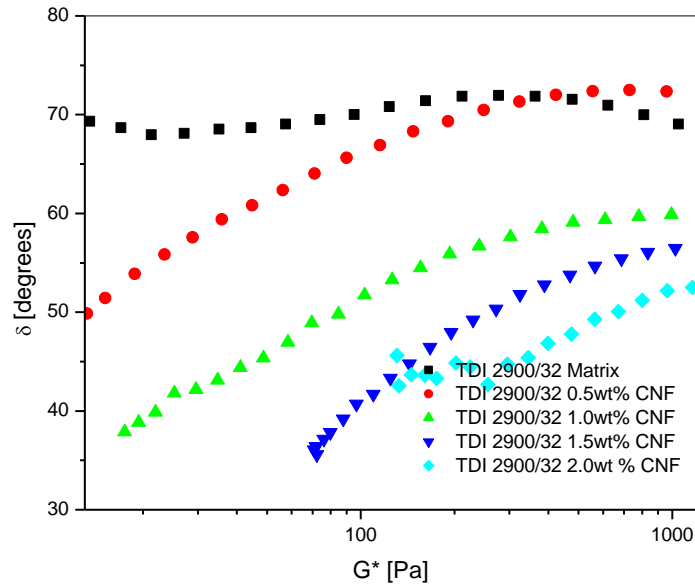
Figure VI-6. Van Gurp-Palmen plot for the TDI 2900/32 nanocomposites.

Finally, the experimental data was modeled as a function of the CNF concentration according to a percolation expression as follows [Du et al., 2004; Mewis & Macosko, 1994; Hough et al., 2004]:

$$G' \propto (m - m_{cG'})^{\beta G} \tag{2}$$

where m is the weight percent of the cellulose nanofibers, $m_{cG'}$ is the concentration at the

percolation threshold, and β_G is an exponent. It is important to note that this equation can only

be applied near the percolation threshold.

The experimental data measured at low frequencies was fitted to the above equation (2) in order

to obtain the concentration at the percolation threshold. Since the model must be used near the

percolation threshold, a CNF concentration range of 1-2 wt% was used. From the results, shown

in Figure VI-7, a critical concentration of 0.93 wt% was found. This value lies within the range

of concentrations for which the qualitative change in suspension behavior was observed. The

experimental data are well fitted with an exponent of 0.70, which is in the range of exponents

reported by other investigators for polymer systems reinforced with short, rigid fibers [Favier et

al., 2004; Dani & Ogale, 1996].
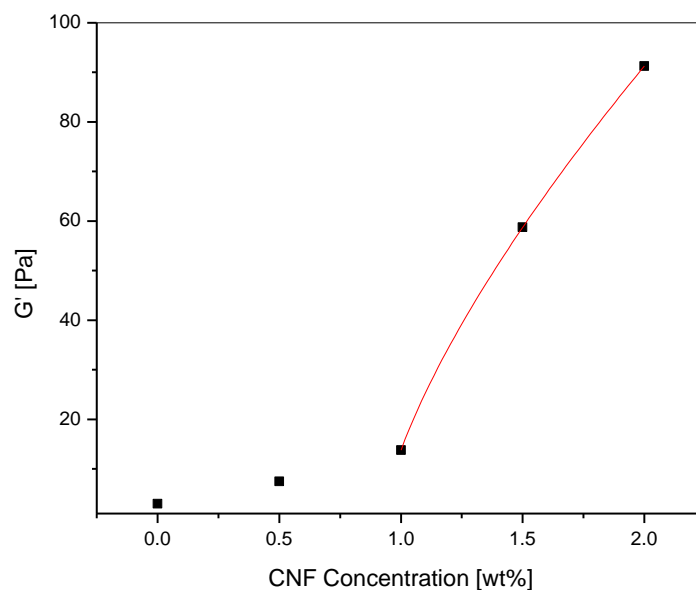
Figure VI-7. Storage modulus (G') versus cellulose nanofiber weight percent behavior fitted using the percolation model given in Equation 2.

Thermal Characterization

Thermal analysis was performed to investigate the interactions between the filler and the polymer on the nanocomposite behavior. The effects of the chemical structure of the polyurethane matrix on the thermal properties were previously discussed in Chapter II. A summary of the transition temperatures and enthalpy of melting for the MDI 2000/32 and MDI 2900/32 systems is shown in Table VI-1. Due to the molecular rearrangement that occurs in the first heating cycle, which was previously discussed in Chapter II, the results from the second thermal cycle were focused upon. From the reported results, it is clear that the addition of a small amount of CNF into the polymer matrices produces a large effect on the thermal behavior. The data shows that a small addition of CNF shifts the melting temperature of the soft segments of the MDI 2000/32 system upwards and increases the heat of melting. This indicates that the

cellulose favors the phase segregation of the polyurethane hard and soft phases. This effect reduces the interruption of soft segment crystallites by reducing order in the hard segment domains. Thus, the soft segment crystallites formed in the presence of the reinforcement are more perfect and melt at higher temperatures than those that are formed in the unreinforced polyurethane matrices. The endotherms corresponding to the melting and crystallization of the hard segment phase of the neat polyurethane and the nanocomposites of the MDI 2900/32 system are small, but noticeable. By addition of the CNF, the endotherm is suppressed. This suppression is due to the polar nature of the cellulose nanofibers, which suggests a preferential association with the hard segments that are more polar than the PTMG soft segments. This association between the CNF and the hard segments interferes with the hydrogen bonding that physically links together the hard segments in crystalline domains, preventing ordering. This effect was previously reported in studies of nanocomposites constructed from segmented polyurethane matrices with clay nanoplatelets [Gregory, 2005]. During that study of nanocomposite morphology, it was found that the polar nanoparticles affected mostly the ordering of the hard segment domains and that the crystallization of the soft segment domains was favored through the increased phase separation.

Sample Designation	CNF Content [wt%]	$T_{melting}$ SS [°C]	$\Delta H_{melting}$ SS(J/g)	T_c SS [°C]	$\Delta H_{c\,SS}$ (J/g)	$T_{melting}$ HS [°C]	$\Delta H_{melting}$ HS (J/g)	T_c HS [°C]	ΔH_c HS(J/g)
MDI 2000/32	0	15.8	27.9	-16.5	19.9	*	*	*	*
	0.5	17.8	64	-17.1	34.4	*	*	*	*
	1.0	19.4	55.1	-20.3	30.6	*	*	*	*
	1.5	21.5	38.2	-23.9	12.9	*	*	*	*
	2.0	15.7	53.1	*	*	*	*	*	*
MDI 2900/32	0	24.2	87.1	-6.4	32.8	202.3	3.0	*	*
	0.5	23.0	81.6	-5.1	33.4	196.0	3.4	163.1	2.3
	1.0	18.4	66.3	-18	21.5	*	*	*	*
	1.5	21.0	60.3	-12.7	30.6	189.7	2.2	142.8	0.8
	2.0	20.9	70.7	-13.8	2.9	195.7	4.2	155.8	2.3

Table VI-1. Thermal transitions for MDI system. * indicates that no transition was observed.

The soft segment transition temperatures and enthalpy of melting for the TDI 2000/32 and TDI 2900/32 systems are shown in Table VI-2. Once again, the results from the second heating cycle are focused upon. The TDI 2000/32 system exhibited only a slight change upon the addition of cellulose nanofibers. The overall behavior remained relatively constant. The addition of cellulose nanofibers to the TDI 2900/32 matrix creates an increase in the melting transition of the soft segments. The melting and crystallization temperatures and enthalpies of melting and crystallization of the soft segments also exhibited an increase. Similar to the MDI system, this is due to the more perfect soft segment crystallites, which are formed in the presence of the reinforcement, that melt at higher temperatures.

Sample Designation	CNF Content [wt%]	$T_{melting}$ SS [°C]	$\Delta H_{melting}$ SS(J/g)	T_c SS [°C]	ΔH_c SS [J/g]
TDI 2000/32	0	18.6	47.6	-23.0	18.5
	0.5	21.8	77.4	-22.3	9.7
	1.0	18.7	78.9	-20.1	24.1
	1.5	17.9	58.4	-19.1	23.8
	2.0	16.7	48.8	-20.5	19.5
TDI 2900/32	0	23.2	45.6	-9.0	28.1
	0.5	22.6	85.0	-3.7	44.1
	1.0	18.2	46.4	-3.2	43.5
	1.5	24.2	126.9	-3.4	45.4
	2.0	24.4	78.2	-3.3	61.8

Table VI-2. Thermal transitions for TDI system.

Mechanical Characterization

The tensile properties of the nanocomposites were evaluated at room temperature. The modulus values for the segmented polyurethane matrices vary greatly from the values listed in Chapter II. This discrepancy is due to the transition temperature of the soft segments, which is very close to room temperature. The mechanical behavior is greatly affected by the temperature. If the matrices are tested at a temperature above the melting temperature of the soft segment, the samples will exhibit a lower modulus but a higher elongation at break. Conversely, if the samples are tested below the melting temperature of the soft segments, they will exhibit a higher modulus but lower elongation at break. In order to evaluate the behavior of the nanocomposites in relation to the matrices, all samples were tested on the same day to remove the effect of temperature. The stress versus strain curves for all samples exhibited typical elastomeric behavior.

147

Table VI-3 summarizes the mechanical properties for nanocomposites constructed with MDI 2000/32 and MDI 2900/32 as the matrices. The addition of high modulus cellulose nanofibers to the segmented polyurethane matrix increases the Young's modulus (E) of the elastomers, but simultaneously, the cellulose nanofibers may interfere with the formation of the hard segment domains which leads to a decrease in modulus. The latter effect is not as noticeable in this case where cellulose is added after the reaction as it was in the previous chapter where cellulose nanofibers were added during the reaction. The results indicate that the addition of a small amount of CNF (0.5 wt%) produces a significant increase in the tensile modulus. However, addition of increasing amounts of CNF produces only a small increase in the tensile modulus. The effect of the rigid fibrils on the polymer matrix is the dominant effect. The effect of the addition of nanoreinforcements with a high modulus outweighs the detrimental effect the nanoparticles have on the ordering of the hard segment domains.

The elongation at break (ε_b) of the samples is also affected by the addition of cellulose nanofibers. For the MDI system, the behavior is expected for an elastomer reinforced with rigid particles. In this system, the higher CNF content produces a lower the elongation at break. The major change occurs by addition of a minimum amount of cellulose. In this system, a greater degree of phase separation and ordering of the soft and hard domains is present prior to the addition of the CNF due to the structure of the isocyanate and the soft segment lengths.

Sample Designation	CNF Content [wt%]	E [MPa]	σ_y [Pa]	ε_b [%]
MDI 2000/32	0.0	1.4 ± 0.4	0.7E6±0.2E5	507.5±150.0
	0.5	13.0 ± 1.4	1.5E6 ± 2.1E4	99.4 ± 12.0
	1.0	7.7 ± 1.1	1.06E6 ± 1.9E5	94.3 ± 6.1
	1.5	19.4 ± 3.4	2.3E6 ± 3.7E5	96.2 ± 8.8
	2.0	10.4 ± 1.4	1.3E6 ± 1.3E5	76.1 ± 24.4
MDI 2900/32	0.0	1.1 ± 0.2	0.3E6 ± 0.5E5	896.6 ± 203.2
	0.5	5.9 ± 0.6	1.2E6 ± 7.6E3	152.0 ± 12.2
	1.0	6.6 ± 1.0	1.3E6 ± 1.0E5	172.7 ± 14.6
	1.5	4.5± 0.9	0.9E6 ± 3.9E4	103.0 ± 33.4
	2.0	5.0± 0.6	1.5E6 ± 8.8E4	727.2 ± 58.2

Table VI-3. Mechanical properties for nanocomposites with the MDI system as a matrix.

The mechanical properties of the TDI 2000/32 system nanocomposites were not evaluated because they were very soft and pliable at room temperature making measurement impossible. The mechanical performance of nanocomposites constructed with TDI 2900/32 as a matrix is outlined in Table VI-4. The initial addition of nanofibers created a decrease in the Young's modulus and strength of the nanocomposites. However, addition of increasing amounts of nanofillers produced an increase in the properties. At 2 wt% CNF, the maximum nanoreinforcement content studied, the properties were the same as the unfilled matrix. In the future, higher particle loadings should be studied. The main effect of nanoreinforcement addition was the sizable increase in the elongation at break. Many researchers have reported a decrease in elongation upon addition of nanofillers, which was observed in the MDI 2000/32 and MDI 2900/32 systems [Paul & Robeson, 2008; Shah et al., 2005]. However, the chemical structure of the TDI 2900/32 system creates a different effect when the sample is elongated. The addition of cellulose nanofibers creates greater phase segregation and domain organization,

which is visible from the DSC results above. When the structure is elongated the cellulose

nanofibers align and orient within the polymer matrix and allow for greater elongation.

Sample Designation	CNF Content [wt%]	E [MPa]	σ_y [Pa]	ε_b [%]
TDI 2900/32	0.0	1.2 $\pm$ 0.083	5.5E5 $\pm$ 5.5E4	542.5 $\pm$ 29.0
	0.5	0.4 $\pm$ 0.109	1.7E5 $\pm$ 7.1E4	714.4 $\pm$ 66.5
	1.0	0.7 $\pm$ 0.932	3.4E5 $\pm$ 5.4E4	798.6 $\pm$ 94.7
	1.5	0.9 $\pm$ 0.1	4.4E5 $\pm$ 5.5E4	470.1 $\pm$ 21.8
	2.0	1.1 $\pm$ 0.1	5.5E5 $\pm$ 6.8E4	976.4 $\pm$ 144.7

Table VI-4. Mechanical properties for nanocomposites utilizing TDI 2900/32 as the matrix.

Shape Memory Behavior (SMB)

Similar to Chapter II, shape memory behavior of the CNF/PU nanocomposites was evaluated at

60°C using a deformation rate of 20 mm/min through a series of cyclic thermomechanical tests.

A maximum deformation of 100% was chosen. Nanocomposites constructed using the TDI

2900/32 system as a matrix were given attention.   The results for fixity and recovery ratios from

the first 4 cycles are shown in Table VI-5.

From the results it is clear that the addition of CNF to the polyurethane matrix in the range of

particle loadings studied does not make a significant impact on the shape fixity or recovery.

While no change is observed, this is an important result due to other researchers who have

observed a decrease in or elimination of the shape memory properties with the addition of

nanoreinforcements [Auad et al., 2009; Razzaq & Frormann, 2007].

TDI 2900/32 T = 60°C 20mm/min	CNF [wt%]	1st cycle [%]	2nd cycle [%]	3rd cycle [%]	4th cycle [%]
Fixity	0	95.51±0.01	96.97±0.90	94.92±2.72	96.62±0.88
	0.5	98.32±1.07	98.68±0.06	98.78±0.25	98.76±0.45
	1.0	97.06±0.54	96.66±0.03	96.16±0.23	96.76±0.62
	1.5	97.64±1.36	98.16±0.23	98.32±0.79	97.36±0.23
	2.0	97.04±2.77	97.22±1.95	98.46±0.59	96.94±0.37
Recovery	0	82.09±3.01	82.34±0.48	77.78±0.76	75.32±3.33
	0.5	83.84±5.89	76.84±1.65	76.50±3.54	66.34±3.77
	1.0	87.64±5.37	79.48±4.47	78.16±2.60	74.64±1.47
	1.5	86.16±1.64	73.75±8.84	74.14±1.95	67.78±1.16
	2.0	80.45±0.95	79.38±0.08	70.64±0	70.2±1.70

Table VI-5. Shape memory testing results of the nanocomposites.

Experimental Parameters

In order to evaluate the effect of recovery time, the unfilled TDI 2900/32 matrix was tested at 60°C using a strain rate of 100 mm/min and a maximum deformation of 100%. This sample was compared to a nanocomposite containing 1.5 wt% cellulose nanofibers. The results are shown in Table VI-6. From the results, it is clear that the fixity and recovery increase with recovery time for the unfilled matrix as well as the nanocomposites. This result was expected and similar behavior was shown for other deformation rates and conditioning temperatures in Chapter II. With the addition of cellulose nanofibers, a slight increase is observed in the fixity along with a small reduction in the recovery. This result was also expected and corresponds to the DSC data. The fixity is governed by the soft segments, which exhibited an increase in enthalpy of melting during differential scanning calorimetry experiments. This increase indicates more perfect crystalline structures are formed upon the addition of CNF and so an increase in shape fixity is the resultant effect. By increasing the recovery time from 5 to 10 minutes, the CNF/PU

nanocomposites exhibited very little change in shape fixity but a sizable increase was observed in shape recovery. Once again, this was the expected result. The increase in recovery time allows additional time for the hard segments to recover the original shape.

Recovery Time [mins]	CNF [wt%]		1st cycle [%]	2nd cycle [%]	3rd cycle [%]	4th cycle [%]
5	0	Fixity	96.32	95.56	96.52	96.84
		Recovery	90.44	87.72	81.88	74.12
5	1.5	Fixity	97.96	98.44	97.88	98.08
		Recovery	82.68	72.20	77.60	77.60
10	0	Fixity	97.08	97.92	95.56	97.32
		Recovery	95.88	93.56	91.61	86.16
10	1.5	Fixity	97.76	97.44	97.36	96.88
		Recovery	96.00	96.00	90.44	70.64

Table VI-6. Shape memory results comparing the recovery time of the unfilled TDI 2900/32 matrix and a nanocomposite containing 1.5 wt% CNF tested at a strain rate of 100 mm/min and a temperature of 60°C.

In addition to the thermomechanical testing, the effect of the recovery time of the nanocomposites was evaluated using dynamic mechanical analysis at 40°C and 20 mm/min with a maximum deformation of 300%. Recovery times of 5, 10, and 20 minutes were evaluated. The procedure was discussed in Chapter II.   The results for a recovery time of 5 minutes are shown below in the stress versus strain curve pictured in Figure VI-8. The graph shows the behavior of the sample during the initial run and the recovery behavior 5 minutes later (indicated by the dashed line).
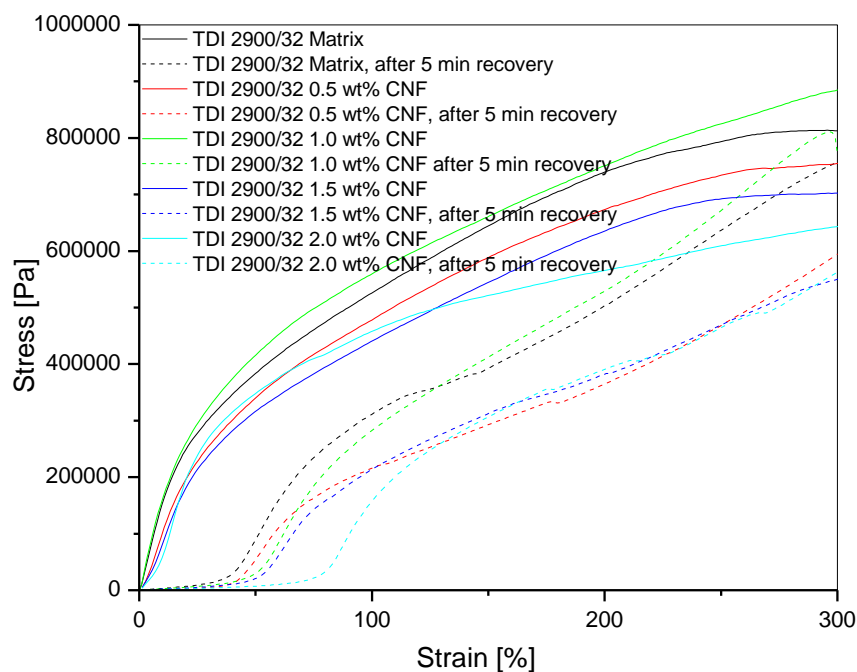
Figure VI-8. Evaluation of a recovery time of 5 minutes on TDI 2900/32 nanocomposites. The dashed lines indicate the recovery behavior.

Tests were performed to evaluate recovery times of 10 and 20 minutes. Graphs similar to Figure VI-9 were generated and the recovery was evaluated. Figure VI-9 is a better representation of the recovery. The calculation of the recovery values from the graph was previously discussed in Chapter II. The graph shows the percent recovery versus the CNF concentration. When the samples were allowed to recover for 5 minutes, a clear decrease with an increase in CNF concentration was observed. By allowing additional time for recovery to occur, the samples exhibit increased recovery at higher CNF concentrations of 2 wt%. This result is expected as the addition of CNF creates more perfect crystalline soft segments, as exhibited earlier by the DSC, which must be recovered by the hard segments. Increasing the recovery time allows the hard segments to recover more of the original shape.

153
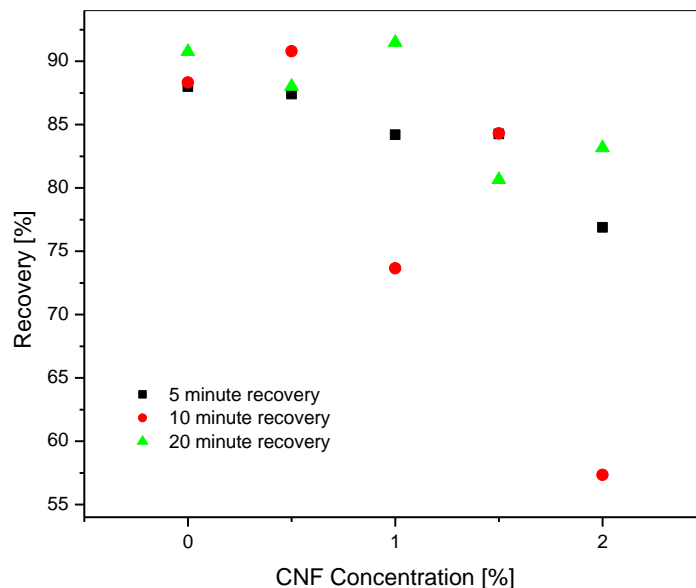
Figure VI-9. Comparison of recovery versus CNF concentration over time.

CONCLUSIONS

Cellulose nanofibers were incorporated into segmented shape memory polyurethanes matrices after the polymerization. The incorporation of cellulose nanofibers induced changes in the micro-structure of the polyurethane matrices, which in turn affected the thermal and mechanical performance of the nanocomposites. Generally, the cellulose nanofibers favored the phase separation between the soft and hard domains generating an upward shift in the melting temperatures of the crystalline phases, an increase in the Young's modulus, and a decrease in deformation at break. These results are similar to those for nanocomposites in which cellulose nanofibers were added during the first step of the polymerization. However, the main difference is that nanocomposites with CNF incorporation post polymerization retain their shape memory behavior.

154

REFERENCES

1. Aranguren, M. I. ; Mora, E. ; DeGroot Jr., J.V. ; Macosko, C.W. Effect of Reinforcing Fillers on the Rheology of Polymer Melts. *J. Rheol*., **1992**, *36*, pp 1165.

2. Auad, M. L.; Mosiewicki, M. A.; Richardson, T.; Aranguren, M. I.; Marcovich, N. E. Tailored Shape Memory Polyurethane Reinforced with Microcrystalline Cellulose Nanofibers. Accepted for publication in *Journal of Applied Polymer Science*, **2009**.

3. Dani, A. ; Ogale, A. A. Electrical Percolation Behavior of Short-Fiber Composites : Experimental Characterization and Modeling. *Composites Science and Technology*, **1996**, *56*, pp 911-920.

4. Du, F. ; Scogna, R. C. ; Zhou, W. ; Brand, S. ; Fisher, J. E. ; Winey, K. I. Nanotube networks in Polymer Nanocomposites : Rheology and Electrical Conductivity. *Macromolecules,* **2004**, *37*, pp 9048.

5. Favier, V. ; Cavaille, J. Y. ; Canova, G. R. ; Shrivastava, S. C. Mechanical Percolation in Cellulose Whisker Nancomposites. *Polymer Engineering and Science*, **2004**, *37* (10), pp 1732-1739.

6. Gregory, S. P. Synthesis and Characterization of Silk-inspired Thermoplastic Polyurethane Elastomers. PhD Thesis, Massachusetts Institute of Technology, Dept. of Chemical Engineering, USA (2005).

7. Guth, E. Theory of Filler Reinforcement. *J. Appl. Phy*., **1945**, *16*, pp 20.

8. Han, C. D. *Rheology and Processing of Polymeric Materials*, Vol. 2. Oxford University Press : New York, 2007.

9. Hough, L. A. ; Islam, M. F. ; Janmey, P. A. ; Yohd, A. G. Viscoelasticity of Single Wall Carbon Nanotube Suspensions. *Phys. Rev. Lett*., **2004**, *93*, pp 168102.

10. Kotsilkova, R.; Ed. *Thermoset Nanocomposites for Engineering Applications*. iSmithers Rapra Publishing: Shawbury, UK, 2007.

11. Krieger, I. M. Rheology of Monodisperse Latices. *Adv. Colloid Interface Sci*., **1972**, *3*, pp 111-136.

12. Marcovich, N. E. ; Auad, M. L.; Bellesi, N. E.; Nutt, S. R.; Aranguren, M. I. Cellulose Micro/Nanocrystals Reinforced Polyurethane. *J. Mater. Res.*, **2006**, *21* (4), pp 870-880.

13. Mewis, J. ; Macosko, C. W. Suspension Rheology. In *Rheology, Principles, Measurements, and Applications*. Macosko, C. W. , Ed. ; Wiley-VCH Publishers : New York, 1994.

14. Orts, W. J.; Shey, J.; Imam, S. H.; Glenn, G. M.; Guttman, M. E.; Revol, J-F. Application of Cellulose Microfibrils in Polymer Nanocomposites. *Journal of Polymers and the Environment*, **2005**, *13* (4), pp 301-306.

15. Panaitescu, D. M.; Vuluga, D. M.; Paven, H.; Iorga, M. D.; Ghiurea, M.; Matasaru, I.; Nechita, P. Properties of Polymer Composites with Cellulose Microfibrils. *Mol. Cryst. Liq. Cryst.*, **2008**, *484*, pp 86/[452]-98/[464].

16. Paul, D. R. ; Robeson, L. M. Polymer Nanotechnology: Nanocomposites. *Polymer*, **2008**, *49*, pp 3187-3204.

17. Payne, A. R. ; Whittaker, R. E. Effect of Vulcanization on the Low-Strain Dynamic Properties of Filled Rubbers. *Journal of Applied Polymer Science*, **1972**, *16*, pp 1191.

18. Razzaq, M. Y. ; Frormann, L. *Journal of Applied Polymer Science*, **1998**, *69*, pp 1563-1574.

19. Shah, R. K. ; Hunter, D. L. ; Paul, D. R. Nanocomposites from poly(ethylene-co-methacrylic acid) ionomers : Effect of Surfactant Structure on Morphology and Properties. *Polymer*, **2005**, *46* (8), pp 2646-2662.

CHAPTER VII.

COMMERCIAL POLYURETHANE NANOCOMPOSITES

INTRODUCTION

The aim of this portion of the research was to investigate the effect of reinforcing commercially available shape memory polyurethane. The incorporation of nanoreinforcements was expected to produce an increase in the mechanical properties of the material while maintaining the shape memory behavior. Additionally, the use of nanoreinforcements was believed to be a pathway to overcome the disadvantages, such as low stiffness and recovery, associated with unfilled polyurethane. The advantages of cellulose nanofibers as nanoreinforcements in synthesized polyurethanes have previously been evaluated and discussed in detail. During this work, conductive cellulose nanofibers (C-CNF) and carbon nanotubes (CNT), in addition to cellulose nanofibers, were used to reinforce a commercial polyurethane, Irogran[TM] PS455-203. These types of conductive nanofillers open the door to a new type of shape memory polymers in which the actuation of the polymer is induced through the temperature changes that occur as a result of the electrical conductivity of the nanofillers.

The use of conductive cellulose nanofibers (C-CNF) is a new approach to the creation of a conducting polymer composite. Conducting polymers, such as polyaniline and polypyrrole, have been investigated for deposition on a variety of substrates such as particles, fibers, polymer films, and membranes. [Stejskal et al., 2005]. The use of polyaniline is desirable due to its

environmental stability, easy polymerization, low cost, and potential applications in biosensors, electrodes, batteries, and gas sensors [Li et al., 2009; Mo et al., 2009]. The main drawback, however, is the low mechanical properties of the conducting polymer. Other researchers have sought to take advantage of polyaniline's conductive properties while overcoming its low mechanical properties by coating nanoreinforcement materials, such as cellulose nanofibers or wood sawdust [Dutta et al., 2005; Sapurina et al., 2003]. The desired effect is that the produced nanocomposites will gain the increase in mechanical properties from the nanoreinforcement and the conductive properties from the polyaniline coating.

Carbon nanotubes (CNT) have gained increasing attention due to their superior mechanical properties, high electrical/thermal conductivity, and high specific surface area [Chen et al., 2006; Mondal & Hu, 2006]. Many other researchers have found that a substantial increase in Young's modulus, tensile strength, and hardness can be achieved through the incorporation of CNT at contents as low as 1 wt% [Chen et al., 2006; Zhang et al., 2004; Frogley et al., 2003]. Similar to the C-CNF, the motivation of this area of the research is the potential of creating a conductive shape memory polyurethane nanocomposite with the increased mechanical properties made possible by use of CNT and the added benefit of a possible new actuation mechanism for the shape memory behavior.

MATERIALS AND METHODS

All nanoreinforcements utilized in nanocomposite construction after the modifications outlined in Chapter IV. A commercial polyurethane matrix (Irogran^{TM} PS455-203, Huntsman, USA) was received in pellet form and dissolved in DMF solvent to be utilized as the polymer matrix for

construction of nanocomposites. The properties shown in Table VII-1 for the chosen polyurethane were obtained from the Huntsman website [www.huntsman.com].

Melt Flow Index	177°C/2.16kg-22
Softening Onset	110°C
Tensile Strength	22.0 MPa
100% Tensile Modulus	3.0 MPa
300% Tensile Modulus	6.0 MPa
Ultimate Elongation	700%

Table VII-1. Listed properties for Irogran[TM] PS455-203 on the Huntsman website.

Cellulose Nanofibers (CNF) and Conductive Cellulose Nanofiber (C-CNF) Nanocomposites

CNF and C-CNF nanocomposites were constructed in a similar manner as outlined in Chapter VI. The CNF and C-CNF, which had been previously freeze dried, were dispersed in DMF using ultrasonic treatments. The CNF/DMF and C-CNF/DMF suspensions were then incorporated into a 30 wt% dissolved commercial polyurethane/DMF solution. A speedmixer (DAC 150) was used at 2000 rpm for 18 minutes to aid in dispersion. Nanocomposite solutions with varying percentages of nanofillers were prepared. The suspensions were cast in open Teflon® molds and dried in a convection oven at 80°C for 24 hours in order to achieve films.

Carbon Nanotubes (CNT)

A similar procedure to that of the CNF and C-CNF was used to prepared CNT nanocomposites. CNTs were dispersed in DMF using limited ultrasonic treatments. Ultrasonication time was limited to 10 minutes to avoid breakage and degradation of the CNT structure. The CNT suspension was then added to a 30 wt% dissolved commercial polyurethane/DMF solution. The speedmixer was used to aid in dispersion. Nanocomposite solutions with 1 and 2 wt% CNTs

were prepared. The suspensions were cast in open Teflon® molds and dried in a convection oven at 80°C for 24 hours in order to achieve films.

TECHNIQUES

Differential scanning calorimetry (DSC), thermal gravimetric analysis (TGA), tensile measurements, scanning electron microscopy (SEM), and evaluation of shape memory behavior were performed following the procedures outlined in Chapter II. Rheological characterization was performed following the procedure outlined in Chapter VI, however, the molten state of the commercial polyurethane matrix was determined to be 160°C in the temperature sweep experiments.

Conductivity

The electrical conductivity of the composites prepared with different concentrations of nanocrystals was determined at room temperature using and ad-hoc equipment (two probe method).

RESULTS AND DISCUSSION

Cellulose Nanofibers (CNF)

Rheological Characterization

Rheological experiments were used to investigate the percolation composition of the reinforced polyurethane. Figure VII-1 shows the frequency dependence of storage modulus, G', for melted films at 160°C and 1% strain with varying percentages of CNF. It is immediately apparent from this figure that cellulose nanofibers (CNF) have a dramatic effect on nanocomposites at very

small particle loadings. Samples prepared with less than 1 wt% CNF exhibited Newtonian liquid behavior in the frequency range analyzed. At concentrations higher than 1.0 wt% a clear non-Newtonian behavior is introduced by the presence of CNF. From these results, it is suggested that a qualitative change occurs in the range of 1-2 wt% of CNF. A plateau appearing at 1 wt% CNF is in the range previously reported by other investigators [Marcovich et al., 2006].
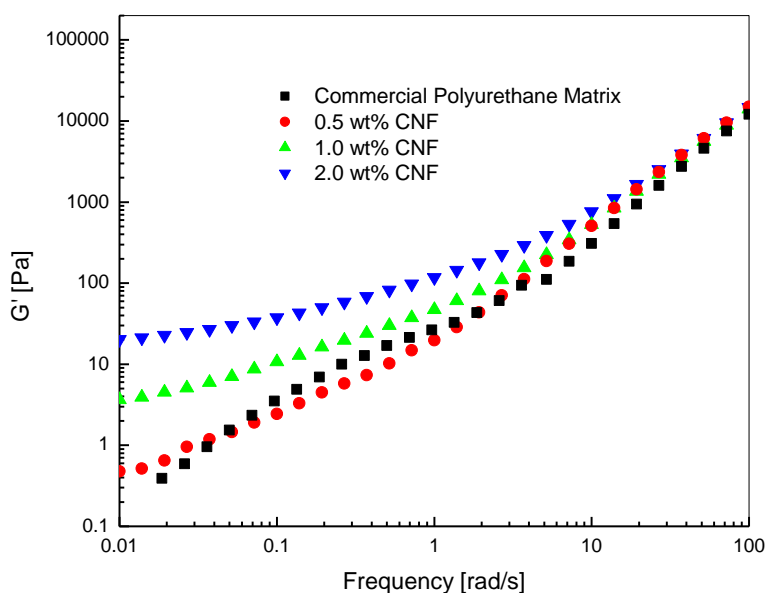
Figure VII-1. Storage modulus, G', versus frequency for the CNF/PU nanocomposites.

Thermal Characterization (DSC)

The effect of cellulose nanofibers on the thermal behavior of the segmented polyurethanes was studied by differential scanning calorimetry (DSC). The data corresponding to the first temperature cycles are analyzed and the data is presented in Table VII-2. From the results, it is clear that the presence of cellulose nanofibers do not produce a significant change in the thermal properties of the commercial polyurethane matrix.

Filler [wt%]		$T_{melting}$ SS [°C]	$\Delta H_{melting}$ SS (J/g)
Commercial Polyurethane Matrix		20.6	5.6
CNF	0.5	21.3	3.1
	1.0	17.9	1.9
	1.5	19.2	4.6
	2.0	20.2	4.5

Table VII-2. Soft segment transitions of CNF/PU nanocomposites.

Mechanical Characterization

The mechanical properties of the CNF/PU nanocomposites are presented in Table VII-3. All the nanocomposite samples exhibited increased Young's modulus (E) and strength (σ_y) over the unfilled commercial polyurethane matrix. Additionally, all the nanocomposite samples presented an elongation at break (ε_b) of more than 500%. The elongation at break of the samples reinforced with 1.5 and 2 wt% CNF actually exceeded that of the unfilled matrix. The decrease in elongation exhibited by the 0.5 and 1.0 wt % sample may be due to inadequate dispersion or agglomerations of the nanoparticles. These aggregations would behave as defects in the polymer matrix and create breaking points therefore resulting in a decreased elongation at break. Overall, the elongation at break exhibited an increase with increasing filler content. This behavior was unexpected and is opposite of the decrease with increasing filler content that has been observed by other researchers [Marcovich et al., 2006; Meincke et al., 2004]. The Young's modulus and strength also exhibited an increase with increasing filler content. The most significant increase occurs in the Young's modulus where the value doubles with the addition of only 0.5 wt% CNF. This is a substantial increase in modulus in comparison to that reported by other investigators [Gall et al., 2002].

Filler [wt%]		E [MPa]	σ_y [MPa]	ε_b [%]
Commercial Polyurethane Matrix		8.70 ± 1.43	1.51 ± 0.15	1664.07 ± 49.43
CNF	0.5	16.43 ± 1.41	2.00 ± 0.76	526.80 ± 22.80
	1.0	21.54 ± 0.56	1.88 ± 0.22	829.50 ± 24.00
	1.5	24.44 ± 10.47	2.83 ± 0.30	1715.63 ± 255.62
	2.0	26.82 ± 2.13	3.18 ± 0.11	1884.93 ± 92.23

Table VII-3. Mechanical properties of CNF/polyurethane nanocomposites.

Scanning Electron Microscopy (SEM)

Scanning electron microscopy was used to view the fracture surface of both the unfilled polyurethane and the polyurethane nanocomposites. The fracture surface of the unfilled polyurethane can be viewed in Figure VII-2. The fracture surface is mostly featureless except for a few features which are characteristic of a brittle fracture.
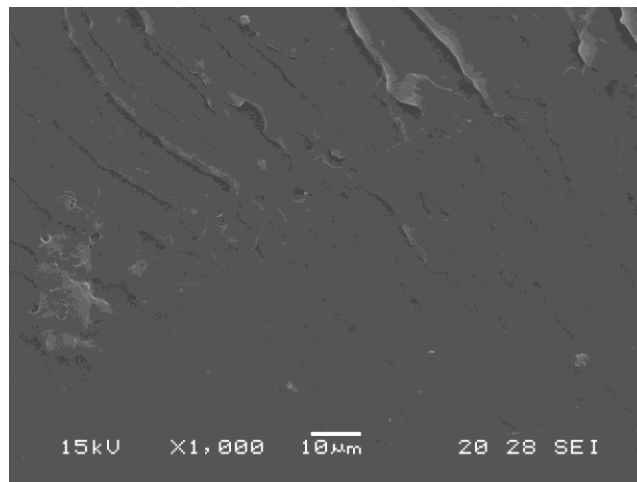
Figure VII-2. SEM image of the commercial polyurethane matrix.

In contrast to the unfilled commercial polyurethane matrix, the 0.5 and 1 wt% CNF reinforced films, which are shown in Figure VII-3 a and b, respectively, exhibit a very different fracture

surface. The rougher surface indicates increased energy dissipation during fracture due to changes in the crack trajectory. Due to the reinforcements, the crack pathway must change to avoid or go around the rigid filler material. This is further evidenced by the increasing roughness of the nanocomposite containing 1 wt% CNF over that which contains only 0.5 wt% CNF.
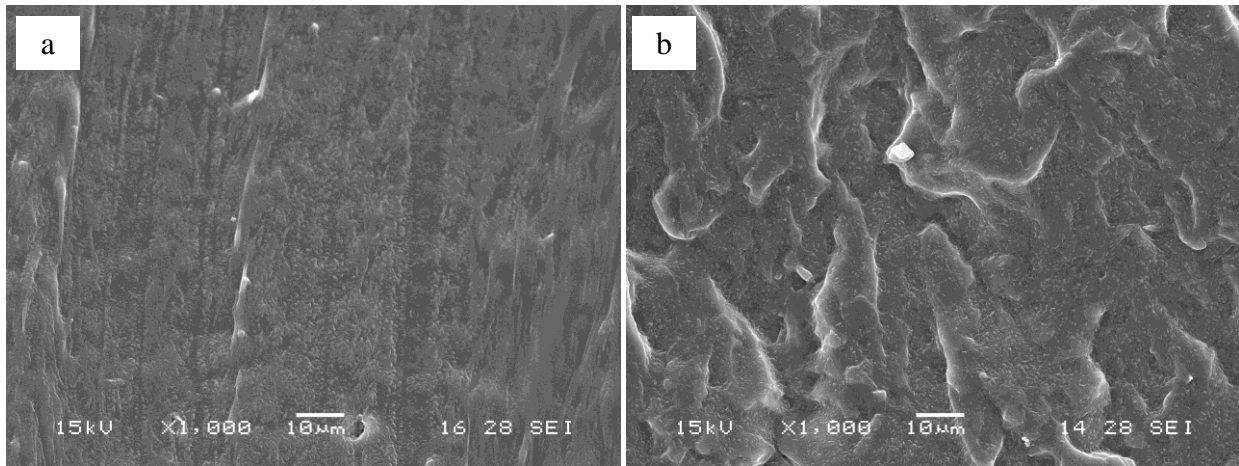
Figure VII-3. SEM images of CNF/PU nanocomposites with a) 0.5 wt% and b) 1.0 wt% CNF.

Shape Memory Behavior (SMB)

The shape memory behavior of the unfilled polyurethane matrix and the CNF/PU nanocomposites was tested through a series of thermomechanical cycles. The temperature selected for the shape memory testing was 60°C, which was an intermediate temperature between the melting of the soft and hard segments. The results are summarized in Table VII-4. Although there is a slight variation in the fixity (R_f) and recovery ratios (R_r), there was no significant variation in the nanocomposites prepared with 1 wt% CNF over that of the unfilled commercial polyurethane matrix. As previously discussed, the stiffness of the material could be

increased with the addition of CNF. The improvement in stiffness does not appear to negatively

impact the shape memory behavior of the nanocomposites.

CNF [wt%]	1st cycle		2nd cycle		3rd cycle	
	% R_f	% R_r	% R_f	% R_r	% R_f	% R_r
0	92.6±1.1	72.5±5.3	91.9±0.2	67.7±9.9	90.5±0.1	63.1±12.9
0.5	94.4	72.3	94.4	71.7	94.2	73.9
1.0	96.9	73.3	96.8	98.9	85.6	62.5

Table VII-4. Shape memory behavior of CNF/PU nanocomposites.

Conductive Cellulose Nanofibers (C-CNF)

Rheological Characterization

Figure VII-4 shows the storage modulus, G', versus the frequency in the linear viscoelastic range

(small strains) for the composite polyurethane films in the liquid molten state (at 160°C). The

storage modulus of the liquid experiences an increase with C-CNF concentration. The largest

variations are observed at low frequencies, where the structure of the C-CNF is more effective in

increasing the relaxation times of the material. Addition of a low concentration of C-CNF

produces a non-Newtonian response and thus, the storage modulus is a function of the frequency

for all the composites at concentrations above 4 wt %.

From these results, it is suggested that a qualitative change occurs in the range of 4 - 10 wt% of

C-CNF. The concentration threshold is much lower than usually found in macroscopic filler

composites [Marcovich et al., 2004], however it is higher than the threshold previously found for

CNF/Polyurethane nanocomposites. This difference can be attributed to the "gluing" action of

the polyaniline as it grows on the surface of the nanofibers. The conductive polymer may act to

link the C-CNFs, which consequently causes them to behave as thicker fibers of lower aspect ratio than the nonconductive CNFs.
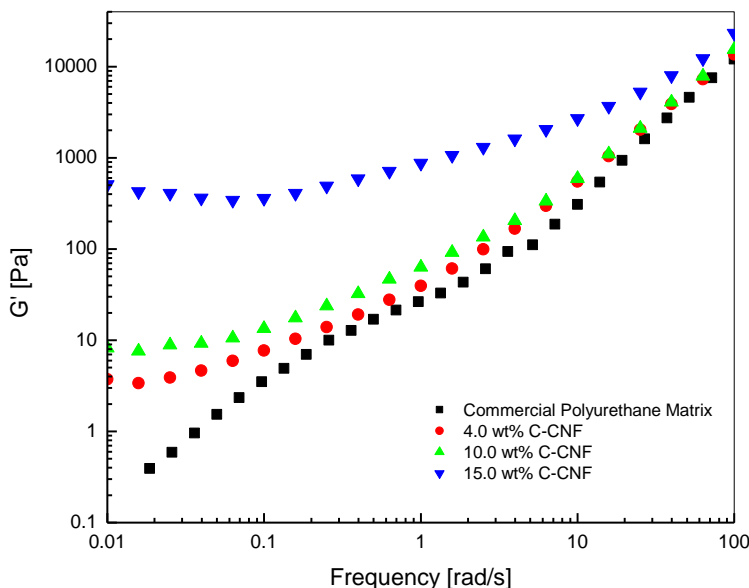
Figure VII-4. Storage modulus, G', versus frequency of the melted polyurethane composites containing different concentrations of C-CNF.

Thermal Characterization (DSC)

The thermal transitions are summarized in Table VII-5. Overall, the trend exhibited is an increasing melting point of the soft segments with increasing C-CNF concentration. A similar trend is observed for the enthalpy of melting of the soft segments, which is about 4 times bigger for the 15 wt% composite than for the commercial polyurethane matrix. These changes indicate that the C-CNF favors phase separation, leading to the formation of more perfect crystals and to increased crystallinity (higher melting temperature and higher heat of melting, respectively). The effect of nanofillers as crystallization nucleating agents has been discussed in the literature in the case of a silica reinforced polyurethane, where the crystallization of the soft segment phase was

also preferentially affected by the presence of the nanoparticles [Nunes et al., 2001]. Furthermore, this behavior was previously reported for a polyurethane system containing unmodified cellulose nanocrystals [Auad et al., 2008] and was explained as the result of the cellulose nanofibrils, CNF, acting as heterogeneous nucleating agents for the polymer crystallization of the soft segments. During that work, the enthalpy of melting associated with the soft segment phase exhibited an increase of 80% with the addition of just 1 wt% of cellulose nanofibers (CNF). Comparatively, a higher C-CNF content is needed to obtain the same increase in the enthalpy of melting (between 4 and 10 wt %).

Filler [wt%]		$T_{melting}$ SS [°C]	$\Delta H_{melting}$ SS (J/g)
Commercial Polyurethane Matrix		20.6	5.6
C-CNF	2.0	22.8	5.3
	4.0	28.4	7.3
	7.0	25.5	7.5
	10.0	26.4	16.4
	15.0	32.6	21.2

Table VII-5. Thermal transitions of C-CNF/PU nanocomposites.

Mechanical Characterization

The mechanical properties of the C-CNF/PU nanocomposites are listed in Table VII-6. As expected, addition of C-CNF has the overall effect of increasing the elastic modulus of the films. Films containing C-CNF reinforcements exhibited no real yield stress response. The value reported corresponds to the intersection of the extrapolated straight lines that can be drawn at low and large deformations. The values follow the same trend observed for the Young's modulus, while a reduction in the elongation at break occurs. These results are expected for the

reinforcement of an elastomer with rigid particles. A large effect is observed in the range of C-CNF concentrations utilized. The modulus of the 10 wt% C-CNF sample is more than three times the modulus of the unreinforced polyurethane matrix. Even though the ultimate elongation is reduced, it is clear that the material maintains the ability to stretch to more than eight times the initial length before rupture, which is still a significantly large extensibility.

Filler [wt%]		E [MPa]	σ_y [MPa]	ε_b [%]
Commercial Polyurethane Matrix		8.70 ± 1.43	1.51 ± 0.15	1664.07 ± 49.43
C-CNF	2.0	11.40 ± 1.76	2.17 ± 0.19	1534.29 ± 91.818
	4.0	17.61 ± 2.07	2.81 ± 0.04	1112.273 ± 109.83
	10.0	31.01 ± 2.35	3.15 ± 0.07	753.00 ± 22.00

Table VII-6. Mechanical properties of C-CNF/PU nanocomposites.

Scanning Electron Microscopy (SEM)

The SEM images of the cryo-fractured surfaces of the C-CNF/polyurethane nanocomposite films with 4 and 10 wt% C-CNF are shown in Figure VII-5. The images show increased roughness in the fracture surface of the 4 wt% sample over the unreinforced polyurethane matrix, which is the obvious result of the decreased crack propagation at points where the rigid cellulose particles deflect the crack towards an easier fracture path. The image corresponding to the surface of the sample containing 10 wt% of C-CNF shows also a very rough surface where the crack path appears to be deflected with higher frequency, in correlation with the increasing concentration of fibrils. There does appear to be some nanofiller aggregation in the sample. Inadequate dispersion problem is practically unavoidable at concentrations above the percolation threshold, such as in this case. Incorporation of relatively high amounts of nanofibrils leads to increasing

dispersion difficulty and to some particle aggregation in the final material, which affects the composite performance.
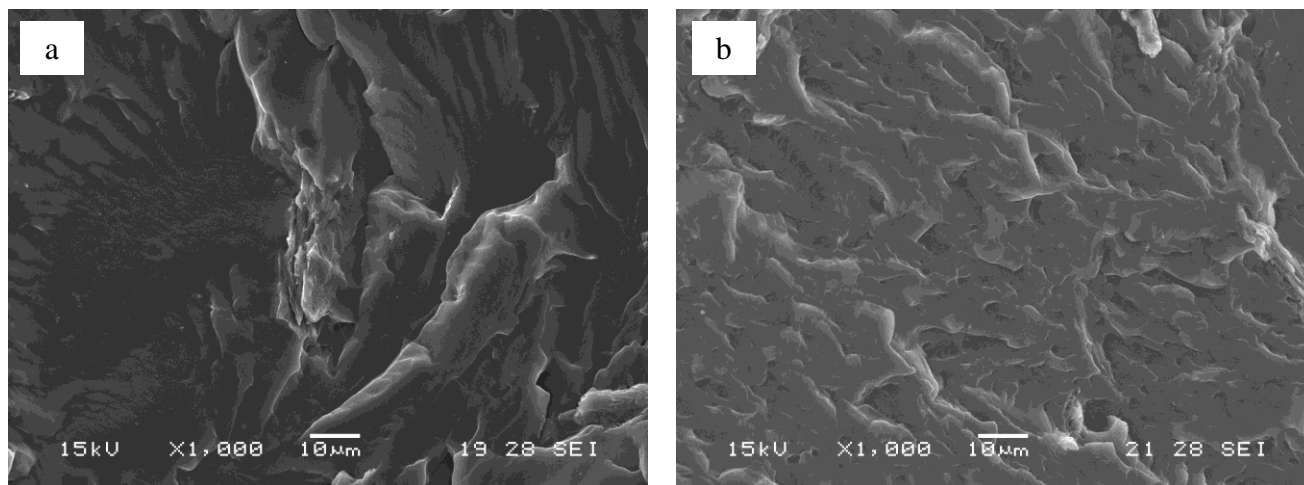
Figure VII-5. SEM images of C-CNF/PU nanocomposites with a) 4 wt% C-CNF and b) 10 wt% C-CNF.

Conductivity

The resistivity of films with varying concentrations of C-CNF is summarized in Table VII-7. At C-CNF concentrations below 4 wt%, the material is non-conductive. However, above this concentration, the sample shows conductivity. Although the conductivity of the samples is low, this method offers an alternate determination of the concentration range at which the percolation of the C-CNF occurs. The electrical percolation threshold appears in the concentration range of 4-10 wt% C-CNF, which is the same concentration range that the rheological percolation was determined. The low values obtained suggest that higher doping should be utilized if more interesting electrical properties are desired [Eichhorn et al., In press]. The use of higher C-CNF concentrations is another option, however, that would lead to reduced extensibility and reduction of the shape memory properties.

Sample	Resistivity (Ω cm)
0 wt% C-CNF	$> 10^{11}$
2 wt% C-CNF	$> 10^{11}$
4 wt% C-CNF	$> 10^{11}$
10 wt.% C-CNF	$2.2 \; 10^{10}$
15 wt% C-CNF	$2.7 \; 10^{10}$
100 wt% C-CNF	$5.3 \; 10^{5}$

Table VII-7. Resistivity values versus C-CNF concentration.

Shape Memory Behavior (SMB)

Table VII-8 summarizes the results for the unreinforced commercial polyurethane sample and for two composite films of different C-CNF concentrations. As previously discussed, the addition of high concentrations of C-CNF increases the tensile modulus of the polyurethane but leads to a reduction in the elongation at break. The effect is important during the high temperature step of the cycle which involved the elongation of the sample at 60°C, for example the 10 wt% composite breaks at about 35 % elongation. Also, by increasing concentrations of the C-CNF larger interactions with the hard segment blocks are produced, which interferes in the arrangement of this phase [Auad et al., 2008]. Increasing dispersion problems should not be underestimated in this respect. The material may still be suitable for some applications, but it does not offer the advantage of large extensibility, which was one of the polyurethane characteristics intended to be preserved, while increasing the modulus.

The fixity and recovery of the samples were calculated according to equations 2 and 3 outlined in Chapter II. The recovery was observed between 63 and 78 % for all the samples up to at least the 4th cycle. Although the recovery calculated with respect to the 100% elongation may seem low, the repeatability of the results in subsequent cycles should be considered. If the actual strain of the tested samples in subsequent cycles (after the first cycle) is considered (ε_m - ε_p), the calculated recoveries would be higher than 85%. Consideration of this value is important because it corresponds to the behavior that the material exhibits during cycling.

C-CNF [wt%]	1st cycle		2nd cycle		3rd cycle		4th cycle	
	% R_f	% R_r	% R_f	% R_r	% R_f	% R_r	% R_f	% R_r
0	92.6±1.1	72.5±5.3	91.9±0.2	67.7±9.9	90.5±0.06	63.1±12.39	93.3±1.1	60.8±12.8
2	95.1±0.5	77.0±4.2	94.5±2.1	73.9±13.5	93.7±2.4	69.4±14.9	93.6±0.8	64.6±13.8
4	90.7±2.8	75.0±17.9	91.5±4.5	73.6±14.5	73.0±0.7	71.2±14.1	78.4±9.0	65.1±2.36

Table VII-8. Recovery and fixity of C-CNF/PU nanocomposites.

The fixity is above 90%, with the exception of the 3rd and 4th cycles of the 4 wt% sample. This drop in fixity of the 4 wt% sample as cycling progresses is suggested to be the result of the interactions of the C-CNF with the hard segment phase of the PU, which leads to increasing morphology disruption during cycling. However, further cycling proved to be repeatable at the elongation used in the study.

Carbon Nanotubes (CNT)

Rheological Characterization

Figure VII-6 shows the frequency dependence of storage modulus, G', for melted samples with varying percentages of CNT. From the graphs, it is observed that G' increases with nanofiller concentration. The most important differences in the graphs are observed in the low frequency range. At higher frequencies, nanofiller effects are comparatively weaker. This phenomenon has been observed for other polymeric nano-systems where the short length dynamics are approximately unchanged but the terminal behavior is strongly modified. At low frequencies, samples begin to show an equilibrium plateau with the addition of as little as 2 wt% CNT. This plateau can be attributed to structural changes that occur due to discrete particles forming crystal networks in the melts. These networks of crystals restrict the long-range motions of the polymer strands. The percolation threshold can be associated with the extensive interactions that occur between the crystals at these concentrations.
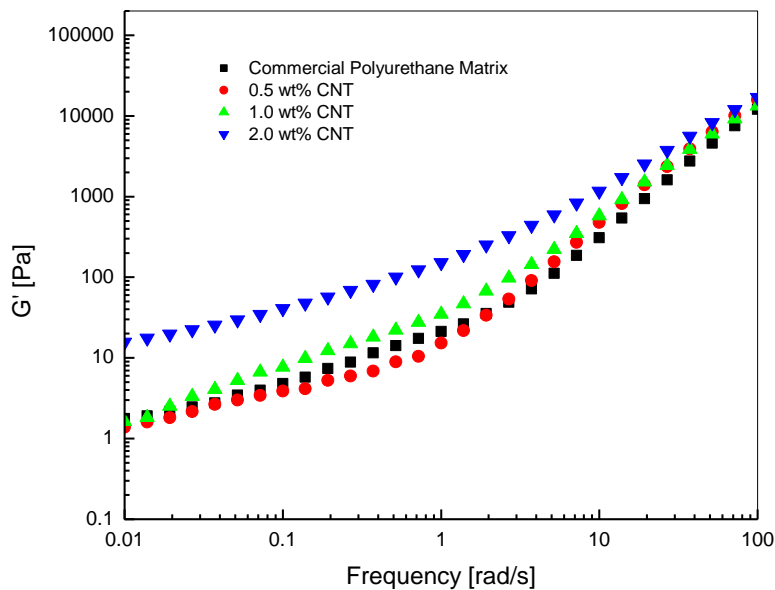
Figure VII-6. Storage modulus (G') versus frequency for CNT/PU nanocomposites.

Thermal Characterization (DSC)

Table VII-9 shows the melting temperatures of the soft segments, corresponding to the first heating of the polyurethane matrix without reinforcement and the nanocomposites prepared with the addition of 0.5 wt% and 1 wt% of CNT.   The addition of carbon nanotubes to the polyurethane matrix does not cause a measurable change in the melting temperatures of the nanocomposite material.

Filler [wt%]		$T_{melting}$ SS [°C]	$\Delta H_{melting}$ SS (J/g)
Commercial Polyurethane Matrix		20.6	5.6
CNT	0.5	23.6	11.3
	1.0	26.3	4.4
	2.0	24.0	2.9

Table VII-9. Melting transitions for CNT/Polyurethane nanocomposites.

Mechanical Characterization

The Young's modulus (E), the yield stress (σ_y), and the elongation at break (ε_b) of the nanocomposite films are presented in Table VII-10. Similar to cellulose nanofibers, the addition of 0.5 wt% CNT produced a 51% increase in the Young's modulus over the unfilled commercial polyurethane. The strength increased dramatically over that of the unfilled commercial polyurethane with the increase of the nanofiller content, reaching a maximum value of 6.58 ± 0.53 MPa at 1 wt% CNT. All the nanocomposite strengths are higher than that of the unreinforced polyurethane. So, it can be confirmed that the nanofiller acts as a reinforcing material with very good fiber-matrix interface. In contrast with microreinforced composites, the elongation at break of this system was not significantly impacted by the presence of nanoreinforcements.

Filler [wt%]		E [MPa]	σ_y [MPa]	ε_b [%]
Commercial Polyurethane Matrix		8.70 ± 1.43	1.51 ± 0.15	1664.07 ± 49.43
CNT	0.5	12.98 ± 1.90	5.55 ± 0.61	1061.10 ± 7.89
	1.0	19.19 ± 1.84	6.58 ± 0.53	1205.72 ± 32.10

Table VII-10. Mechanical properties of CNT/PU nanocomposites.

Scanning Electron Microscopy (SEM)

The scanning electron micrographs of the 0.5 and 1.0 wt% CNT/PU nanocomposites are shown in Figure VII-7 a and b. Similarly to the CNF/PU and C-CNF/PU nanocomposites the roughness of the fracture surface increases with increasing nanoreinforcement content. The reason for this has been previously discussed in this chapter.
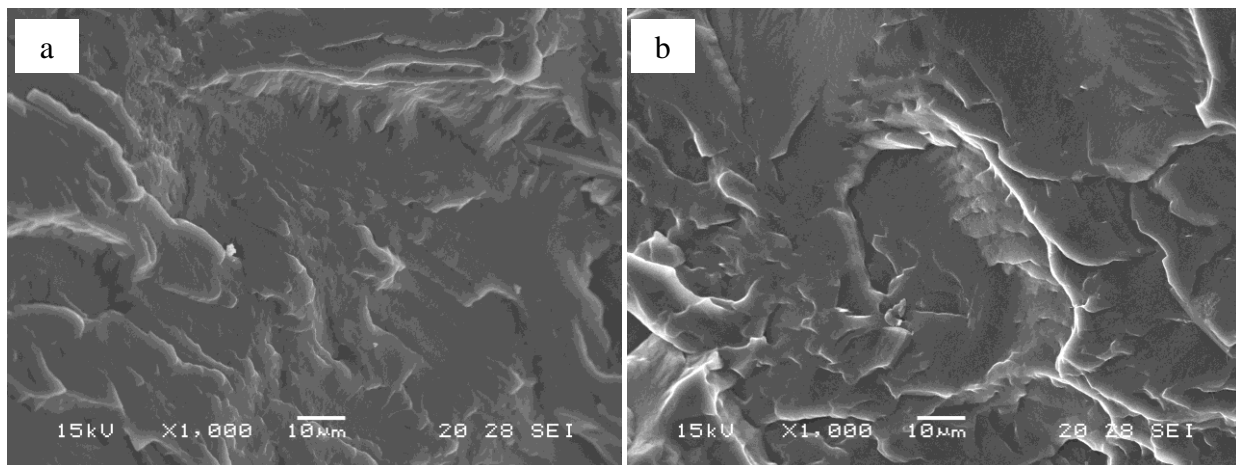
Figure VII-7. Scanning electron micrographs of CNT/PU nanocomposites: a) 0.5 wt% and b) 1.0 wt%.

Shape Memory Behavior (SMB)

It was necessary to verify that the original shape memory properties of the polyurethane were not affected by the incorporation of nanoreinforcements. Shape memory behavior testing was performed on the nanocomposites in order to evaluate the effect of nanoreinforcements on the polyurethane matrix's ability to fix and recovery its shape. Table VII-11 summarizes the shape memory characteristics for the CNT/PU nanocomposite films. The recovery ratio decreased with increasing number of cycles, while the fixity increased (or remained largely unaffected) for both, CNT/PU composites and the unfilled commercial polyurethane matrix. However, the fixity and recovery ratios did not vary significantly in the range of CNT loadings studied. Note that other researchers have found that the addition of nanoparticles to a shape memory polymer decreased the recoverable strain limit, a factor attributed to the inability of the finite fraction of particles to exhibit shape memory behavior, but increased the attainable recovery stress [Gall et al., 2002]. In the present study, this behavior was not observed because of the low concentration of nanoreinforcements employed. However, researchers in other studies have found an opposite effect where the incorporation of multi-walled carbon nanotubes into a shape memory

polyurethane matrix created an increased recovery ratio and recovery stress of the nanocomposites [Mondal & Hu, 2006; Koerner et al., 2004]. The results of this study more closely resemble the latter findings.

	1st cycle		2nd cycle		3rd cycle		4th cycle	
	% R_f	% R_r	% R_f	% R_r	% R_f	% R_r	% R_f	% R_r
Commercial PU Matrix	92.6±1.1	72.5±5.3	91.9±0.2	67.7±9.9	90.5±0.06	63.1±12.39	93.3±1.1	60.8±12.8
0.5 wt% CNT	91.48	80	93.92	74.33	93.36	73.83	93.68	72.25
1 wt% CNT	92.9 ± 2.0	73.2 ± 9.6	95.7 ± 2.6	67.0 ± 9.0	94.16 ± 1.1	98.5 ± 7.5	94.1 ± 0.6	68.7 ± 5.0

Table VII-11. Shape memory behavior results for CNT/PU nanocomposites.

CONCLUSIONS

Nanocomposites were constructed using a commercially available thermoplastic polyurethane as the matrix and CNF, C-CNF, or CNT as the nanoreinforcements. The effect of the nanoreinforcement on the nanocomposite properties was evaluated. The percolation thresholds of each of the nanocomposite systems was evaluated and found to be 1-2 wt%, 4-10 wt%, and approximately 2 wt% for CNF, C-CNF, and CNT, respectively. The higher percolation threshold of the C-CNF nanocomposite system was attributed to the gluing action of the polyaniline coating on the surface of the cellulose nanofibers. All of the nanoreinforcements evaluated created an increase in the mechanical properties of the nanocomposites over those of the unfilled commercial polyurethane. Additionally, the shape memory behavior was maintained in the range of particle loadings studied.

REFERENCES

1. Auad, M. L.; Contos, V.; Nutt, S.; Aranguren, M.; Marcovich, N. E. Characterization of Nanocellulose Reinforced Shape Memory Polyurethanes. *Polymer International*, **2008**, *57,* pp 651–659.

2. Chen, W.; Tao, X.; Liu, Y. Carbon Nanotube-Reinforced Polyurethane Composite Fibers. *Composites Science and Technology*, **2006**, *66*, pp 3029-3034.

3. Dutta, D.; Sarma, T. K.; Chowdhury, D.; Chattopahyay, A. J. Colloid Interface Sci., **2005**, *283*, pp 153.

4. Frogley, M. D.; Ravich, D.; Wagner, H.D. Mechanical Properties of Carbon Nanoparticles-Reinforced Elastomer. *Comp Sci Technol.*, **2003**, *63*, pp 1647-1654.

5. Gall, K.; Dunn, M. L.; Liu, Y.; Finch, D.; Lake, M.; Munshi, N.A. Shape Memory Polymer Nanocomposites. *Acta Materialia*, **2002**, *50* (20), pp 5115-5126.

6. Eichhorn, S. J.; Dufresne, A.; Aranguren, M.; Marcovich, N.; Capadona, J. R.; Rowan, S. J.; Weder, C.; Thielemans, W.; Roman, M.; Renneckar, S.; Gindl, W.; Veigel, S.; Yano, H.; Abe, K.; Nogi, M.; Nakagaito, A. N.; Mangalam, A.; Simonsen, J.; Benight, A. S.; Bismarck, A.; Berglund, L. A.; Peijs, T. Review: Current International Research into Cellulose Nanofibres and Nanocomposites. In press *Journal of Materials Science* (2009).

7. Koerner, H.; Price, G.; Pearce, N. A.; Alexander, M.; Vaia, R. A. Remotely Actuated Polymer Nanocomposites – Stress-recovery of Carbon-Nanotube-Filled Thermoplastic Elastomers. *Nature Materials*, **2004**, *3*, pp 115-120.

8. Li, D.; Huang, J.; Kaner, R. Polyaniline Nanofibers: A Unique Polymer Nanostructure for Versatile Applications. *Accounts of Chemical Research*, **2009**, *42* (1), pp 135-145.

9. Marcovich, N. E.; Reboredo, M. M.; Kenny, J. M.; Aranguren, M. I. Rheology of Particle Suspensions in Viscoelastic Media. Wood Flour - Polypropylene Melt. *Rheologica Acta*, **2004**, *43*, pp 293-303.

10. Marcovich, N. E.; Auad, M. L.; Bellesi, N. E.; Nutt, S. R.; Aranguren, M. I. Cellulose Micro/Nanocrystals Reinforced Polyurethane. *J. Mater. Res*., **2006**, *21* (4), pp 870-881.

11. Meincke, O.; Kaempfer, D.; Weickmann, H.; Friedrich, C.; Vathauer, M.; Warth, H. Mechanical Properties and Electrical Conductivity of Carbon-Nanotube Filled Polyamide-6 and its Blends with Acrylonitrile/Butadiene/Styrene. *Polymer,* **2004**, *45*, pp 739.

12. Mondal, S.; Hu, J. L. Shape Memory Studies of Functionalized MWNT-Reinforced Polyurethane Copolymers. *Iran Polymer Journal*, **2006**, *15*, pp 135-142.

13. Mo, Z.; Zhao, Z.; Chen, H.; Niu, G.; Shi, H. Heterogeneous Preparation of Cellulose-

Polyaniline Conductive Composites with Cellulose Activated by Acids and its Electrical Properties. *Carbohydrate Polymers*, **2009**, *75*, pp 660-664.

14. Nunes, R. C. R.; Pereira, R. A.; Fonseca, J. L. C.; Pereira, M. R. X-ray Studies on Compositions of Polyurethane and Silica. *Polymer Testing,* **2001**, *20*, pp 707.

15. Sapurina, I.; Frolov, V. I.; Shabsels, B. M.; Stejskal, J. R. Conducting Composite of Polyaniline and Wood. *J. Appl Chem.,* **2003**, *76*, pp 863-867.

16. Stejskal, J.; Trchova, M.; Sapurina, I. Flame-retardant Effect of Polyaniline Coating Deposited on Cellulose Fibers. *Journal of Applied Polymer Science*, **2005**, *98*, pp 2347-2354.

17. http://www.huntsman.com/pu/eng/Products/Thermoplastic_Polyurethane/Product_Information/IROGRAN/Applications/Technical_Extrusion/IROGRAN%C2%AE/index.cfm?PageID=6067

18. Zhang, W. D.; Shen, L.; Phang, I. Y.; Liu, T. X. Carbon Nanotubes Reinforced Nylon-6 Prepared by a Simple Melt-Compounding. *Macromolecules*, **2003**, *37*, pp 256-259.

CHAPTER VIII.

NANOREINFORCED SEGMENTED SHAPE MEMORY POLYURETHANES

PROCESSED BY EXTRUSION

INTRODUCTION

Smart fibers, fibers made from shape memory materials, are able to sense a variety of stimuli, such as electrical, thermal, chemical, or magnetic, from the environment and adapt or respond [Ji et al., 2006]. A new class of textiles constructed from smart materials is emerging for industrial, technical, medical, and military purposes. These "smart textiles" integrate the functionalities of smart materials into the textile structure [Ji et al., 2006]. Smart fibers, or shape memory fibers, find their most immediate application in the textile and clothing industry where they are used to create intelligent textiles capable of self-regulating in response to external stimuli [Meng & Hu, 2007; Tang & Stylios, 2006].

Polyurethane fibers can be produced through a variety of processing techniques such as dry, wet, chemical, and melt spinning [Meng & Hu, 2008]. During this work, the goal was to construct shape memory polyurethane fibers reinforced with cellulose nanofibers (CNF) and carbon nanotubes (CNT) by an extrusion process. The impact of cellulose nanofibers (CNF) and carbon nanotubes (CNTs) as reinforcement for segmented shape memory polyurethane fibers was studied. The morphology and mechanical properties of the fibers were evaluated.

MATERIALS

Multi-walled carbon nanotubes (Shengzhen Nanotech Port Co., China) and microcrystalline cellulose (MCC, Avicel PH-101, FMC BioPolymer, USA) were used after corresponding chemical modifications, which were previously detailed in Chapter III. A commercial shape memory polyurethane matrix (Irogran PS455-203, Huntsman, USA) was received in pellet form and dissolved in dimethylformamide (DMF) solvent to be utilized as the polymer matrix for construction of nanocomposites.

METHODS

Preparation of Nanoreinforced Segmented Shape Memory Polyurethane Suspensions

Polymer solutions were obtained by dissolving 30 wt% commercial polyurethane pellets in DMF solvent. Samples containing 0, 0.5, and 1.0 wt% nanofillers were prepared. Cellulose nanofibers (CNF) were subjected to ultrasonication for approximately 1 hour in DMF prior to their addition into the polyurethane (PU) matrix. Ultrasonication of the CNF in DMF prior to addition to the polyurethane matrix aids in dispersion. After addition of the CNF/DMF suspension to the dissolved polyurethane matrix, a speedmixer (DAC 150) was used at 2000 rpm for 18 minutes to further aid in dispersion of the CNF in the polyurethane matrix. A similar procedure was used to prepare carbon nanotube based composites. However, the ultrasonication time was limited to 10 minutes in order to avoid degradation of the carbon nanotube structure.

Preparation of Nanoreinforced Shape Memory Polyurethanes Fibers by Extrusion

Nanofiller/polyurethane/DMF suspensions were extruded to produce continuous fibers with a fixed cross-sectional profile. Sample solutions were poured into a HPLC syringe pump fitted

with a spinning pack and a single hole spinneret. Each of the prepared suspensions were extruded by dry jet-wet spinning at a temperature of 12.5°C, spinneret diameters of 1.3mm, throughput ranging from 0.05-0.4 mL/min.

The suspensions were filtered through a screen pack containing a 325 mesh screen before passing through the spinneret. Filaments were obtained by forcing the composite suspension through the hole in the spinneret. The spinneret's hole shape determines the final cross section and shape of the finished fiber. As seen in Figure VIII-1 fibers were extruded directly into the coagulation bath with no air gap being used. The system was equipped with a pair of stepped cylinder godets with four levels. This allows three drawing steps, which leads to a total of four draw ratios. In order to produce a variety of fiber sizes and orientations, multiple pump speeds, solution draw down rates, and draw ratios were utilized. After drawing and further exposure to the distilled water coagulation bath, the fiber exits to a take-up package as seen in Figure VIII-2. After take-up, the fiber was soaked in distilled water overnight before being allowed to dry.

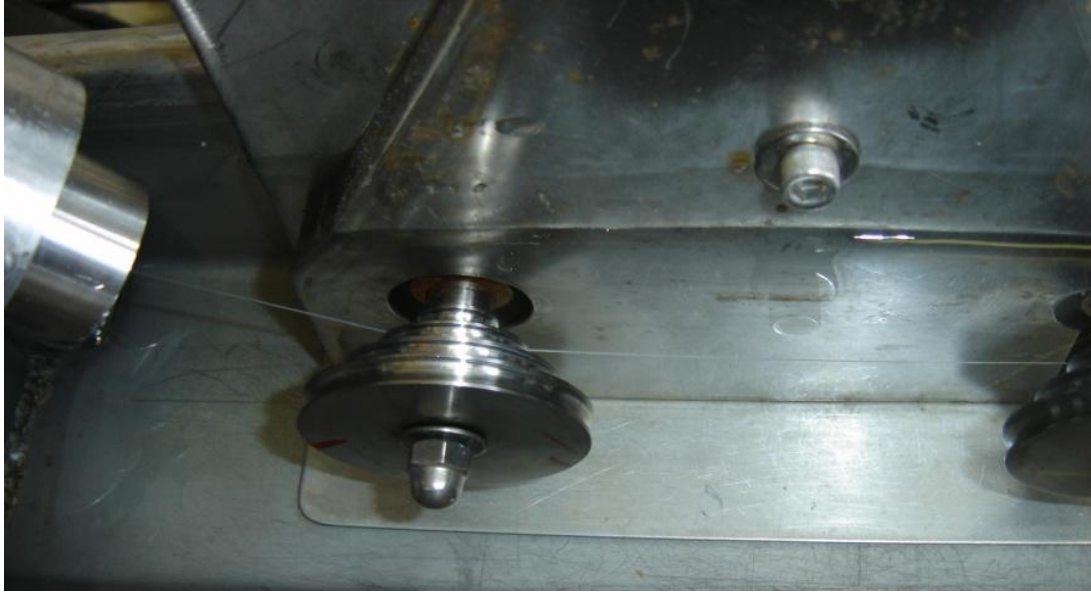Figure VIII-1. Fiber extrusion with no air gap onto a pair of stepped cylinder godets.

Figure VIII-2. Fibers exit coagulation bath onto take up package.

TECHNIQUES

Scanning electron microscopy (SEM) was performed following the procedures outlined in Chapter VI. The thermal and rheological characterization of samples containing CNF and CNT nanofillers was previously performed and discussed in Chapter VII.

Tensile Analysis of fibers

Stress/strain measurements were obtained from an Instron 4400R Model 1122. The gauge length was 15 mm and the extension speed was 37 mm/min. The initial modulus, breaking tenacity and elongation at break were calculated following ASTM D3822-96. Fiber tex was obtained by measuring the length of the extruded fibers and weighing a specified length. The following conversion was used to calculate the fiber tex and/or fiber denier: tex = 1 gram / 1000 meters, denier = 1gram/ 9000 meters.

RESULTS AND DISCUSSION

Scanning Electron Microscopy (SEM)

Extruded fibers were evaluated using scanning electron microscopy (SEM) to evaluate CNF and CNT orientation within the fibers. Figure VIII-3 shows extruded CNF/PU and CNT/PU fibers containing 1 wt% nanofibers at different magnifications. While it is not clearly observable in the SEM micrographs below, other researchers have found evidence in melt spun multi-walled carbon nanotubes (MWNTs)/shape memory polyurethane nanocomposite fibers of preferential alignment of the MWNTs to the fiber axis. During fiber processing, a number of parameters can influence this alignment process. In the melt spinning process, where this phenomenon has previously been observed, higher shear force and drawing ratio contribute to the axial alignment of the MWNTs [Meng et al., 2007]. While alignment of the nanofillers within the polyurethane matrix is not clearly visible in the SEM micrographs, it is clearly observed that overall alignment along the fiber axis is occurring. The draw ratio, 1:2, has an influence on orientation and alignment of the polymer chains along the fiber axis.

The fiber surface is also of interest and can be observed in Figure VIII-3. From the SEM micrographs taken at 500x magnification, the surface of the fibers reinforced with 1 wt% CNF is clearly much smoother than those reinforced with 1 wt% CNT. The surface of the CNT fibers may be more rough and coarse due to CNT aggregates which are exposed on the fiber surface. Similar effects have been reported in CNT reinforced polyurethane fibers [Meng et al., 2007]. This must be considered for the final application of the fibers. For example, hand is of major importance in textile applications.
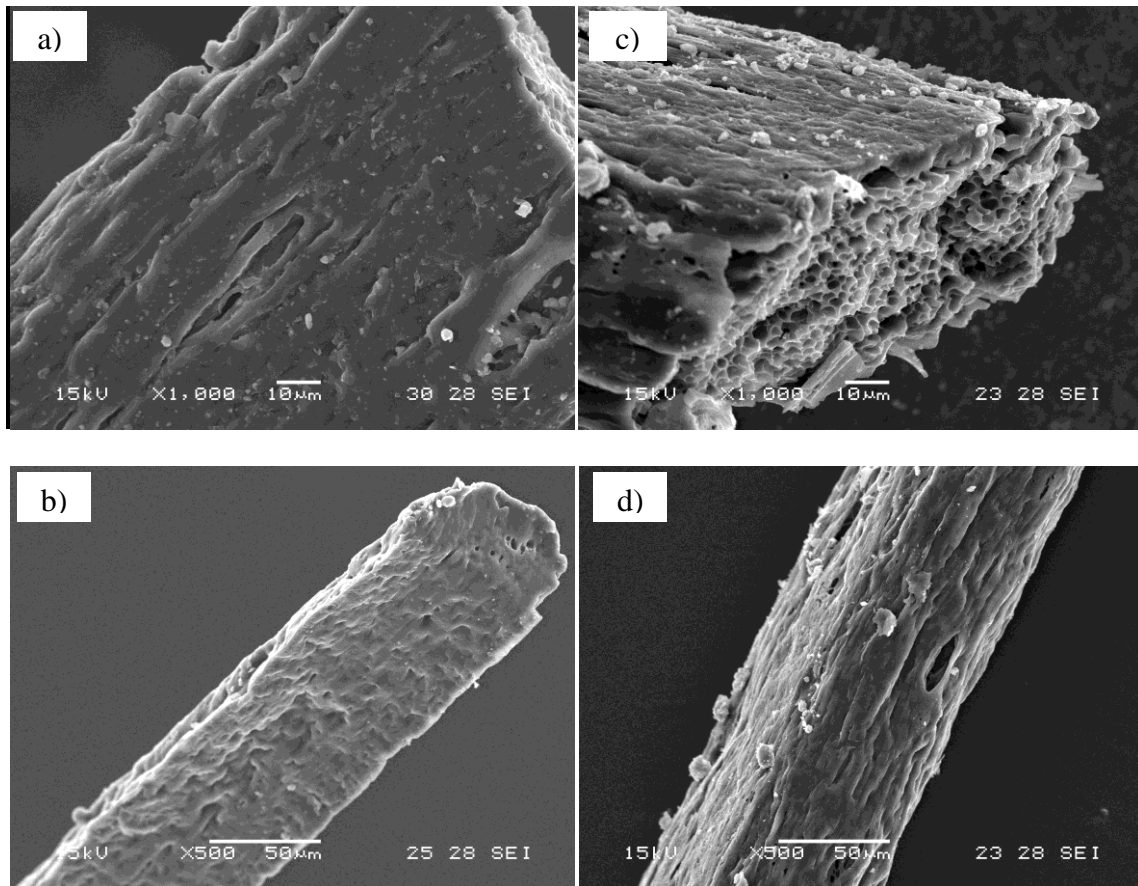

Figure VIII-3. Extruded fibers at varying magnifications: a) and b) CNF/PU fiber (1wt% CNF); c) and d) CNT/PU fiber (1wt% CNT).

184

Tensile Analysis

In order to examine the mechanical properties of the nanocomposite fibers, tensile testing was performed at room temperature. A summary of the results is shown in Table VIII-1.

Filler [wt%]		Flow Rate [mL/min]	Tex	Initial Modulus [cN/dtex]	Deformation at Break [%]	Breaking Tenacity [cN/dtex]
Commercial Polyurethane Matrix		0.4	48.9	0.027 ± 0.0063	682.41 ± 102.67	0.085 ± 0.011
CNT	0.5	0.4	58.5	0.044 ± .0049	711.17 ± 82.15	0.11 ± 0.024
	1.0	0.2	7.0	0.013 ± .048	682.65 ± 87.24	0.25 ± 0.010
	1.0	0.2	5.2	0.011 ± .040	677.00 ± 144.45	0.35 ± 0.011
	1.0	0.1	3.0	0.012 ± .052	667.48 ± 104.97	0.39 ± 0.081
	1.0	0.05	4.3	0.093 ± 0.022	642.95 ± 73.71	0.25 ± 0.017
	1.0	0.05	3.1	0.067 ± 0.024	830.33 ± 204.31	0.30 ± 0.061
CNF	0.5	0.4	20.0	0.064 ± 0.016	670.63 ± 127.66	0.18 ± 0.036
	1.0	0.2	6.2	0.087 ± 0.019	638.19 ± 69.12	0.55 ± 0.84
	1.0	0.1	5.8	0.095 ± 0.072	657.50 ± 119.21	0.44 ± 0.072
	1.0	0.05	8.6	0.094 ± 0.046	783.38 ± 82.95	0.31 ± 0.064

Table VIII-1. Tensile properties of the commercial polyurethane matrix and nanocomposite fibers.

The fibers were produced with a draw ratio of 1:2. As discussed previously, the draw ratio leads to an increase in molecular orientation. From other studies [Meng & Hu, 2008], molecular orientation had led to shape memory polyurethane fibers with outstanding mechanical properties when compared to those that lack molecular orientation. From the table, it is clearly visible that the nanocomposite fibers experience a significant increase in breaking tenacity over the unreinforced polyurethane fibers. Fibers with the addition of 0.5 wt% CNF showed an increase in breaking tenacity of 110% over that of the control matrix and 30% over fibers with 0.5 wt%

CNT. An increase in modulus was also observed with the addition of nanoreinforcements, which correlates to the findings of the commercial polyurethane nancomposite films in Chapter VII. A slight increase in the deformation at break was observed after the addition of nanoreinforcements. From the samples tested, the increase in mechanical properties was overall, more significant for fibers containing CNF. This effect can be seen in Figure VIII-4.
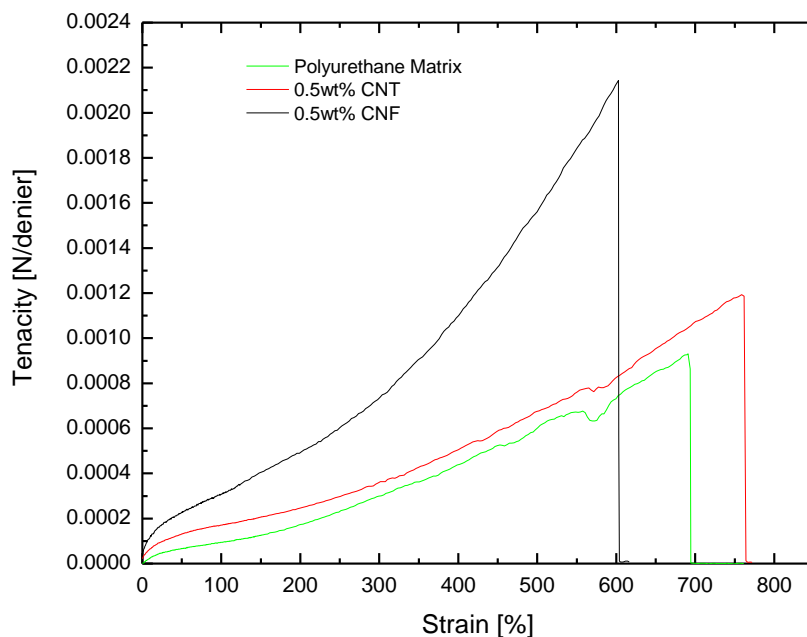

Figure VIII-4. Tenacity versus strain for extruded fibers with 0.5 wt% nanoreinforcements.

This behavior indicates good dispersion of the CNT in the matrix and additional mechanisms of energy dissipation. Chen et al. observed similar behavior in CNT/PU composite fibers fabricated through a twin-screw molten extrusion method. Similarly, composite fibers exhibited an increased modulus and yield stress without diminished elongation at break. It was observed that this behavior is not only attributable to the CNT nanoreinforcements but also to their impact on the behavior of the soft segment crystallization which would allow for larger deformations [Chen

186

et al., 2006]. The values obtained for elongation at break for fibers with a much lower linear density exceed the range of values reported for Spandex, which provides an elongation at break ranging from 500-600% for much larger fibers with a range of linear density in the range of 11-2500 dtex [Meng & Hu, 2008].

CONCLUSIONS

Shape memory polyurethane fibers reinforced with cellulose nanofibers and modified carbon nanotubes were prepared. Tensile tests of the extruded fibers showed an increase in the initial modulus and elongation at break with the incorporation of nanoreinforcements. A more significant effect in the initial modulus and elongation at break was observed in the fibers reinforced with cellulose nanofibers. An important result was that the elongation at break remained largely unaffected by the incorporation of nanoreinforcements and even slightly increased in some cases.

REFERENCES

1. Chen, W.; Tao, X.; Liu, Y. Carbon Nanotube-Reinforced Polyurethane Composite Fibers. *Composites Science and Technology*, **2006**, *66,* pp 3029-3034.

2. Ji, F.; Zhu, Y.; Hu, J.; Liu, Y.; Yeung, L.; Ye, G. Smart Polymer Fibers with Shape Memory Effect. *Smart Mater. Struct*., **2006**, *15*, pp 1547-1554.

3. Meng, Q.; Hu, J. Study on poly(ε-caprolactone)-based Shape Memory Copolymer Fiber Prepared by Bulk Polymerization and Melt Spinning. *Polymers for Advanced Technologies*, **2008**, *19*, pp131-136.

4. Meng, Q.; Hu, J.; Zhu, Y. Shape Memory Polyurethane/Multiwalled Carbon Nanotube Fibers. *Journal of Applied Polymer Science*, **2007**, *106*, pp 837-848.

5. Meng, Q.; Hu, J. Influence of Heat Treatment on the Properties of Shape Memory Fibers. I. Crystallinity, Hydrogen Bonding, and Shape Memory Effect. *Journal of Applied Polymer Science*, **2008**, *109*, pp 2616-2623.

6. Tang, S. L. P.; Stylios, G. K. An Overview of Smart Technologies for Clothing Design and Engineering. *Int J Cloth Sci Technol*, **2006**, *18*, pp 108.

7. Zhu, Y.; Hu, J.; Yeung, L-Y.; Liu, Y.; Ji, F.; Yeung, K. Development of Shape Memory Polyurethane Fiber with Complete Shape Recoverability. *Smart Mater. Struct.*, **2006**, *15*, pp 1385-1394.

CHAPTER IX.

CONCLUSIONS

During this work, the main focus was to study the effect of chemical structure on the properties and shape memory behavior of thermoplastic segmented shape memory polyurethanes. Additionally, nanoreinforcement of the polyurethane matrix was studied as a pathway to overcome the inherent disadvantages of low stiffness and low recovery force. Particular focus was placed upon hard segment content, hard segment composition, soft segment length, the timing of nanoreinforcement addition, the type of nanoreinforcement, and dispersion properties of the polymer suspensions.

Early in the research, segmented shape memory polyurethanes with 32 wt% hard segment content were found to exhibit the best combination of mechanical, thermal, and shape memory properties. For this reason, samples created with 32 wt% hard segments were concentrated on during the remainder of the research with particular emphasis placed on the TDI 2900/32 system. Since little focus has been given to polyurethanes constructed with TDI hard segments in the literature, this research adds substantially to the existing body of knowledge regarding the behavior of polyurethanes constructed using this particular isocyanate. By examining the structure of the polyurethanes, it was found that the hard segment composition plays an important role in the thermal and mechanical properties due to the structure of the utilized isocyanate, which greatly impacts the phase separation and crystallinity of the hard segments.

The soft segment length was found to have a significant influence on the ultimate deformation at break, thermal properties, and shape fixity.

In order to gain a better understanding of the gathered data for the shape memory behavior testing, the influence of the testing parameters was evaluated in depth. It was found that the testing parameters are of great importance and may have a significant influence the obtained shape memory behavior results. For this reason, careful selection of the testing parameters is important and the end application of the polymer system should be taken into consideration. Additionally, this study found that in order to achieve shape memory behavior the following must be present: adequate phase separation of the hard and soft segments, effective hard segments for shape recovery, and crystallinity of the soft segments for shape fixity.

The next step was to determine the influence of sample age and thermal treatment on the morphology and thermal and mechanical properties of the synthesized linear, thermoplastic polyurethanes. It was determined that the properties and morphology of samples composed of TDI hard segments reached equilibrium in a very short period (1 hour) as opposed to those composed of MDI hard segments which took much longer to reach equilibrium (approximately 20 days). The use of thermal treatment was effective at producing equilibrium in the MDI systems but showed little effect on the TDI system. Overall, it was found that the sample age has a significant impact on the polymer properties and that this effect must be taken into account not only in research but also when considering the end use or application of the polymer system. This examination was important because the current understanding and discussion of how aging affects the mechanical properties of the polyurethanes was limited in the literature.

The nanofillers selected for this research were desirable for the potential improvements to the polyurethane matrices as well as the possibility of introducing a new type of shape memory actuation to the polymer matrices (in the case of conductive cellulose nanofibers and carbon nanotubes). The commercial applicability of the nanofillers was also a consideration. For example, cellulose is desirable in commercial nanocomposites due to its availability and low cost while carbon nanotubes, which are more expensive, have excellent mechanical properties and stand to make substantial improvements in polymer properties at very low particle contents. Nanofiller incompatibility was overcome through modification. In order to improve nanofiller dispersion and adhesion to the polymer matrices, cellulose nanofibers were subjected to acid hydrolysis while carbon nanotubes were acidified and functionalized with MDI groups.

The effect of the incorporation of nanofillers into the polymer matrix was studied. The timing of the addition of nanofillers was also of interest. It was found that when cellulose nanofibers were added during the polymerization of the segmented shape memory polyurethanes, changes in the micro-structure of the polyurethanes occurred which affected the thermal, mechanical, and shape memory performance of the nanocomposites. The CNF tended to favor the phase separation of the soft and hard segments, which was observed in the upward shift of the melting temperatures of the crystalline phases. An increase in the Young's modulus, a decrease in the deformation at break, and elimination of the shape memory behavior were observed. Since retention of the shape memory behavior was of great concern during the construction of the nanocompistes, it was determined that addition of the CNF to the polymer matrix during the polymerization reaction is not an adequate path to achieve the desirable properties of the CNF/PU nanocomposite system. However, when cellulose nanofibers were added after the

polymerization the shape memory behavior was retained. Similarly, the incorporation of cellulose nanofibers induced changed in the microstructure of the polyurethane matrices, which was observed in the thermal and mechanical properties. The nanocomposite system exhibited behavior similar to that of CNF added during the first step of the reaction with the main difference being the retention of the shape memory behavior. The timing of nanofiller addition on the polymer properties has not previously been investigated in literature and the findings of this study are significant for other studies involving nanofillers that are capable of chemically interacting with the polymer matrices.

The impact of different types of nanofillers, CNF, C-CNF, and CNT, was evaluated using the commercial thermoplastic polyurethane provided by Huntsman. The mechanical and thermal properties of the nanocomposites were evaluated and compared. Additionally, a great deal of attention was directed to the impact of the nanofillers on the shape memory behavior of the nanocomposite system. All of the utilized nanoreinforcements were found to create an increase in the mechanical properties of those of the unfilled polyurethane matrix. The only nanoreinforcement to create a change in the thermal properties of the matrix was the C-CNF, in which much higher particle loadings were studied. The electrical percolation threshold of the C-CNF/PU nanocomposite system was determined to be in the range of 4-10 wt%, which corresponds to the rheological percolation threshold determination. The percolation threshold was determined to be approximately 1.5 wt% for the CNF and approximately 2 wt% for the CNT. The shape memory behavior of the polymer nanocomposite systems was maintained in the range of particle loadings studied and was even slightly enhanced over the unfilled polyurethane matrix.

192

Finally, extrusion processing of shape memory polyurethane nanocomposite fibers was evaluated. The evaluation of nanoreinforcement on fiber properties was important to this research because the material is suitable for and often used in intelligent textile materials. It was found that through utilization of nanoreinforcements such as cellulose nanofibers or carbon nanotubes, a significant improvement could be made over the unfilled polyurethane fibers in the initial modulus and yield stress without sacrificing the elongation at break.